PLASMA WAKEFIELD ACCELERATORS USING MULTIPLE ELECTRON BUNCHES

by

Efthymios Kallos

A Dissertation Presented to the
FACULTY OF THE GRADUATE SCHOOL
UNIVERSITY OF SOUTHERN CALIFORNIA
In Partial Fulfillment of the
Requirements for the Degree
DOCTOR OF PHILOSOPHY
(ELECTRICAL ENGINEERING)

August 2008

Epigraph

We are at the very beginning of time for the human race. It is not unreasonable that we grapple with problems. But there are tens of thousands of years in the future. Our responsibility is to do what we can, learn what we can, improve the solutions, and pass them on.

- Richard Feynman

Dedication

To the world

Acknowledgements

It must have been a warm November afternoon in Florida when on our way from Orlando to Miami after a conference Bing asked us to urgently make a stop to go to a restroom. After pulling over at some random building in a rush, Bing went inside and she returned moments later to the car with the remark that we had accidentally stopped by a fashion model agency! Within a few femtoseconds Erdem, Reza, Xiaodong and I had jumped off our car seats and ran through the building doors to check out the models, only to find ourselves in front of the surprised faces of a large number of buttoned-up employees of what turned out to be a … bank.

There were memorable moments like this one that made the everyday life of a student pursuing a Doctor of Philosophy a rather wonderful experience. The first person to be acknowledged of course is my advisor, Tom Katsouleas, who maintained a rather joyful atmosphere in our research group and inspired us to produce great research results by getting the best out of every one of us. I will never forget my first interaction with Tom back in the fall of 2003 when as an aspiring young scientist who had just arrived at the University of Southern California (USC) I walked into his office and asked him to describe to me some of the research he was involved with. I had never heard the words “plasma accelerators” until that moment of my life and, truth be told, I did not understand a single thing of what he explained that evening of what seemed to me – at the time – a very obscure field of physics.

Walking[1] on my way back home after this meeting, the words of the great artist Pablo Picasso kept ringing in my head: “*I am always doing that which I cannot do, in order that I may learn how to do it*”. I decided to embrace this philosophy and joined Tom’s group hoping that

[1] Oddly enough, I managed to live without a car in Los Angeles until 2 years later.

this was the best way for me to gain the most knowledge; that turned out to be – in retrospect – a very wise choice. After five exciting years I am graduating from the group having analyzed millions of experimental data points, having run thousands of simulations, having derived countless equations, and having made more good friends that I could have ever hoped for, ultimately experiencing a personal adventure of the greatest magnitude. During this unique process my understanding for the field of plasma accelerators and for the subject of physics in general has grown exponentially, the collaboration with other physicists allowed me to produce some very interesting scientific results, and Tom turned out to be a great advisor and one of the few people on the planet that no person could ever possibly dislike. Such is the aura of Tom that most people are grateful to meet such an individual once in their lives, while we lucky enough to be around him for 5 years. So, thank you, Tom.

The work presented in this dissertation would not have had its current form without the contributing help of many individuals. Patric Muggli, with who we frequently left our homes back in Los Angeles in order to visit the Brookhaven National Lab (BNL) and conduct our experiments, has had an indelible impact in shaping my way of scientific thinking. Given the fact that we were spending almost two months every year at BNL, we probably had more dinners together (since we were eating out every day) than with our girlfriends. We managed to cover pretty much every possible topic of discussion during those trips, ranging from Schrödinger's cat and Quantum Chromodynamics to European constitutions and life in tropical islands. Above all though, he has been very pleasant to work with in experiment upon experiment, always having time to listen and investigate any research issue we might have been struggling with.

Most of the experimental data presented in this dissertation were recorded at the Accelerator Test Facility (ATF) at BNL. Many thanks need to go to the facility director, Vitaly

Yakimenko, who managed to efficiently lead the group of scientists and staff at ATF into helping us to conduct the experiments as smoothly as possible[2]. He also brought forth a lot of fresh ideas and solutions to our problems which we would have never imagined on our own. I would also like to warmly thank the rest of the people at the ATF who made all these experiments a reality: Igor Pogorelsky, Igor Pavlishin, Karl Kusche, Daniil Stolyarov, Marcus Babzien, along with Samer Banna and Adam Lichtl for interesting discussions. Last, but not least, Wayne Kimura from STI Optronics has been a wonderful collaborator and generous enough to allow us to continuously use his wide range of equipment.

Another large part of my experimental experience was acquired at the Pulsed Power Laboratory here at USC under the kind supervision of Martin Gundersen. I worked endless hours with his student, Jessica Hao Chen, trying to analyze, decode and explain the mysterious yet fascinating world of plasma discharges. It was a pleasure to work and discuss with her every single time, even if at times nothing was working properly. We became good friends outside the lab and she has provided to me a unique authentic look into the Chinese culture.

The University of Southern California overall has provided me with a very comfortable and pleasant working environment to develop world-class research. Special mention needs to go to the USC machine and glass shops that constructed several key elements for my experiments, as well as to the USC Supercomputer Cluster (HPCC) that made possible the simulations of the complex interactions between trillions of particles and fields in one of the fastest computers in the world. I am certain that Isaac Newton would have been proud to see the incredible results of his second law of motion applied to our systems.

[2] Yet he repeatedly failed to convince us to bring our bathing suits to Long Island.

Probably the second most important contribution to the life of a Ph.D. student (after the advisor) is the interaction with the other students in the research group. To this regard, I was blessed to work with a unique array of personalities and philosophies from all over the world: Erdem Oz, Reza Gholizadeh, Wang Xiaodong, Bing Feng, Xiaoying Li, Chris Fenton, Ali Ghalam, Suzhi Deng and Brian Allen. Whether it was matters of science (like evaluating an impossible integral, following an electron trajectory in the plasma, or disproving the conservation of energy[3]), or matters of life (like driving for 8 hours in the middle of the night to Los Angeles after an exhausting hike at Grand Canyon during a hot summer day, philosophizing about the existence of aliens under the Yerkes astronomical observatory in Lake Geneva, or witnessing the ingenious flash-forwards in Lost), or both (like estimating on our way to Las Vegas that the earth would slightly slow down if all humans decided to start walking westwards), I would like to thank them for being such a great company all these years during my adventure.

I also feel that I should thank the people I worked with at the summer school on particle accelerators, with who we had some of the best two weeks during those intense studies at Ithaca which went on from morning till after midnight. Among others, we bonded very well with the marathon-runner Diktys Stratakis, the warm Brazilian Karen Fiuza and the awesome Matt Leone. It felt weird one day to calculate together the betatron frequencies and the next one to get soaked in the thunderous waters of the Niagara Falls. I am happy that we have stayed in contact and we meet again every once a while at the conferences.

Aside from those people that where directly related to my research, a number of other people influenced my life during the Ph.D. years. First of all it was my father, my mother and my brother that supported my decision to come to United States for such an extended period of

[3] This is not meant to be a joke. For example, the total amount of dark energy increases as it smoothly fills the space that is created through the expansion of the universe – see also Noether's theorem.

time and have always been there for me when I needed them. I am not sure when I was born 27 years ago whether my parents imagined that I would become the first doctor among our extended family (especially in a field that didn't even exist at the time). Furthermore, my companion in life, Dora, has always followed my steps and trusted in me, even when she had to move not just between zip codes but between whole continents for us to be together. Her support through all these years has surpassed my wildest expectations, and I will probably never be able to return her kindness in full.

I want to wholeheartedly thank my housemates, Andrew Yick and Rajay Kumar, for managing to turn an otherwise dull apartment into a fun and lively place. Ever since our first Quantum Mechanics class (where on my sight of Andrew I exclaimed "*this is exactly the kind of person I could never relate to*"), we went to graduate school together, we lived together and we earned our doctorates together. Andrew and I shared a special passion for technology and science that allowed us to work miracles with our class projects, our home theater system and our gadgets, a situation I will probably never encounter again in my life. I also need to thank the first non – Greek person that I became a close friend with, Yao Wen, with who the 3 am trips to late-night eateries and our movie-going experience at the dodgy University Village theaters became a regular thing.

The Greek community in USC and around Los Angeles in general has had a great impact on making California not look totally foreign to my eyes. Sotiris Zogopoulos took the time to first introduce me to the tricks of living in the US, while Costas Christodoulou and Violetta Ettare helped me tremendously during my first few months of settling down here. Dimitrios Pantazis was always available for a chat or just to hang out, and with Fragiskos Papadopoulos we went to almost every possible movie and movie theater in the greater Los Angeles area. With Stavros

Gonidakis we shared a lot of interesting discussions as well as the unforgettable jet-ski ride on the crystal-clear waters of Paradise Island in the Bahamas (which also gave me an unforgettable whole body skin burn). Melania Apostolidou and Nikos Zygouras were always fun to hang out with and to share our thoughts on the past, present and future. Finally, our love for convertible cars between me and Panagiotis Galiotos led to one of the most exciting day road trips of my life: from Los Angeles to Las Vegas, with the hood down both ways for the whole drive, driving in the serene desert landscape in the middle of the summer. Nothing compares to experiencing a full sunset and a full sunrise with the wind blowing at 70 mph (we were back by 9am the next morning just in time to go the lab without anyone noticing).

I also wish to thank my professors and the members of my qualifying exam and defense committees, Aluizio Prata, Stephen Haas, Werner Däppen, John O' Brien, Armand Tanguay and William Steier. They all transferred some part of their wisdom to me one way or another through homework problems, stories, suggestions and constructive criticism.

My guess is that people tend not to thank deceased persons in their dissertation acknowledgements; however I will have to break that rule and salute the late Richard Feynman, to my eyes the archetypal physicist. It was as if he was still alive when I was reading his books, listening to his derivations or watching his masterful lectures. His poster always stood on the wall of my desk and in the darkest moments of my Ph.D., an inspirational story from the master was the best cure to get me out of the dead-ends and put me back on track with real physics. He was the last true genius of our time.

There is an old African proverb that says "*If you want to go quickly, go alone. If you want to go far, go together*". The work that is described in the following pages of this dissertation would not have had its present form if it weren't for the 48 people that are acknowledged in this

section. From the bottom of my heart, I thank you all again for sharing with me the greatest adventure in life: the intoxicated feeling of being the first person in the world to discover something for the first time.

Table of Contents

List of Figures

Abstract

Particle accelerators are the tools that physicists use today in order to probe the fundamental forces of Nature, by accelerating charged particles such as electrons and protons to high energies and then smashing them together. For the past 70 years the acceleration schemes have been based on the same technology, which is to place the particles onto radio-frequency electric fields inside metallic cavities. However, since the accelerating gradients cannot be increased arbitrarily due to limiting effects such as wall breakdown, in order to reach higher energies today's accelerators require km-long structures that have become very expensive to built, and therefore novel accelerating techniques are needed to push the energy frontier further.

Plasmas do not suffer from those limitations since they are gases that are already broken down into electrons and ions. In addition, the collective behavior of the particles in plasmas allows for generated accelerating electric fields that are orders of magnitude larger than those available in conventional accelerators. Such wakefields have been demonstrated experimentally, typically by feeding either single electron bunches or laser beams into high density plasmas. As such plasma acceleration technologies mature, one of the main future challenges is to monoenergetically accelerate a second trailing bunch by multiplying its energy in an efficient manner, so that it can potentially be used in a future particle collider.

The work presented in this dissertation is a fruitful combination of theory, simulations and experiments that analyzes the use of multiple electron bunches in order to enhance certain plasma acceleration schemes. Specifically, the acceleration of a trailing electron bunch in a high-gradient wakefield driven by a preceding bunch is demonstrated experimentally for the first time by using bunches short enough to sample a small phase of the plasma wakes. Additionally,

it is found through theoretical analysis and through simulations that by using multiple bunches to drive the wakefields, the energy of a trailing bunch could be efficiently multiplied in a single stage, thus possibly reducing the total length of the accelerator to a more manageable scale. Relevant proof-of-principle experimental results are also presented, along with suggested designs that could be tested in the near future. Furthermore, electron beam and plasma diagnostics are analyzed and presented, which are necessary for properly completing and understanding any plasma wakefield experiment. Finally, certain types of plasma sources that can be used in related experiments are designed, diagnosed and tested in detail.

In science one tries to tell people, in such a way as to be understood by everyone, something that no one ever knew before. But in poetry, it's the exact opposite.

- Paul Dirac

Chapter 1

Introduction

1.1 Physics and Particle Accelerators

"*We are trying to prove ourselves wrong as quickly as possible, because only in that way can we find progress*". This is how the celebrated physicist Richard Feynman described the evolution of physics in his famous series of lectures he gave at Cornell University in 1965 regarding the character of physical laws [60]. Indeed, the experimenters are not very interested in confirming already-established laws under regular conditions. Rather, they prefer to look carefully in those places where the laws are most likely to be falsified. Consider for example the experiments that measured the blackbody spectrum [151] and the bending of light near the sun [46] in the early 20^{th} century which challenged our understanding of nature, thus allowing Max Planck and Albert Einstein, respectively, to suggest that energy is quantized [142] and that space is not flat [48], ultimately giving birth to the modern theories of Quantum Mechanics and General Relativity.

Today and for the past 70 or so years, the most successful tools that we use to look into those new regimes are particle accelerators [138]. These machines use strong electric fields to

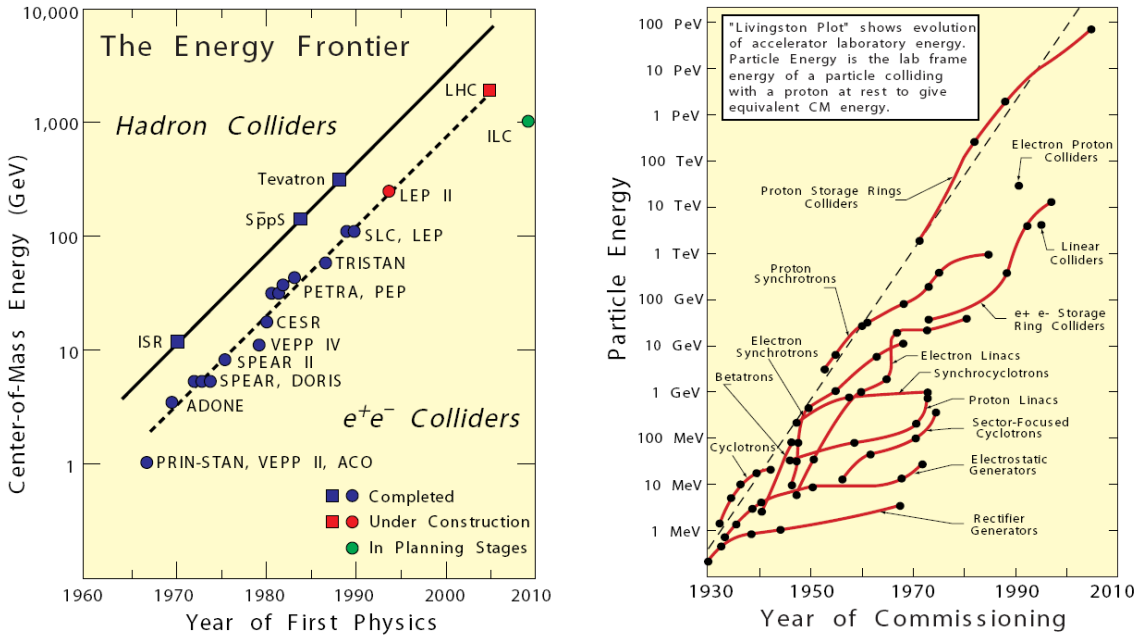

Figure 1.1: The Livingston curve shows the progress of the energy of various accelerators with time. From [138].

accelerate charged particles such as electrons and protons to high energies which are then smashed against each other at near the speed of light[1]. By observing the behavior of the products of those collisions, the elementary constituents of matter can be analyzed and new fundamental laws can be formed [11]. The ongoing success of these colliders has relied on the technological developments that allow them to accelerate particles at ever higher energies: From Einstein's famous mass-energy equivalence equation, $E = mc^2$, higher energies translate to more massive particles that can be created and detected in the accelerators. The progress of the accelerator energy over the past decades is depicted in Figure 1.1 .

The energy of accelerators has increased almost 10 orders of magnitude since the first cyclotrons where constructed in the early 1930s, and this scaling has produced some amazing discoveries in the field of particle physics as the higher energies allowed for heavier particles to

[1] If a proton from the 14 TeV Large Hadron Collider was to race a photon around the earth, it would finish the race in 145 μs, lagging only 1 mm behind the photon.

be detected. Most of the quark structure inside protons and neutrons was identified in the 1970s and 1980s at the Stanford Linear Accelerator Center (SLAC) [8], with masses that range between 1 MeV/c^2 (for the up quark) to 5 GeV/c^2 (for the bottom quark). The carriers of the electroweak force, W and Z bosons, were discovered in 1983 at CERN's Super Proton Synchrotron (SPS) and were found to have masses 80 GeV/c^2 and 90 GeV/c^2, respectively. The heaviest elementary particle known to date, the top quark, was discovered only in 1995 at Fermilab's Tevatron accelerator [39] with a mass of 171 GeV/c^2. Without particle accelerators, our understanding of the four fundamental forces of nature would have been limited to Einstein's theory of gravity [48] from 1915 and Maxwell's equations for electromagnetism [121] from 1865.

This success though has not happened without cost, as accelerators have come a long way since Lawrence's first 1 MeV cyclotron in 1932 which was a mere 10 cm long [103]. The price, complexity and size of the latest particle accelerators have skyrocketed along with their energy. This dissertation is written in 2008, the year that the Large Hadron Collider (LHC) is commissioned. The LHC is the largest and most complicated machine ever constructed by humans, a circular 14 TeV proton – proton collider built underground in a 27 km tunnel at CERN [1], near the French-Swiss borders[1]. This worldwide effort of 2,000 scientists from 34 countries will look for, among other things, the Higgs Boson with an upper expected mass of 144 GeV/c^2 (which may provide the tools to unify the three of the four fundamental forces), evidence for supersymmetric particles (which may explain the excess of non-baryonic matter in

[1] 14 TeV is roughly the energy needed to pick up a piece of hair from the floor and place it on a table (this is mostly kinetic energy – the rest mass energy of a proton is $E = mc^2 \simeq 1GeV$). The total energy circulating in the 2×2800 bunches of LHC with 10^{11} protons each is 724 MJ or the energy of a TGV train running at full speed (320 km/h).

the universe) and string theory's extra dimensions (which may explain why gravity is so weak compared to the other forces in nature). The price tag for LHC is between $5 – 10 billion.

LHC – scale accelerators are very close to the limit of what we can practically afford to build using conventional technologies, even collaboratively. The International Linear Collider (ILC) [3], a proposed 1 TeV lepton smasher, is estimated to cost $7 billion and extend over 30 km in length, more than 10 times the length of SLAC. The Compact Linear Collider (CLIC) [175] is another scenario of a proposed lepton collider at 3 TeV with a length of 33 km and similar cost. Any such projects will be extremely hard to finance and may ultimately follow the path of the Superconducting Super Collider (SSC), a 87 km circumference accelerator that was cancelled after the projected cost exceeded $12 billion in 1993[1].

The reason why the cost has been scaling with the collider energy is that the accelerating gradients (i.e., the energy gained per unit length) have more or less remained constant over the past few decades, in the order of 10 – 100 MV/m. Therefore, the only way to scale into higher energies is to simply make the accelerating portion longer, thus increasing the construction and maintenance costs at the same time. Those conventional techniques rely on radio-frequency electric fields that propagate inside metallic cavities. One of the major limitations of this technology is that if the accelerating fields are increased beyond a certain point, the modules are damaged [23] because the energy from these fields is approaching the energy that binds electrons to the atoms in the cavity walls and tears them apart. This is why the ILC gradient can only be 40 MV/m [3] (limited by the loss of superconductivity in the niobium cavities due to heat), only two times larger than the 20 MV/m of the 40 year old SLAC. Clearly, a revolution is

[1] 24 km of the underground tunnel were bored in Texas after 2 years of construction before cancellation.

needed here; a new acceleration technology that will do for the accelerators what the transistor did for the electronics 60 years ago: miniaturize them.

1.2 Plasma Accelerators

1.2.1 Basic Principles

The new particle acceleration technology that is the subject of this dissertation is plasma accelerators [50, 51]. The main principle behind it is that one can use a relativistic electron beam (Plasma Wakefield Acceleration – PWFA) or a laser pulse (Laser Wakefield Acceleration – LWFA) to excite relativistically moving waves in plasmas (ionized gases). The electric fields excited in those waves are at least 2 – 3 orders of magnitude stronger than the ones supported by the conventional metallic cavities, and thus, when utilized properly, they are used to accelerate particles to high energies in much smaller distances (thus reducing the cost). In addition, since plasma accelerating cavities (which are created dynamically every time) consist of already ionized particles, they do not suffer from the material breakdown damage like the conventional metallic cavities. Figure 1.2 illustrates the basic physical principles of a plasma accelerator.

As the relativistic electron beam or the laser beam propagates inside the plasma, the electric field of the beam displaces the plasma electrons[1], while the plasma ions are much heavier and stay static. Eventually the electrons are drawn back on the axis from the force of the positively charged ions, overshoot the axis, and they start to oscillate (perpendicular to the propagation direction of the beam in this figure). This sets up a charge density wave behind the beam, since the regions where the electrons cross the axis are more negatively charged than the regions where the electrons are far away from the axis. This charge difference creates a very

[1] The electric field of a relativistic beam is mostly transverse to its direction of motion.

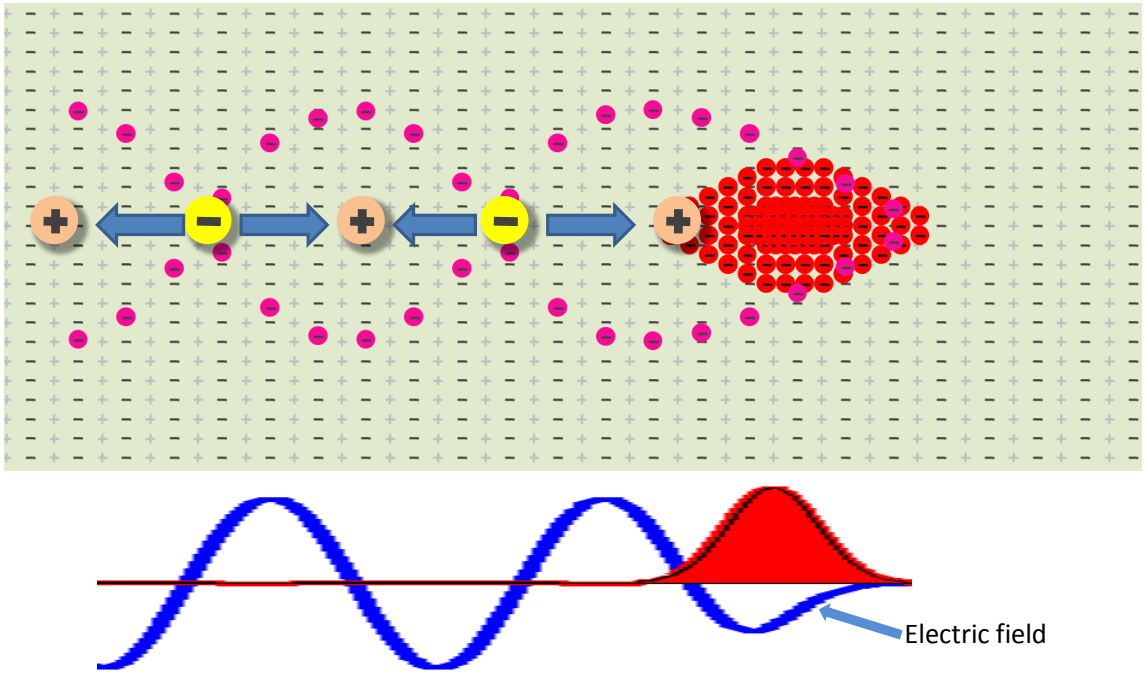

Figure 1.2: The main physical picture of a plasma accelerator. A relativistically moving electron beam or laser pulse is moving to the right inside a uniform plasma. The electric field of the driver displaces the light plasma electrons, which are then drawn back on axis from the static ions, setting up an electron density oscillation. The corresponding electric field that is generated on axis is plotted in the bottom.

strong electric field that propagates at the velocity of the beam. As a result, if a witness electron beam is placed at the proper phase, it will experience this accelerating field and be propelled to high energies.

A simple estimate for the strength of the electric field oscillation amplitude can be made by using Gauss's law:

$$\nabla \cdot \vec{E} = \frac{\rho}{\varepsilon_0} \tag{1}$$

Assuming a one – dimensional plane wave perturbation of the charge density, $\rho = e\Delta n e^{+ik_p z}$, where e is the electron charge, Δn is the plasma density perturbation, and $k_p = \omega_p / c$ is the plasma wavenumber, then the electric field perturbation is $\vec{E} = \hat{z} E_0 e^{+ik_p z}$, with $\nabla = \hat{z}\partial / \partial z$ (c is

the speed of light in vacuum). For a density perturbation on the order of the neutral plasma density, $\Delta n \sim n_0$, the electric field amplitude E_0 is roughly

$$eE_0 \simeq mc\omega_p \simeq \sqrt{\frac{n_0}{10^{16}\, cm^{-3}}} \times 10 \frac{GeV}{m} \tag{2}$$

Note that the plasma frequency ω_p is given by

$$\omega_p = \sqrt{\frac{e^2 n_0}{\varepsilon_0 m}} \tag{3}$$

For a plasma with a neutral density $n_0 = 10^{16} cm^{-3}$, equation (2) indicates that an accelerating electric field (wakefield) of 10 GV/m could be supported by the plasma. These extremely large wakefields are the single most important reason that has motivated the plasma accelerator community over the last 30 years to investigate the details of using plasmas as accelerating structures.

The physical reason why plasmas can support those high gradients is the collective effect of the plasma electrons. As opposed to the other three states of matter where the particles and molecules are distributed in a fuzzy and incoherent way, inside a plasma its billions of freed electrons can be manipulated together and forced to act coherently. The success of the future plasma accelerator will rely on maintaining this nice collective behavior over long enough distances. Moreover, it should be pointed out that the plasma accelerator is merely an energy transformer. It does not provide energy; it may only transfer the energy of an existing beam to a trailing beam. As such, it still requires a pre-created driver to provide the initial energy to be extracted. Therefore, the plasma accelerator will not replace existing accelerators; it will rather extend them to higher energies [81].

1.2.2 Progress of Plasma Accelerators

In order to put the work presented in this dissertation into perspective, a review of the history of plasma accelerators until today is necessary [42] and the purpose of this section.

Plasmas where identified as early as 1879 [40] (dubbed *radiant matter*), by Langmuir's time in the 1920s [102] they were known to support propagation of electron waves [169] and became well understood by the 1950s [5, 41]. Fainberg in 1956 was the first to suggest [56] that if one would generate plasma waves that propagated at relativistic speeds ($v_{ph} \simeq c$) then particles could be accelerated by sampling the relativistic electric fields inside the plasma. Although some first demonstrations of the interaction of an electron bunch train with a plasma happened in the mid-1970s by Berezin et al. [17, 57] showing 250 kV/m gradients, it wasn't until the rigorous work of Tajima and Dawson in their seminal 1979 paper [168] that a significant effort to conduct research on plasma accelerators was seriously initiated [43, 82]. In this paper the idea of using a laser to excite the relativistic waves in the plasma was first proposed. By 1985 the excitation of the first GV/m unloaded relativistic waves in plasmas was reported by Clayton et al. [36] using laser beat – wave techniques[1].

Earlier in the same year Chen et al. [31, 93] analyzed the excitation of plasma waves by relativistic electron beams instead of lasers. In 1988 Rosenzweig et al. demonstrated experimentally for the first time the interaction of a trailing electron beam with the wakefield excited by a preceding drive electron beam [148]. They fed a 21 MeV drive beam with 2 – 3 nC charge which was 7 ps long into a 33 cm long plasma with a neutral density of 10^{13} cm^{-3} and observed 50 keV energy shifts of the witness beam at 5 MV/m gradients. Those experiments were later extended in the mildly nonlinear regime in 1989 [14, 149] (by allowing the plasma

[1] Single laser pulses were not intense enough at the time to excite those wakes, thus the beating between two laser pulses was utilized.

density n_0 to become smaller than the beam density n_b), as was analyzed theoretically in 1987 also by Rosenzweig [146].

By 1991 the so-called blowout or bubble regime of the plasma wakefield accelerators was identified through simulations [13, 147]. In this highly nonlinear regime the drive beam is much denser than the plasma, $n_b \gg n_0$, and as a result the region behind the driver is void of electrons leaving a uniform density ion column [15, 113, 114, 115]. A witness beam placed in that region was found to experience simultaneously uniform accelerating and focusing forces along its transverse size, an extremely desirable situation that is not possible with linear drivers.

The first evidence of accelerated electrons using a laser-driven plasma were reported by Kitagawa et al. in 1992 [99] by trapping electrons in a beat-wave setup. Soon after, in 1993, in a series of very well monitored experiments, Clayton et al. showed the acceleration of externally injected electrons in a laser beat-wave plasma with 0.7 GV/m gradients [37], which was later followed by acceleration of trapped electrons up to 28 MeV by sampling 2.8 GV/m gradients, as reported by Everett et al. in 1994 [55]. By 1995 Modena et al. [122] reported the use of an intense 5×10^{18} W/cm^2 laser to drive the plasma to wave breaking by inducing the Raman Forward Scattering instability, thus producing the most energetic electrons from a laser-driven accelerator at the time (44 MeV)[1]. Still, the laser pulse needed to be many times longer than the plasma wavelength for these schemes to work.

As lasers became more powerful in the early 2000s reaching multi – TW levels, it became possible to excite plasma waves in the blowout regime [112] by using a single short pulse (with length comparable to the plasma wavelength). In 2002, Malka et al. published the first such results [119] by accelerating trapped electrons to 200 MeV using 1 Joule energy 30 fs

[1] The LWFA gradients where much higher than the PWFA gradients at the time due to the difference in the driver intensities: typically 10^{19} W/cm^2 for laser beams, 10^{12} W/cm^2 for particle beams.

long Titanium:Sapphire laser pulses onto 2×10^{19} cm^{-3} density gas jets, albeit with 100% electron energy spread at the exit. Soon it was clear from the first 3D LWFA simulations [117, 145, 170] that in this regime very low energy spread bunches could be produced; it wasn't long before three groups independently reached this "sweet spot" in 2004 [58, 63, 120] by trapping and accelerating 0.5 nC bunches to over 100 MeV with less than 10% energy spread. More than 20 groups worldwide have since repeated those results, and in 2006 the output energy was increased to 1 GeV by propagating similar laser pulses inside a cm-scale capillary plasma by Leemans et al. [106, 127]. This last record-breaking result for laser-driven accelerators also brought forth the main issue with these schemes, the fact that laser pulses tend not to propagate focused over long distances due to diffraction, and it is challenging to extend these acceleration techniques to meter-scale plasmas that are required for particle-physics-quality energies.

Relativistic charged particle beam drivers on the other hand are "stiffer" and do not suffer from diffraction as severely[1]. While the laser-driven acceleration was flourishing, the PWFA community had set forth to demonstrate that plasma accelerators can work over meter-scales by using the 50 GeV SLAC electron beam as a driver in the ultrarelativistic blowout regime[2] [73]. This collaboration produced a wide array of wonderful experimental results in the 2000s, such as the transverse beam-envelope dynamics by Clayton et al. in 2002 [35], the study of positron focusing by Hogan et al. [75] and the 56 MV/m positron acceleration in positron-driven wakefields by Blue et al. [19] in 2003, the 150 MV/m acceleration of the electron beam by Muggli et al. in 2004 [123], the first multi-GeV energy gain for any plasma accelerator by

[1] The effective relativistic parameter γ for a laser is $\simeq \omega_0 / \omega_p \sim 10$ for a 1 μm laser at 10^{19} cm^{-3} density, while the SLAC beam has $\gamma \simeq 10^5$.

[2] This was initially proposed by John Dawson.

Hogan et al. in 2005 [74], and the production of ultra-short trapped electron bunches by Oz et al. in 2007 [136], culminating with the doubling of the energy for some of the electrons of the beam from 42 GeV to 84 GeV in a little less than one meter of plasma as reported by Blumenfeld et al., also in 2007 [18, 20]. Although the energy spread of those electrons was an undesirable 100%, this latest remarkable result proved that over 50 GV/m accelerating gradients can be maintained in long plasmas.

1.3 Present Challenges for PWFAs and Scope of the Dissertation

In this section we will analyze the upcoming challenges that plasma wakefield accelerators have to surpass in the next 10 – 20 years in order to realize a future plasma-based lepton collider, and how the work described in this dissertation is placed along that roadmap.

1.3.1 Future Collider Design Requirements

We initially need to briefly summarize the requirements that a future lepton (electron-positron) collider must satisfy in order to produce interesting new physics [3, 175], since a plasma accelerator must be designed according to them [178]. First, the particle energy needs to be at least 250 GeV[1]. For comparison the previous largest electron-positron collider, CERN's Large Electron-Positron (LEP), accelerated particles up to 105 GeV.

Equally important is the luminosity L, or the number of collisions per cross-sectional area, defined as

$$L = f \frac{N^2}{A} \tag{4}$$

Here f is the repetition rate of the collisions (per turn for circular colliders), N is the number of particles per collision in each beam, and A is the area of each beam. The Tevatron at

[1] For a total of 500 GeV per collision.

Fermilab has enough energy to create the Higgs Boson, but its luminosity is too low to provide a satisfying measurement, on the order of 10^{32} $cm^{-2}s^{-1}$. This is why LHC, CLIC and ILC luminosities are targeted towards the 10^{34} $cm^{-2}s^{-1}$ value. Furthermore, in order to produce high-quality data the beam quality also needs to be very high, which translates to 0.1 – 10% energy spread and emmitance of 0.01 – 0.1 mm-mrad.

In order for this design to be constructible at a fraction of the present design cost estimates for CLIC and ILC, currently at $10 billion per TeV, an average accelerating gradient larger than 100 MV/m is required along with a wall-plug efficiency (the fraction of electrical power that translates to beam power) of 10 – 20%. In comparison, SLAC operated at 40 MW and CLIC & ILC will require a constant supply of 200 – 300 MW of AC power to operate at those efficiencies.

1.3.2 Roadmap to a Plasma-Based Collider

Presently the most promising technology for a plasma accelerator appears to be an electron-beam driven PWFA as opposed to a laser-driven LWFA, for two primary reasons. First, lasers are limited by diffraction and it is not straightforward to extend the laser-plasma interaction length from 1 cm (which is the case now [106]) to several meters, required to achieve multi-GeV particle energies. Second, despite today's PW-scale power, lasers do not provide enough energy: a required 250 GeV beam with 6×10^{9} electrons (1 nC charge) contains 250 Joules of energy, as opposed to 1 Joule of energy that most present-day LWFA lasers can offer at a very low repetition rate. In contrast, the 50 GeV SLAC electron beam provides about 100 Joules of very-low-entropy energy hundreds of times every second.

PWFAs have already demonstrated that energy doubling at 50 GV/m gradients over a meter-long plasma is achievable. With that starting point, the following major milestones will need to be reached in the next few years in order to realize a future plasma-based collider:

1. High-energy acceleration of a trailing electron beam with high charge and low energy spread
2. High-energy acceleration of a trailing positron beam
3. Wake excitation from a high-efficiency driver
4. Multiply the energy gain either by staging or by increasing the transformer ratio[1]

All 4 of the above milestones may depend on the use of multiple bunches, which is the main focus of this dissertation.

Regarding item 1, the accelerated electrons observed in PWFA experiments to date have originated either from the same bunch that drove the wakefield or from unshaped witness bunches that were much longer than a plasma wavelength, thus sampling a large phase of the wake which increased the energy spread and spoiled the beam emmitance. Eventually a witness bunch that is much shorter than the plasma wavelength will have to be placed appropriately and accelerated with high-gradients. Such an experiment was performed at the Accelerator Test Facility (ATF) of the Brookhaven National Lab (BNL), and the main results are presented in Chapter 4 here (also published in [85]). Specifically, it is shown that a trailing bunch which is shorter than the plasma wavelength is accelerated under 150 MV/m loaded gradients for the first time. This result, combined with SLAC-type propagation in a meter-scale plasma experiment could lead to the realization of the first milestone. The process would then have to be repeated for an injected positron witness bunch (item 2).

[1] For a definition of the transformer ratio, see section 2.3.

Items 3 and 4 deal with high efficiency and multiplication of the energy in a single-bunch PWFA stage. Coupling 250 Joules of energy (required for a strong 250 GeV witness bunch as we showed earlier) with a realistic 10% efficiency using plasma acceleration requires 2,500 Joules of input beam energy. This is one order of magnitude more energy than a single electron bunch can carry today. As a result, multiple bunches will most likely need to be used to provide the necessary energy, either through staging (by placing many single-bunch PWFA cells in series), or by using multiple bunches in a single stage [118]. As we will analyze in Chapter 5, the latter solution not only could provide the necessary energy but also optimize the beam-to-plasma energy transfer efficiency without the need for specially shaped bunches (only their positions and charge need to be tuned).

Furthermore, staging significantly reduces the average energy gradient of the total accelerator because it requires relatively long non – PWFA modules to be inserted between the different stages to achieve extraction of spent beams and injection of new ones. On the other hand, multiple bunch PWFA schemes can multiply the energy of a witness bunch in a single stage, thus eliminating the need for staging and preserving the high gradients. Such high transformer ratio scenarios will also be analyzed theoretically and through simulations in Chapter 5. In addition, some preliminary experimental results using multiple electrons bunches to drive wakefields will also be presented in Chapter 6.

Multiple bunch schemes are favored in the linear or mildly nonlinear regime of plasma acceleration because the sensitive nature of the phasing of the bunches in the waves is not affected by the nonlinear frequency shifts that occur in the blowout regime. In addition, although the transverse focusing properties are not optimized in this regime and the gradients may not be as large, the linear regime offers design simplicity and symmetry in the acceleration

between electron and positron witness bunches (neglecting for now spot size constraints imposed by luminosity requirements). It is also less susceptible to instabilities such as the hose instability [44] which may prevent the beam propagation over very long distances otherwise.

The rest of the dissertation is organized as follows. Chapter 2 analyzes results from the PWFA linear theory relevant to understanding the experiments and simulations presented later. Chapter 3 provides a series of experimental data regarding the design and diagnosis of plasma sources. Chapter 4 demonstrates the high-gradient witness bunch acceleration in the wake driven by a preceding bunch. Chapter 5 presents designs and simulations for high-transformer-ratio and high-efficiency multibunch PWFA drivers. Chapter 6 demonstrates experimentally some preliminary schemes for multibunch PWFA accelerators. Finally, Chapter 7 summarizes the results and points out future research directions.

1.4 Chapter Conclusions

The following items are concluded from this chapter:

- Particle accelerators are the main tool for doing modern physics but they have limited gradients; fields greater than 150 MV/m cause cavity wall breakdown.

- Plasma – based accelerators overcome the gradient limitations because of the collective motion of the free electrons and provide a promising potential alternative.

- A future electron-positron collider will require high energy (> 250 GeV), high luminosity (10^{34} $cm^{-2}s^{-1}$) and high beam quality (low emmitance and energy spread) achieved over relatively short distances. Present plasma accelerator schemes do not solve these issues satisfactorily.

- This dissertation demonstrates high – gradient acceleration of a trailing bunch and proposes the use of multiple electron bunches to multiply the energy of short trailing beams at a fraction of the conventionally required distances in an efficient manner.

In mathematics you don't understand things. You just get used to them.

- Johann von Neumann

Chapter 2

PWFA Linear Theory

In this chapter the basic principles of plasma wakefield theory will be analyzed. The focus will be in the linear regime and specifically in those aspects fundamental to the understanding of the physical principles of the simulations and the experiments presented the in later chapters of this dissertation. Apart from the generated wakefield amplitude we will analyze the transformer ratio, energy efficiency, beam loading and also the transverse effects.

In principle the linear regime is valid when the plasma density perturbation δn is small compared to the neutral plasma density n_0, or $\delta n / n_0 \ll 1$. Since the density perturbation is typically on the order of the peak beam density n_{b0}, this criteria is equivalent to $n_{b0} / n_0 \ll 1$. In practice and through simulations it is found that the predictions of the linear theory are good up to $n_{b0} / n_0 \sim 1$ [116].

2.1 Longitudinal Wakefields

2.1.1 Basic Equations

A number of assumptions are made when deriving the plasma wakefield equations in the two-dimensional linear regime. 1) There is azimuthal symmetry, $\partial / \partial \varphi = 0$. 2) The plasma ions remain static since their mass M_i is much larger than the electron mass m. 3) The second order perturbations of all the quantities are much smaller than the first order perturbations. 4) The plasma electrons and ions are cold and have uniform neutral density. 5) The beam velocity is close to the speed of light c, i.e. $\vec{v}_b \simeq c\hat{z}$.

Next we define the electron beam density distribution as follows

$$n_b\left(z,\varphi,r,t\right) = n_b\left(\xi = z - ct, r\right) = n_{b\parallel}\left(\xi\right)\cdot n_{b\perp}\left(r\right) \tag{5}$$

Hence the beam charge density is $\rho_b = -en_b$ and the beam current $\vec{J}_b = -\hat{z}ecn_b$. Here $\xi = z - ct$ is a variable in the frame of the moving beam, and $n_{b\perp}\left(r\right)$ is an amplitude-normalized to 1 unitless probability distribution such that $n_{b\perp}\left(0\right) = 1$. Combining Maxwell's equations [121], Newton's second law of motion for the electrons [130] and the equation of continuity for the plasma, it can be found (see Appendix A) that the plasma electron density is then $n_e \simeq n_0 + n_1$, where $n_1 = \delta n$ is the density perturbation which follows the harmonic oscillator equation

$$\frac{\partial^2 n_1}{\partial \xi^2} + k_p^2 n_1 = -k_p^2 n_b \tag{6}$$

and its solution as a function of ξ is given by the Green's function integral

$$n_1\left(r,\xi\right) = -k_p n_{b\perp}\left(r\right) \underbrace{\int_{-\infty}^{\xi} n_{b\parallel}\left(\xi'\right)\sin\left(k_p\left(\xi - \xi'\right)\right)d\xi'}_{=\varepsilon_0 k_p Z\left(\xi\right)/e} \tag{7}$$

Here $k_p = 2\pi / \lambda_p$ is the plasma wavenumber. The corresponding longitudinal electric field perturbation $E_z(r,\xi)$ can be split into a longitudinal component $E_{\|}(\xi)$ and a transverse component $R(r)$ as $E_z(r,\xi) = E_{\|}(\xi) \cdot R(r)$ which are given by [92, 116, 174]

$$\begin{aligned} E_{\|}(\xi) &= \frac{e}{\varepsilon_0} \int_{-\infty}^{\xi} n_{b\|}(\xi') \cos\left(k_p(\xi - \xi')\right) d\xi' \\ R(r) &= \frac{k_p^2}{2\pi} \int_{\varphi'=0}^{2\pi} d\varphi' \int_{r'=0}^{+\infty} n_{b\perp}(r') K_0\left(k_p \sqrt{r^2 + r'^2 - 2rr'\cos\varphi'}\right) r' dr' \end{aligned} \tag{8}$$

Notice that $E_{\|}(\xi) = Z'(\xi)$. For a complete derivation see Appendix A. K_0 is the zeroth order modified Bessel function of the second kind [4]. $R(r)$ is a unitless function that describes the transverse dependence of the wakes and it has the property that $R(r) \simeq n_{b\perp}(r)$ for transversely wide beams. The equality is satisfied exactly when $R(r) = n_{b\perp}(r) = 1$. It is interesting to point out that in that 1D limit, equation (8) shows that the longitudinal wakefield after the beam is proportional to the cosine Fourier transform of the beam density.

2.1.2 Transverse Component

Experimentally the most common transverse beam density profile is a Gaussian, defined through $n_{b\perp}(r) = e^{-r^2/2\sigma_r^2}$. We shall examine these profiles closer since they are most commonly assumed throughout this dissertation. Using equation (8), the transverse component $R(r)$ of the longitudinal wake can be evaluated numerically and is plotted in Figure 2.1 for different beam spot sizes. The on-axis value $R(r=0)$ as a function of σ_r is plotted also in Figure 2.1 for different asymptotic expressions and it is given by the formula [116]

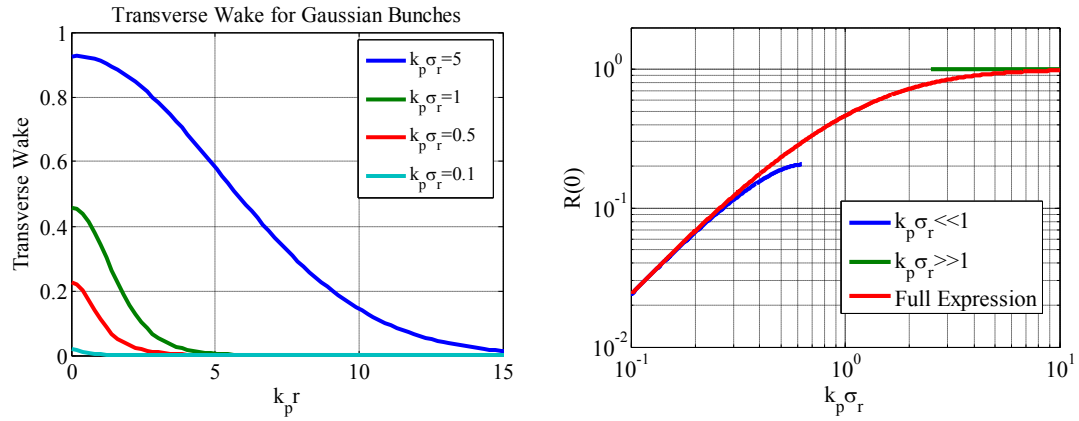

Figure 2.1: Left: Transverse dependence $R(r)$ of the longitudinal wakefield for transversely Gaussian bunches. Right: The on-axis transverse component of the longitudinal wakefield $R(0)$. The two asymptotic expressions for extreme values are also plotted here.

$$R(0) \simeq \begin{cases} k_p^2\sigma_r^2\left[0.05797 - \ln\left(k_p\sigma_r\right)\right] & , \quad k_p\sigma_r \ll 1 \\ \left(\frac{k_p^2\sigma_r^2}{2}\right) e^{+\frac{k_p^2\sigma_r^2}{2}} E_1\left(\frac{k_p^2\sigma_r^2}{2}\right) & , \quad \forall\, k_p\sigma_r \\ 1 & , \quad k_p\sigma_r \gg 1 \end{cases} \tag{9}$$

Here $E_1(b) \equiv \int_1^{+\infty} \frac{e^{-bt}}{t} dt$ is the exponential integral of the first kind. We observe that for beams narrower than $k_p\sigma_r \sim 1$ the transverse effects become important, specifying the transition between 1D and 2D regimes.

2.2 Transverse Wakefields

In this section we will investigate the transverse wakefield of a beam in the linear regime, which for the relativistic beams studied here is equal to $W_\perp(r,\xi) \equiv F_\perp / e = E_r - cB_\varphi$, and determines the transverse forces on the beam [33, 129, 167]. The transverse wakefield can be estimated once the longitudinal wakefield $W_\parallel = E_z$ is known by using the Panofsky-Wenzel theorem [139]

– or simply by taking the transverse component of Faraday's law: $\frac{\partial W_{\parallel}}{\partial r} = \frac{\partial W_{\perp}}{\partial \xi} \Rightarrow W_{\perp} = \int \frac{\partial E_z}{\partial r} d\xi = Z(\xi) R'(r)$. Equivalently [30, 33, 166]

$$W_{\perp}(r,\xi) = \frac{e}{\varepsilon_0 k_p} \int_{-\infty}^{\xi} n_{b\parallel}(\xi') \sin\left(k_p(\xi - \xi')\right) d\xi' \cdot \frac{dR}{dr} \tag{10}$$

2.2.1 Focusing

The envelope equation of a transversely Gaussian beam in one dimension (neglecting space charge effects which are of the order of $1/\gamma^2$) [35, 72, 161] is

$$\frac{d^2\sigma_x}{dx^2} + K\sigma_x = \frac{\varepsilon_N^2}{\gamma^2 \sigma_x^3} \tag{11}$$

Here σ_x is the transverse spot size of the beam along the dimension x, K is the focusing strength, and ε_N is the normalized emmitance of the beam. Deviations in the initial spot size of the beam are minimized when the beam emmitance is matched such that $\frac{d^2\sigma_x}{dx^2} = 0$, or

$$\varepsilon_N = \gamma \sqrt{K} \sigma_x^2 \tag{12}$$

Inside an ion channel (void of electrons) there is no azimuthal magnetic field ($B_{\varphi} = 0$) and the remaining transverse electric field E_r (calculated from Gauss's law) increases linearly with r, while the focusing strength is a constant:

$$K = \frac{eE_r / r}{\gamma mc^2} = \frac{n_0 e^2}{2\varepsilon_0 \gamma mc^2} = \frac{k_p^2}{2\gamma} \tag{13}$$

The matched emmitance is then given by the formula

$$\varepsilon_N = \sqrt{\frac{\gamma}{2}} k_p \sigma_x^2 \tag{14}$$

This scenario, which often occurs in the blowout regime of PWFAs, is highly desirable since either the beam spot size remains constant (if the emmitance is matched) or it stably oscillates around the equilibrium value.

In other cases though, the focusing strength is not constant and it may depend on the longitudinal position along the bunch. It can be proven from first principles that it is then given by the more generalized equation [72]

$$K\left(\sigma_x\right)=\frac{e}{\gamma mc^2\sigma_x^2}\left(\overline{x\cdot W_\perp\left(x\right)}\right) \tag{15}$$

Here $W_\perp$ is the transverse wakefield acting on the beam in that dimension and

$$\overline{x\cdot W_\perp\left(x\right)}\equiv\int_{-\infty}^{+\infty}x\cdot W_\perp\left(x\right)\cdot n_x\left(x\right)dx \tag{16}$$

In the above expression $n_x\left(x\right)$ is the 1D density probability distribution of the beam in that dimension[1].

2.2.2 Emmitance Balancing in the Linear Regime

Specializing now in the linear regime of PWFAs, by replacing the transverse wakefield from equation (10) on equation (15) we have

$$K\left(\xi;\sigma_x\right)=\frac{eZ\left(\xi\right)}{\gamma mc^2\sigma_x^2}\underbrace{\int_{-\infty}^{+\infty}x\cdot R'\left(x\right)\cdot n_x\left(x\right)dx}_{I(\sigma_x)} \tag{17}$$

The approximately "matched" or balanced emmitance is then found from equation (12) as

$$\varepsilon_N\left(\xi;\sigma_x\right)=\sqrt{\gamma}\sqrt{\frac{eZ\left(\xi\right)}{mc^2}I\left(\sigma_x\right)}\cdot\sigma_x \tag{18}$$

[1] For a Gaussian beam density $n_x\left(x\right)=1/\sqrt{2\pi}\sigma_x\cdot\exp\left(-x^2/2\sigma_x^2\right)$ the constant value of $K=k_p^2/2\gamma$ is retrieved for an ion channel, independent of σ_x.

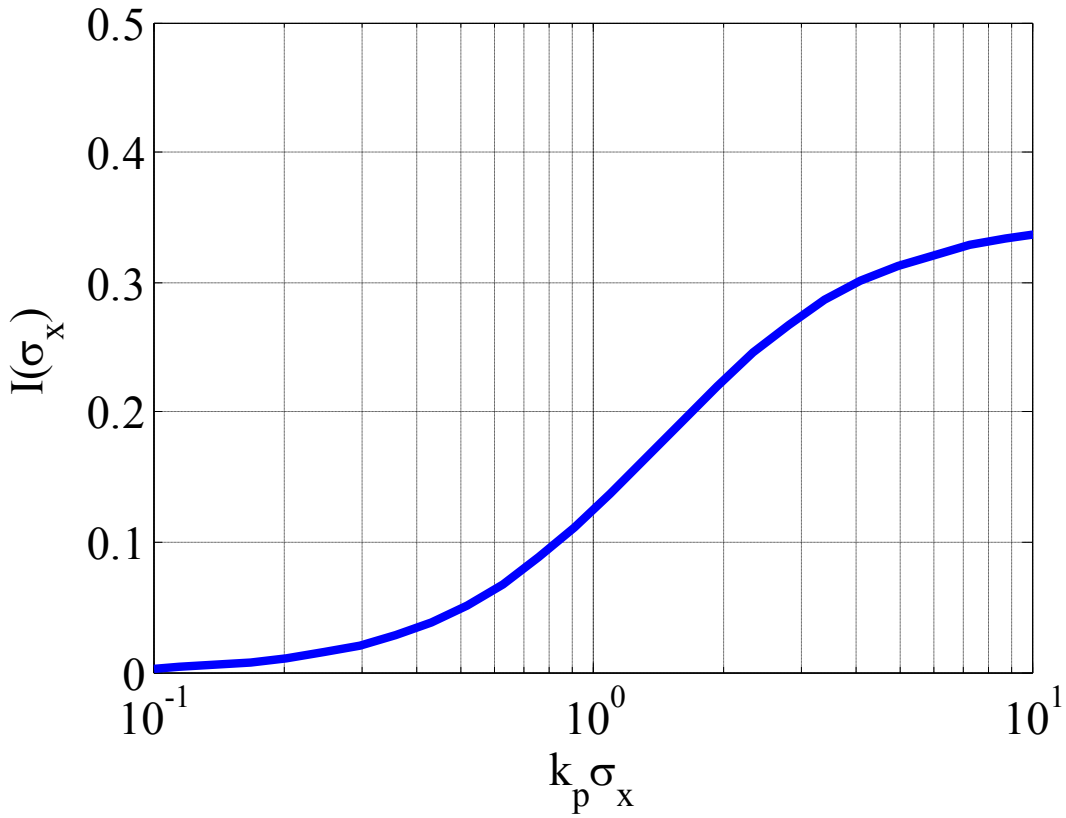

Figure 2.2: Transverse focusing dependence for a Gaussian distribution, useful for calculating the emmitance that balances the plasma's transverse focusing force.

The function $I(\sigma_x)$ defined in equation (17) can be evaluated numerically for a Gaussian beam distribution $n_x(x) = \frac{1}{\sqrt{2\pi}\sigma_x} e^{-\frac{x^2}{2\sigma_x^2}}$. The minimum value of the emmitance that can prevent a single beam from collapsing under the focusing force is found by assuming a transverse wakefield on the order of $Z \simeq E_0 / k_p$, where E_0 is the maximum value of the longitudinal wakefield $E_{\parallel}$ inside the beam. Then we find that

$$\varepsilon_N(\sigma_x) \geq \sqrt{\gamma} \sqrt{\frac{e E_0}{mc\omega_p} I(\sigma_x)} \cdot \sigma_x \tag{19}$$

2.3 Transformer Ratio

2.3.1 Physical Interpretation

The transformer ratio R is defined as the ratio of the maximum accelerating wakefield behind a bunch $E_{\max}^{+}$, divided by the maximum decelerating wakefield inside the bunch $E_{\max}^{-}$. It is an artificial measure on how efficiently energy is transported from a drive bunch into a witness bunch through the plasma oscillations.

$$R \equiv \frac{E_{\max}^{+}}{E_{\max}^{-}} \tag{20}$$

The importance of the transformer ratio can be illustrated in an ideal case as follows. Assume that a single point charge Q drives a wake, its total (kinetic) energy being W_0. The charge will generate a maximum decelerating wakefield $E_{\max}^{-}$ and it will lose all its energy after traveling a distance L, such that $W_0 = E_{\max}^{-} L$. Now suppose that another test charge trails behind and gains energy by sampling the wake of the first charge. It can only gain energy over the same distance L, because in principle after that distance the first bunch has deposited all its energy to the plasma waves and has come to a halt. The total energy ΔW gained from the second charge is

$$\Delta W = E_{\max}^{+} L = E_{\max}^{+} \frac{W_0}{E_{\max}^{-}} = R W_0 \tag{21}$$

Therefore the somewhat surprising result is reached that the total energy gained does not depend on the wakefield amplitude, but only on the transformer ratio.

2.3.2 Achieving Large Transformer Ratios

In most plasma acceleration experiments to date the transformer ratio has not been an important factor because the interaction between the plasma and the beam happens over relatively small distances and the drive beams do not have enough time to deposit a significant fraction of their energy. However a realistic future plasma accelerator will have to achieve high transformer ratios in order to effectively multiply the energy of an incoming beam over short distances.

According to the fundamental wakefield theorem, the transformer ratio of a single symmetric bunch in a linear homogeneous lossless plasma has a maximum value of 2 [10, 152, 153] (for a simple proof, see Appendix B.1). In order to achieve higher transformer ratios, either an asymmetric bunch must be used or more than one driving bunches must be fed into the plasma. In the former case, it was found by Bane et al. [9, 32, 104] that a single bunch which has a linearly ramped longitudinal density profile (along with a sharp kick in the beginning[1]) can create a constantly retarding wakefield along the bunch length, with the efficiency approaching 100% and a transformer ratio theoretically up to $2\pi M$, where M is the length of the bunch in units of k_p (see details in Appendix B.2). However these shaped bunches are not trivial to generate using present-day technology [49] and no PWFA experiment has been attempted using a single ramped bunch.

Another promising way to achieve high transformer ratios using regularly shaped beams is the use of more than one drive bunches, as initially hinted by Laziev et al. in 1988 [104, 154]. Power et al. [144] and Jing et al. [78, 79] more recently have proposed schemes for dielectric wakefield accelerators where if the distance between the bunches and the charge in each bunch

[1] The sharp kick brings the wakefield in the optimal value, after which the ramp preserves it.

is adjusted appropriately, then the decelerating wakefield experienced by each bunch could be identical for all bunches and hence the transformer ratio and the efficiency will be enhanced. Those ideas can be extended to plasma accelerators[1] and they will be analyzed in detail in Chapter 5.

2.4 Energy Transfer

In this section we will consider the driving energy efficiency of a plasma accelerator in the linear regime. This is of great interest because the plasma accelerator is essentially an energy transformer, extracting the energy from the drive beam(s) and delivering it through the plasma waves to a trailing beam. The efficiency is a very important parameter in the design of the accelerator as design efficiencies around 20% are highly desirable in order to reduce the cost of the accelerator.

2.4.1 Driving Efficiency

Given an electron beam with a specific initial energy, the *driving efficiency* is defined as the fraction of the total beam energy that has been transferred to the plasma waves at the end of the beam-plasma interaction.

Let us focus on the energy transport between particles and fields using general electromagnetic theory. Assuming a current $\vec{J}$ created by a number of particles that are present in an electric field $\vec{E}$, then the instantaneous power density transferred from the particles to the fields and vice versa is defined by $\vec{J} \cdot \vec{E}$ (with units of W/m^3) . For the case of a charged bunch distribution, the total *instantaneous* power P dissipated at the plasma (in

[1] They are applicable to other wakefield accelerator schemes as well, as long as they share the same formulation.

Watts) is just the integral of the above power density integrated over the whole volume of the bunch:

$$\begin{aligned} P &= \int_{r=0}^{+\infty}\int_{\phi=0}^{2\pi}\int_{\xi=-\infty}^{+\infty} \vec{J}\cdot\vec{E}\; dV = \\ &= \int_{r=0}^{+\infty}\int_{\phi=0}^{2\pi}\int_{\xi=-\infty}^{+\infty} qcn_{b\parallel}(\xi)n_{b\perp}(r)E_{\parallel}(\xi)\cdot R(r)\,rdrd\phi d\xi = \\ &= qc\int_{\xi=-\infty}^{+\infty} n_{b\parallel}(\xi)E_{\parallel}(\xi)d\xi\cdot\int_{r=0}^{+\infty} n_{b\perp}(r)R(r)2\pi rdr \Rightarrow \\ &\Rightarrow P = P_{\parallel}\cdot P_{\perp} \end{aligned} \tag{22}$$

In order calculate the total energy transferred from the beam to the plasma, equation (22) needs to be multiplied by the total time of the interaction, $T = L/c$ (L is the length of the interaction). This assumes that the velocities of the particles in the bunch are identical and do not change with time; in other words, the bunch is rigid[1].

The energy transfer efficiency of the interaction is now defined as the fraction of the total energy of the bunch that has transferred to the plasma after time T. Assuming that there are N particles in the bunch, each having the same initial energy $W_0 \equiv eV_0 = eE_{\max}L$, the efficiency η is written as

$$\begin{aligned} \eta &\equiv \frac{\text{energy dissipated to the plasma}}{\text{total energy in the bunch}} = \frac{T\cdot P}{N\cdot W_0} = \\ &= \frac{\int_{r=0}^{+\infty} n_{b\perp}(r)R(r)2\pi rdr\int_{-\infty}^{+\infty} n_{b\parallel}(\xi)E_{\parallel}(\xi)d\xi}{NE_{\max}} \end{aligned} \tag{23}$$

Note that $E_{\max} \equiv E_0\cdot R(0)$ (assuming the wakefield peaks on-axis). By inspecting the above expression we observe that the efficiency is maximized to unity when the electric field is

[1] Otherwise the time-dependent integral $\int Pdt$ needs to be evaluated.

constant for every point along the bunch distribution, $E_{\max}(\xi)=E_0$, with $R(r)=1$. Physically this means that every particle inside the bunch is depositing its energy to the plasma at the same rate. In that case the efficiency becomes

$$\eta=\frac{E_0\overbrace{\int_{r=0}^{+\infty}n_{b\perp}(r)2\pi r dr\int_{-\infty}^{+\infty}n_{b\|}(\xi)d\xi}^{\triangleq N}}{NE_0}=\frac{NE_0}{NE_0}=1 \tag{24}$$

It may not be obvious right away that the constant electric field E_0 along the bunch (in the enumerator of the above expression) and the electric field that corresponds to the initial energy of the bunch $E_{\max}$ (in the denominator of the above expression) should be the same. However the physical meaning of $E_{\max}$ is the electric field required such that a charge with energy $W_0=eV_0=eE_{\max}L$ will come to a stop after distance L. V_0 then is simply the voltage difference induced between the start and end points. Of course the symmetrical argument can also be applied: It is the electric field required to accelerate a charge e over distance L to an energy $W_0=eV_0=eE_{\max}L$.

2.4.2 Transverse Efficiency

The efficiency specified in equation (23) will be less than unity for bunches for which $R(r)<1$ for some r. For transversely Gaussian bunches, $n_{b\perp}(r)=e^{-r^2/2\sigma_r^2}$, this transverse driving efficiency which is defined as

$$\eta_\perp\equiv\frac{\int_0^{+\infty}n_{b\perp}(r)R(r)rdr}{\int_0^{+\infty}n_{b\perp}(r)R(0)rdr} \tag{25}$$

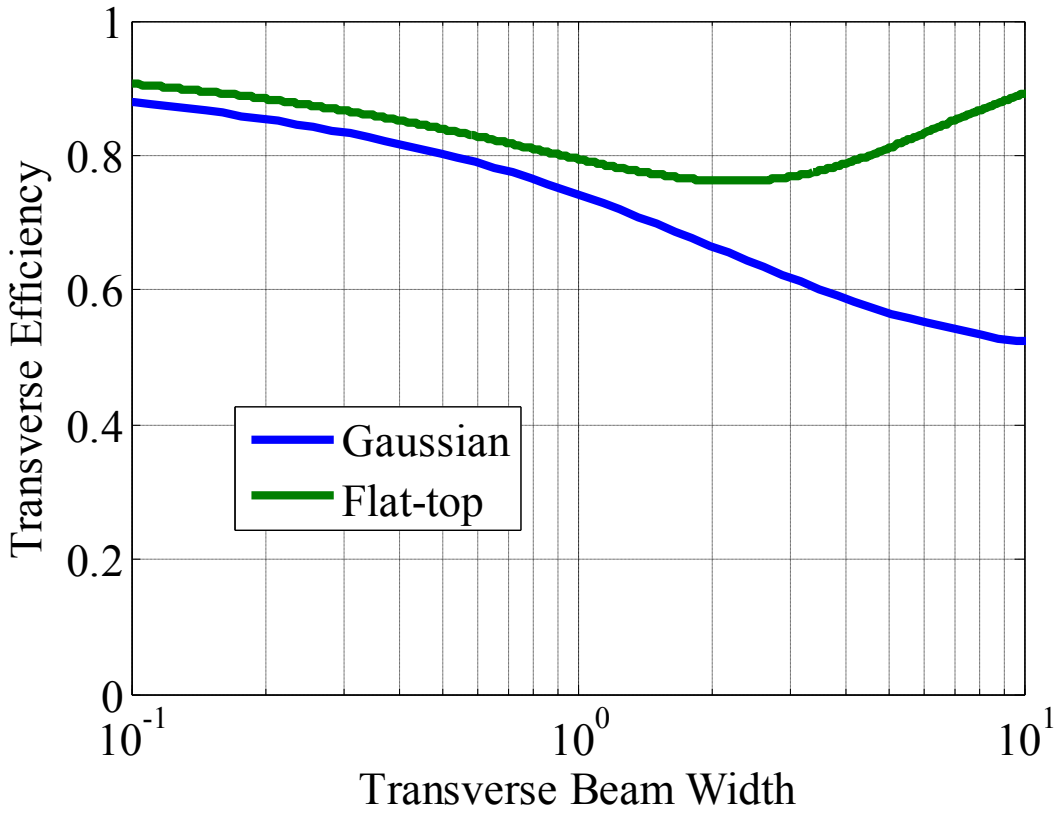

Figure 2.3: Transverse efficiency of a Gaussian bunch (beam width $\sqrt{2\pi}k_p\sigma_r$) and of a flat-top bunch (beam width $k_p\alpha$).

is plotted in Figure 2.3 as a function of the bunch width $k_p\sigma_r$. $R(0)$ is the maximum value of $R(r)$, which here occurs on-axis.

The transverse efficiency increases with decreasing σ_r because the wakefield variation across the beam is less for narrower beams. The efficiency is compared with the transverse efficiency of a transversely flat-top bunch (with an infinitely sharp cutoff at $r = k_p\alpha$). We observe that for narrow bunches ($k_p\sigma_r < 1$ or $k_p\alpha < 1$) the efficiency is independent of the exact bunch shape since the wakefield always extends out to a distance $1/k_p$. However for wide bunches the efficiency of a Gaussian bunch is 50%, unlike the wide sharp flat-top bunch which approaches

100%. This can be explained by invoking physical arguments when realizing that for wide beams ($k_p\sigma_r \gg 1$), the transverse component of the wakefield $R(r)$ and the transverse beam profile $n_{b\perp}(r)$ will overlap very closely since the expelled plasma electrons stay close to the beam ($\lambda_p \ll \sigma_r$). Hence for wide beams $R(r) \to n_{b\perp}(r) = e^{-r^2/2\sigma_r^2}$ with $R(0) \to 1$ and in this case equation (25) will read $\eta_\perp \simeq \frac{1}{2\pi\sigma_r^2}\int_{r=0}^{+\infty}\left(e^{r^2/2\sigma_r^2}\right)^2 2\pi r dr = 1/2$. Wide flat-top bunches consist a special case where $n_{b\perp}(r)R(r) = n_{b\perp}^2(r) = n_{b\perp}(r)$ and therefore yield transverse efficiency of $\eta_\perp = 1$ (equivalent to setting $R(r) = 1$ which is the 1D limit).

2.4.3 Efficiency vs Transformer Ratio

The concepts of driving efficiency and transformer ratio are very closely related. In this section we provide an example to illustrate the similarities and differences between these two parameters. Assume a single longitudinally square bunch centered at ξ_0 with a longitudinal width w containing N_0 particles that has a beam density profile

$$n_b(\xi, r) = \underbrace{\underbrace{\frac{N_0}{2\pi\sigma_r^2 w}}_{n_{b0}} rect\left(\frac{\xi-\xi_0}{w}\right)}_{n_{b\parallel}} \underbrace{e^{-\frac{r^2}{2\sigma_r^2}}}_{n_{b\perp}} \tag{26}$$

Here the function $rect(\xi/w)$ is 1 for $|\xi| < w/2$, ½ for $|\xi| = w/2$ and 0 otherwise. Using equation (8), the electric field generated by this bunch in the 1D limit is

$$\begin{aligned} E_\parallel(\xi) = &+\frac{en_{b0}}{\varepsilon_0 k_p}\sin\left[k_p(\xi-\xi_0+w/2)\right]\cdot rect\left(\frac{\xi-\xi_0}{w}\right)+ \\ &+\frac{en_{b0}}{\varepsilon_0 k_p}2\sin\left(\frac{k_p w}{2}\right)\cos\left[k_p(\xi-\xi_0)\right]\cdot U(\xi-\xi_0-w/2) \end{aligned} \tag{27}$$

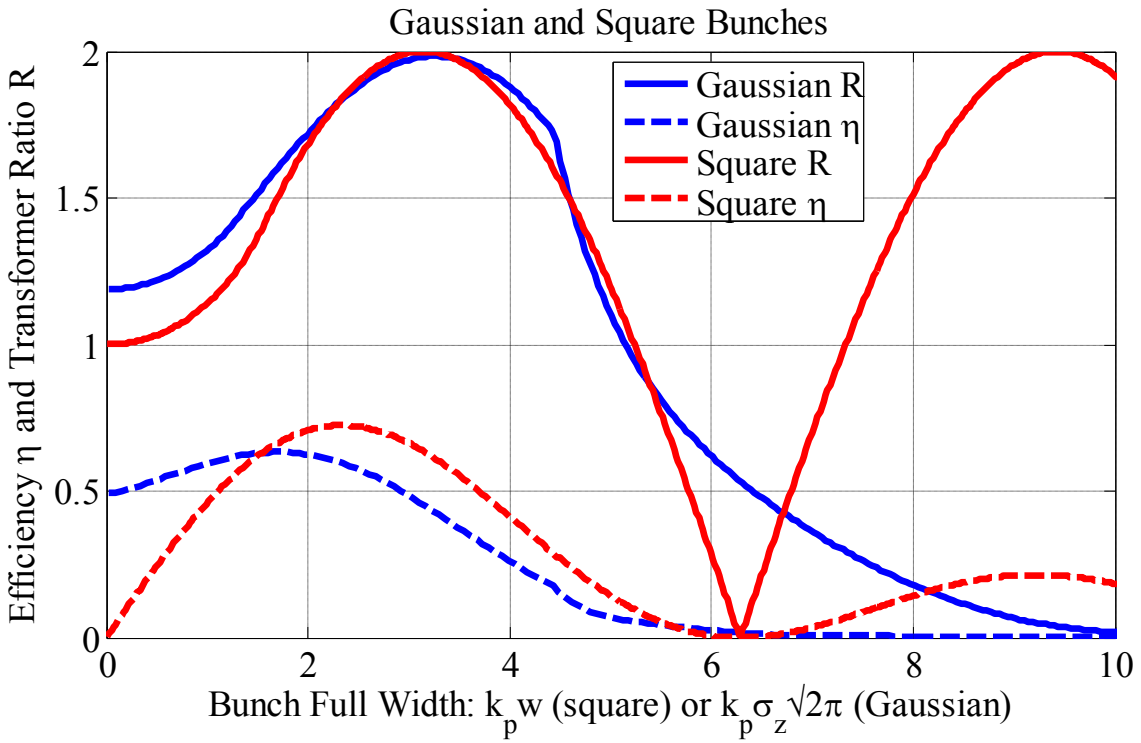

Figure 2.4: Transformer ratio and driving efficiency of a single square bunch as a function of the normalized bunch width $k_p w$. The results are compared with the transformer ratio and efficiency of a Gaussian bunch with normalized width $\sqrt{2\pi}k_p\sigma_z$. The transformer ratio for the Gaussian is defined at 1σ.

Here U is the Heaviside step function. The driving efficiency is calculated from equation (23) and is equal to

$$\eta\left(k_p w\right)=\frac{1-\cos\left(k_p w\right)}{k_p w} \tag{28}$$

The transformer ratio is simply from equations (27) and (20)

$$R\left(k_p w\right)=\begin{cases}\dfrac{1}{\cos\left(k_p w/2\right)} & , \quad k_p w\le\dfrac{\pi}{2}\\ 2\sin\left(\dfrac{k_p w}{2}\right) & , \quad k_p w\ge\dfrac{\pi}{2}\end{cases} \tag{29}$$

The values of the longitudinal efficiency η and the transformer ratio R are plotted in Figure 2.4 as a function of the normalized width of the bunch $k_p w$. For comparison, the

corresponding parameters for a Gaussian bunch of the same number of particles (achieved when $\sqrt{2\pi}\sigma_z = w$) are also plotted in the same graph[1].

It is observed that although the two parameters (η and R) are optimized around the same rough range of values for $k_p w$, they peak at slightly different points. In order to analyze this difference, we can compare the situations where the two above quantities are maximized, namely $k_p w = \pi$ (which maximizes the transformer ratio at $R = 2$ and then the efficiency is $\eta = 2/\pi = 63.6\%$), and $k_p w = 0.742\pi$ (which maximizes the efficiency at $\eta = 72.5\%$ and the transformer ratio then is $R = 1.84$).

In the maximum transformer ratio case, $k_p w = \pi$, the maximum wake inside the bunch is $E_{\max}^{-} = \frac{e n_{b0} w}{\varepsilon_0 \pi}$ and the maximum accelerating wake after the bunch is exactly $E_{\max}^{+} = \frac{e n_{b0} w}{\varepsilon_0 \pi} 2 = 2E_{\max}^{-}$. Assuming that each particle in the bunch has an initial energy W_0, then the interaction length is limited by the length over which the fastest decelerating particle loses all its energy:

$$L = \frac{W_0}{e E_{\max}^{-}} = \frac{W_0 \varepsilon_0 \pi}{e^2 n_{b0} w} \tag{30}$$

The energy left behind (transferred to the plasma) is proportional to the square of the accelerating field amplitude and the length of the interaction (C is a constant):

$$W_{plasma} = C \cdot \left(E_{\max}^{+}\right)^2 \cdot L = C \cdot 4 \frac{n_{b0} w}{\varepsilon_0 \pi} W_0 \tag{31}$$

[1] Strictly, the transformer ratio of a Gaussian bunch is always equal to 1 (since the bunch extends to infinity). Here we evaluate the transformer ratio at a distance 1σ from the center. On the other hand the definition of the efficiency incorporates the bunch profile and does not suffer from this technicality.

In comparison, in the maximum efficiency case, $k_p w = 0.742\pi$, the maximum wake inside the bunch is $E'^{-}_{\max} = \frac{en_{b0}w}{\varepsilon_0 0.742\pi} \simeq 1.35 E^{-}_{\max}$ and the maximum accelerating wake after the bunch is $E'^{+}_{\max} = \frac{en_{b0}w}{\varepsilon_0 0.742\pi} 2\sin\left(\frac{0.742\pi}{2}\right) \simeq 1.24 E^{+}_{\max}$. So in this case the decelerating wake is 35% higher, and the accelerating wake is 24% larger after the bunch. The interaction length now is shorter:

$$L' = \frac{W_0}{eE'^{-}_{\max}} = 0.74L \tag{32}$$

Finally, the total energy transferred to the plasma is

$$W'_{plasma} = C \cdot \left(E'^{+}_{\max}\right)^2 \cdot L' \simeq 1.14 \cdot W_{plasma} \tag{33}$$

So 14% more energy will be transferred to the plasma in the maximum efficiency case, even though the transformer ratio is actually smaller. The lower R is counterbalanced by the higher wake, even if the interaction length is shorter. This is because the energy transferred is proportional to the *square* of the wakefield, but only *linearly* proportional to the interaction length (which is inversely proportional to the decelerating wakefield).

2.5 Beam Loading

In this section we will investigate the process of energy transfer from the plasma wave to a witness bunch. In order for the bunch to gain energy it needs to be phased properly at the accelerating crest of the plasma wakefield. The witness bunch will also suffer energy spread if the longitudinal wakefield is not uniform along its longitudinal and transverse dimensions. Finally, an energy transfer efficiency from the plasma to the bunch electrons is associated with this beam loading. The question is then what is the optimal set of parameters for the witness

bunch (charge, width, phasing) to optimize the acceleration process and produce an accelerating bunch with low energy spread and high efficiency.

2.5.1 Longitudinal Beam Loading

Assume a external longitudinal plasma wakefield that has the form (on-axis)

$$E_{ext}\left(\xi\right)=E_0\cos\left(k_p\xi\right)R_0\left(0\right) \tag{34}$$

Here $R_0\left(0\right)$ is given by equation (9). At this point it is not relevant how this wakefield was created; it may have been generated by a single bunch or by a series of bunches, adding in or out of phase. After the drivers though, the wake that is left behind can be fully described with the above expression.

For simplicity let us assume a square witness bunch with N_w particles and length w phased at a position $\varphi_w=k_p\xi_w$ after the location of the external wakefield maximum $\xi=0$, of the form

$$n_b=\underbrace{\frac{N_w}{2\pi\sigma_w^2 w}}_{n_{b0}}rect\left(\frac{\xi-\xi_w}{w}\right)e^{-\frac{r^2}{2\sigma_w^2}} \tag{35}$$

The total wakefield inside and after the bunch (on-axis) can be found by superimposing the external field from equation (34) to the field generated by the witness bunch from equation (27) . The beam loading efficiency then is found to be

$$\begin{aligned}\eta_b&=\frac{W_{before}-W_{after}}{W_{before}}=1-\frac{E_{after}^2}{E_{before}^2}=\operatorname{sinc}\left(\frac{k_p w}{2}\right)p_0\left[-2\cos\left(k_p\xi_w\right)-p_0\operatorname{sinc}\left(\frac{k_p w}{2}\right)\right]\\ p_0&\equiv\frac{E_{0w}R_w\left(0\right)}{E_0R_0\left(0\right)}\end{aligned} \tag{36}$$

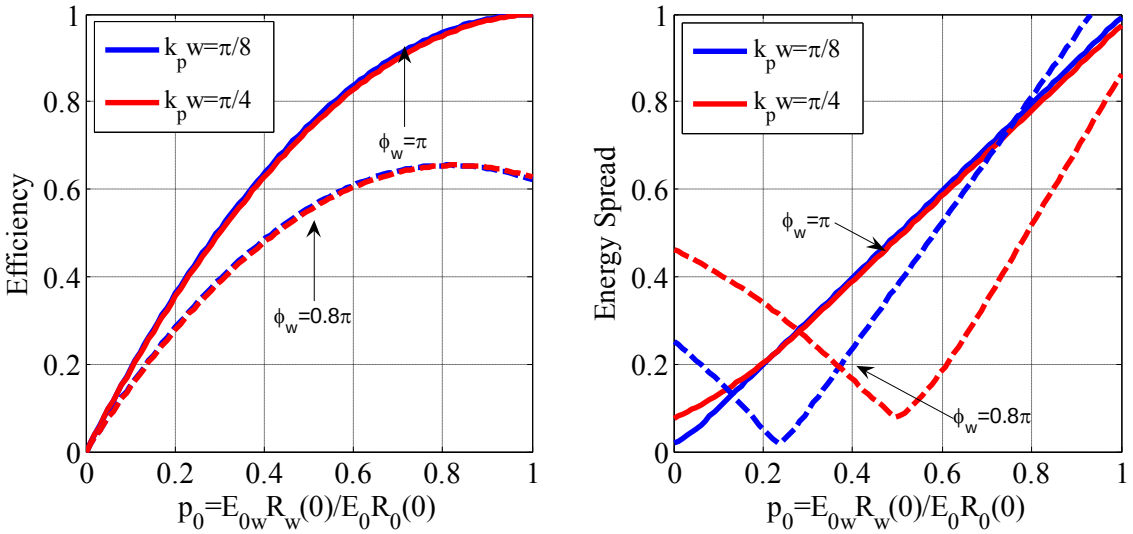

Figure 2.5: Longitudinal beam loading efficiency (left) and fractional longitudinal energy spread (right) of a square bunch accelerated by an external wakefield as a function of the normalized bunch length $k_p w$, the phase φ_w of the bunch in the wake, and the number of particles in the bunch (related to the ratio $p_0 = E_{0w} R_w(0) / E_0 R_0(0)$).

Here $\mathrm{sinc}(x) = \sin(x)/x$ is the unnormalized sinc function and $E_{0w} = \frac{eN_w}{\varepsilon_0 2\pi\sigma_r^2} = \frac{en_{b0}w}{\varepsilon_0}$ is the longitudinal wakefield amplitude per normalized unit length generated by the witness bunch. The maximum efficiency is achieved when the bunch is phased at the most flat portion of the external wave (so that different particles experience as similar as possible accelerating gradient), i.e. $\varphi_w = k_p \xi_w = \pi$. In that case and for very short bunches, $k_p w \to 0$, then in the 1D limit ($R_0(0) = R_w(0) = 1$) the expression derived by Katsouleas et al. in 1987 [92, 174] is retrieved:

$$\eta_b = \frac{E_{0w}}{E_0}\left(2 - \frac{E_{0w}}{E_0}\right) \tag{37}$$

On the other hand, increased efficiency occurs at the expense of larger energy spread for this unshaped bunch. 100% efficiency happens when $E_{0w} = E_0$ (or $N_w = \frac{\varepsilon_0 E_0}{e} 2\pi\sigma_r^2$ particles are loaded into the wake) and means that no wakefield is left behind the bunch, therefore the

wakefield along the bunch will vary from E_0 (in the head) to 0 (in the tail) resulting in 100% energy spread. The fractional energy spread f_w for the square bunch is given by the formula

$$f_w = \frac{\Delta W}{W_0} = p_0 \,\mathrm{sinc}\left(\frac{k_p w}{2}\right) \tag{38}$$

In Figure 2.5 the beam loading efficiency and the energy spread for a square witness bunch are plotted in the 1D limit as a function of the bunch parameters: the bunch width $k_p w$, its phase in the external wake φ_w, and its self-wakefield E_{0w} (which is proportional to the number of particles in the bunch) normalized to the external wakefield amplitude E_0. We observe that although the efficiency is substantially lower when the witness bunch is placed before the peak of the wake, its charge can be adjusted such that the energy spread is minimized (at some expense of the accelerating gradient).

2.5.2 Reverse Ramped Bunch

The tradeoff between efficiency and energy spread can be surpassed if a longitudinally specially shaped bunch is utilized, as described in [89, 92, 174]. The efficiency is maximized with no longitudinal energy spread if all the particles on-axis feel the same accelerating wakefield. Using equation (8) and assuming an external wakefield of the form in equation (34), by requiring the total field inside a bunch with its head phased $k_p \xi_w$ relative to the external wake to be constant, the optimal longitudinal beam distribution is found

$$n_b\left(\xi\right) = \frac{\varepsilon_0 k_p E_0 R_0\left(0\right)}{e}\left[\sin\left(k_p \xi_w\right) + \cos\left(k_p \xi_w\right) \cdot k_p\left(\xi - \xi_w\right)\right] \tag{39}$$

while the phase is adjusted between $\pi/2 \le k_p \xi_w \le \pi$. The (constant) accelerating gradient in this case is $E_a = -E_0 R_0\left(0\right)\cos\left(k_p \xi_0\right)$, the maximum length of the bunch is

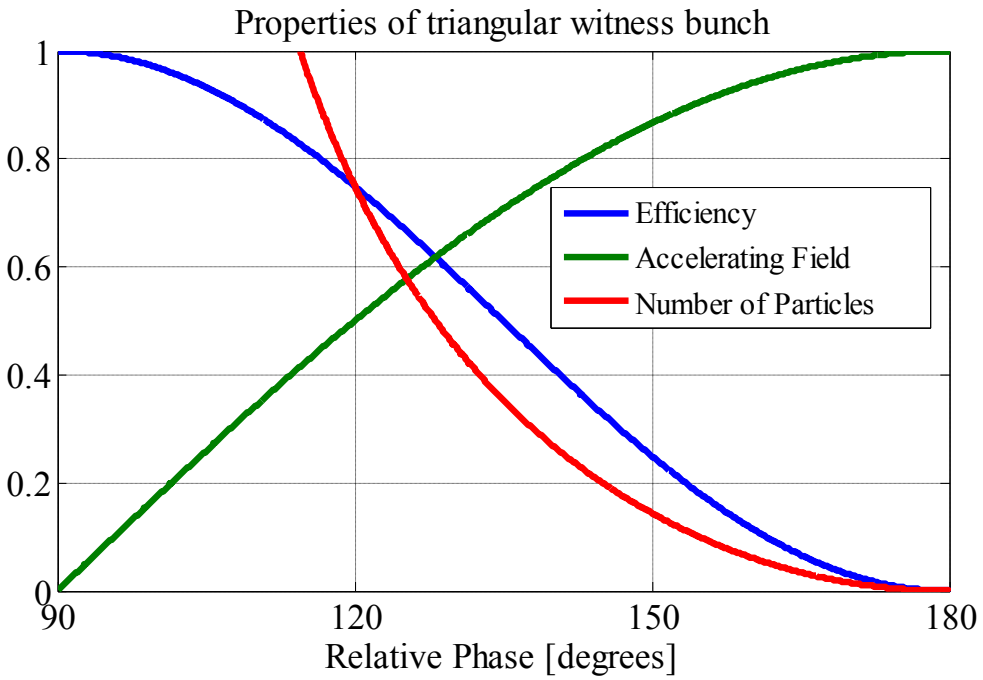

Figure 2.6: The efficiency, accelerating field and the relative number of particles accelerated for a ramped witness bunch in a sinusoidal wakefield as a function of its position relative to the external wakefield. The longitudinal energy spread is zero for this specially shaped bunch.

$k_p L = -\tan\left(k_p \xi_w\right)$, the longitudinal efficiency is $\eta_b = \sin^2\left(k_p \xi_w\right)$ and the total number of particles in the bunch is $N_w = -N_0 \dfrac{\sin^2\left(k_p \xi_0\right)}{2\cos\left(k_p \xi_0\right)}$, with $N_0 = \dfrac{\varepsilon_0 2\pi\sigma_r^2 E_0 R_0(0)}{e}$ for a transversely Gaussian profile. Although now there is no energy spread, the efficiency (and the number of particles) are increased at the expense of the accelerating gradient. Those tradeoffs are depicted in Figure 2.6.

2.5.3 Transverse Beam Loading

So far we have ignored transverse effects in the beam loading process. Now suppose that the same square witness bunch defined in equation (35) is found inside a 2D external axi-symmetric wakefield

$$E_{ext}\left(\xi,r\right)=E_0\cos\left(k_p\xi\right)R_0\left(r\right) \tag{40}$$

The wakefield generated from that witness bunch (after the bunch) has the general form (see also equation (27))

$$E_w\left(\xi,r\right)=E_w\cos\left(k_p\xi+\varphi_w\right)R_w\left(r\right) \tag{41}$$

Here φ_w is the phase shift of the witness wake relative to the wake of the external wakefield. The total energy in the wakefield before the witness bunch over one period of the wave is (for wide beams where the other field components can be neglected)

$$W_{ext}=\int_{r=0}^{+\infty}2\pi rdr\int_{\xi=0}^{2\pi/k_p}d\xi E_0^2\cos^2\left(k_p\xi\right)R_0^2\left(r\right)=\frac{\pi^2}{k_p}E_0^2\int_{r=0}^{+\infty}rdrR_0^2\left(r\right) \tag{42}$$

The *total* wakefield after the bunch is given by the superposition of (40) and (41):

$$\begin{aligned}E_{after}\left(\xi,r\right) \quad &= E_w\left(\xi,r\right)+E_{ext}\left(\xi,r\right)= \\ &= E_0R_0\left(r\right)\sqrt{1+p^2+2p\cos\varphi_w}\,\sin\left(k_p\xi+\varphi_{after}\right) \\ &p\left(r\right)\equiv\frac{E_wR_w\left(r\right)}{E_0R_0\left(r\right)}\end{aligned} \tag{43}$$

After calculating the energy W_{after} in the wake left behind by the witness bunch similar to equation (42), the beam-loading efficiency of the system can be written as

$$\eta_b=1-\frac{W_{after}}{W_{ext}}=1-\frac{\int_0^{+\infty}\left(1+p^2+2p\cos\varphi_w\right)R_0^2\left(r\right)rdr}{\int_0^{+\infty}R_0^2\left(r\right)rdr} \tag{44}$$

Some interesting special cases can be discussed here. First, if $E_w=0$ then $\eta_b=0$ (no energy is transferred from the wake to the bunch). Second, if the bunch that excited the wake and the witness bunch have the same radial dependence (i.e., $R_0\left(r\right)=R_w\left(r\right)$), then the transverse

components of the wakes overlap perfectly in space (albeit with different strengths) and the 1D result of equation (36) is retrieved, yielding the efficiency

$$\eta_b = \frac{E_w}{E_0}\left(-2\cos\varphi_w - \frac{E_w}{E_0}\right) \tag{45}$$

Negative beam loading efficiency means that the bunch transfers energy to the plasma instead of the other way. In order for the witness bunch to absorb energy, the phase of the witness bunch must be selected such that $\cos\varphi_w < 0$. The maximum beam loading efficiency is obtained when $\varphi_w = \pi$, in which case the external wave and the bunch wake are exactly out of phase and cancel out.

To illustrate the principles of beam loading, we can plot in Figure 2.7 the efficiency according to equation (44) when the external wake is of the form (40) with amplitude E_0 and transverse dependence $R_0(r)$ corresponding to a transversely Gaussian bunch with spot size σ_0. The witness bunch is placed at the accelerating phase, $\varphi_w = \pi$. The efficiency is plotted versus the wakefield amplitude ratio, E_w / E_0, where E_w is the amplitude of the sinusoidal wake that the witness bunch alone leaves behind it (proportional to the number of particles in the witness bunch). We also vary in the same plot the transverse Gaussian spot size of the witness bunch, σ_w, by plotting curves for different σ_w / σ_0, for three different values of $k_p\sigma_0$. Note that the $\sigma_w / \sigma_0 = 1$ curves are the same as the $\varphi_w = \pi$ curve in Figure 2.5.

We observe that when the drive and witness bunches have the same transverse width ($\sigma_w / \sigma_0 = 1$) then the beam loading is 100% when $E_w = E_0$. This of course happens with 100% energy spread since the two waves overlap out of phase everywhere in space. For narrower witness bunches, $\sigma_w / \sigma_0 < 1$, the efficiency is reduced and denser bunches (higher E_w) need to

be utilized to compensate for the narrower witness wakes. After the efficiency peaks for each case it eventually becomes negative since the wake energy left behind is mostly that of the witness bunch. Note that simply by changing σ_w will also alter the witness wake E_w by $1/\sigma_w^2$ - see equation (35). For example, for the case of $k_p\sigma_0 = 2.4$ (top panel), if initially $\sigma_w/\sigma_0 = 1$ and $E_w/E_0 = 0.1$ (20% beam loading) then by making the spot size 10 times smaller ($\sigma_w/\sigma_0 = 0.1$) will also cause $E_w/E_0 = 10$, yielding an efficiency of ≈28%.

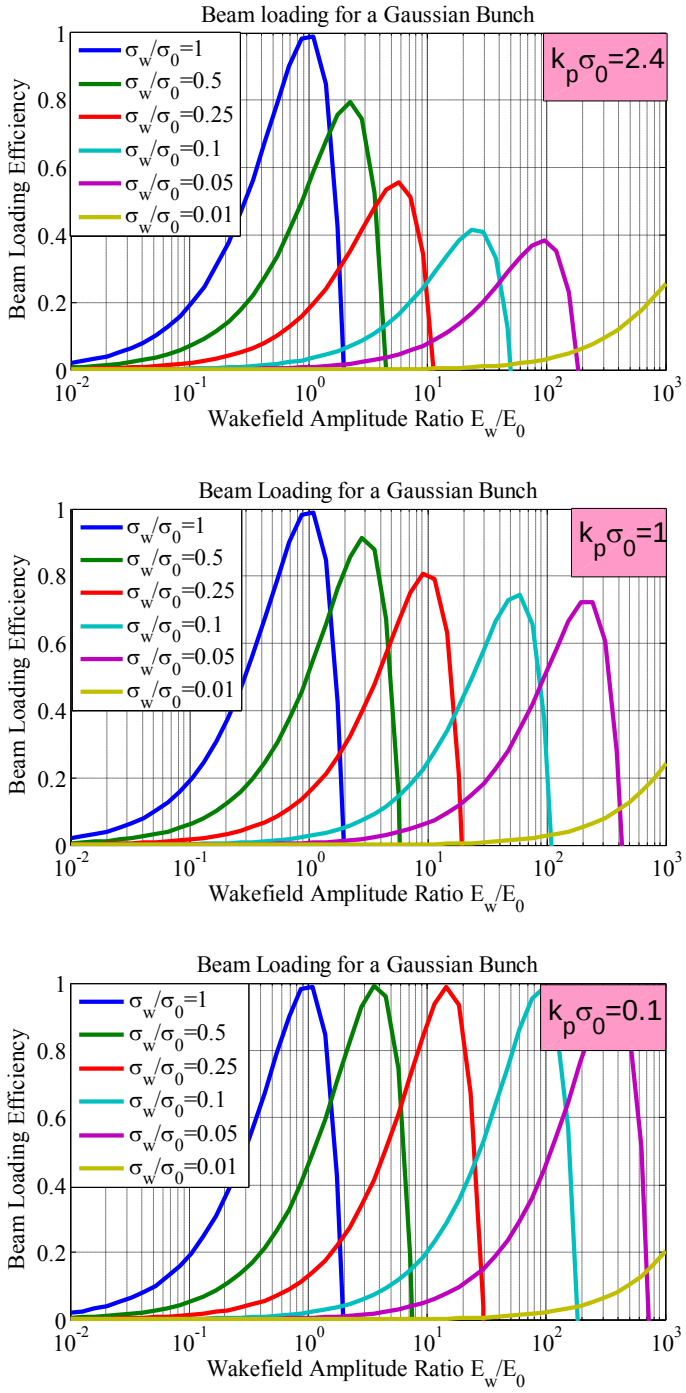

Figure 2.7: Beam loading for a transversely Gaussian witness bunch of spot size σ_w in the presence of an external wave of amplitude E_0 created by transversely Gaussian bunches of spot size σ_0. The wake amplitude left behind by the witness bunch alone is E_w. The different colored curves correspond to narrower witness bunches. The curves for 3 different values of $k_p\sigma_0$ are plotted in this figure.

It is advantageous to use narrower drive bunches (bottom panels) since the wake energy is more efficiently absorbed. The reason for this is that when driving with a narrow bunch then the beam loading is insensitive to the width of the witness bunch since the wake always extends out to a plasma skin depth. Furthermore, narrow drive bunches increase the driving energy transfer efficiency (see Figure 2.3). The drawback is that the absolute number of particles N that can be used in the drive bunch has to reduce as σ_0 decreases, since the drive beam density $n_{b0} \propto N / \sigma_0^2$ cannot be raised arbitrarily without going into the nonlinear regime where these derivations break down (for a fixed plasma density). The plasma density could be decreased to allow for more particles, but only at the expense of the wakefield amplitude which scales as $E \propto \sqrt{n_0}$ for fixed n_{b0} / n_0 (see for example equation (27) for the scaling).

2.5.4 Transverse Energy Spread

As with the longitudinal beam loading, there is always a tradeoff between the transverse beam loading and transverse energy spread. This energy spread is in addition to whatever energy spread may be imparted on the bunch by the longitudinal effects and field variation along the bunch. The transverse energy spread is caused by the off-axis field variation along the radial profile of the bunch. Unlike the transverse beam loading efficiency, it is not independent from the longitudinal profile of the bunch. Therefore, we shall examine the transverse energy spread on a longitudinally square and transversely Gaussian bunch of the form specified in equation (35), which is loaded onto an external wakefield of the form $E_{ext}\left(\xi, r\right) = E_0 \cos\left(k_p \xi\right) R_0\left(r\right)$. Since the wake left behind by the witness bunch alone is equal to $E_w\left(\xi, r\right) = E_w \cos\left(k_p \xi + \varphi_w\right) R_w\left(r\right)$, the total wakefield *inside* the witness bunch is a

superposition of $E_{ext}(\xi,r)$ and the wakefield found by substituting the bunch profile into equation (8), and can be written as

$$\begin{aligned} E_{inside}(\xi,r) &= E_0 R_0(r)\sqrt{1+p'^2+2p'\sin\left(\frac{k_p w}{2}+\varphi_w\right)}\sin\left(k_p\xi+\varphi_{inside}\right) \\ p'(r) &\equiv \frac{1}{2\sin\left(\frac{k_p w}{2}\right)}\frac{E_w R_w(r)}{E_0 R_0(r)} \end{aligned} \tag{46}$$

The fractional transverse energy spread (defined at the radial tail $r=3\sigma_w$ of the bunch[1]) is found

$$f_{w\perp} = 1-\frac{E_{inside}(\xi,r=3\sigma_w)}{E_{inside}(\xi,r=0)} \tag{47}$$

The above energy spread is plotted in Figure 2.8 as a function of the various parameters of the system for $\varphi_w=\pi$.

Two regions are clearly distinguishable in these graphs. For light beam loading (left side), the energy spread is determined by the external wakefield and $E_{inside}\sim R_0(r)$ only. For heavy beam loading (right side), the energy spread is determined by the transverse variation of the bunch wakefield along the bunch, i.e. $E_{inside}\sim R_w(r)$. For transversely similar bunches, $\sigma_w=\sigma_0$, the energy spread is independent of the witness bunch charge since the fields overlap everywhere in space. We observe that in order to retain a small energy spread while loading a significant amount of charge, a witness bunch narrower than the drive wave must be used.

[1] As with the transformer ratio, the energy spread for non-finite bunches strictly is always 100%. The emmitance (area of the beam particles in phase space) is a much better definition of beam quality, although it complicates the issue by including spatial particle information as well.

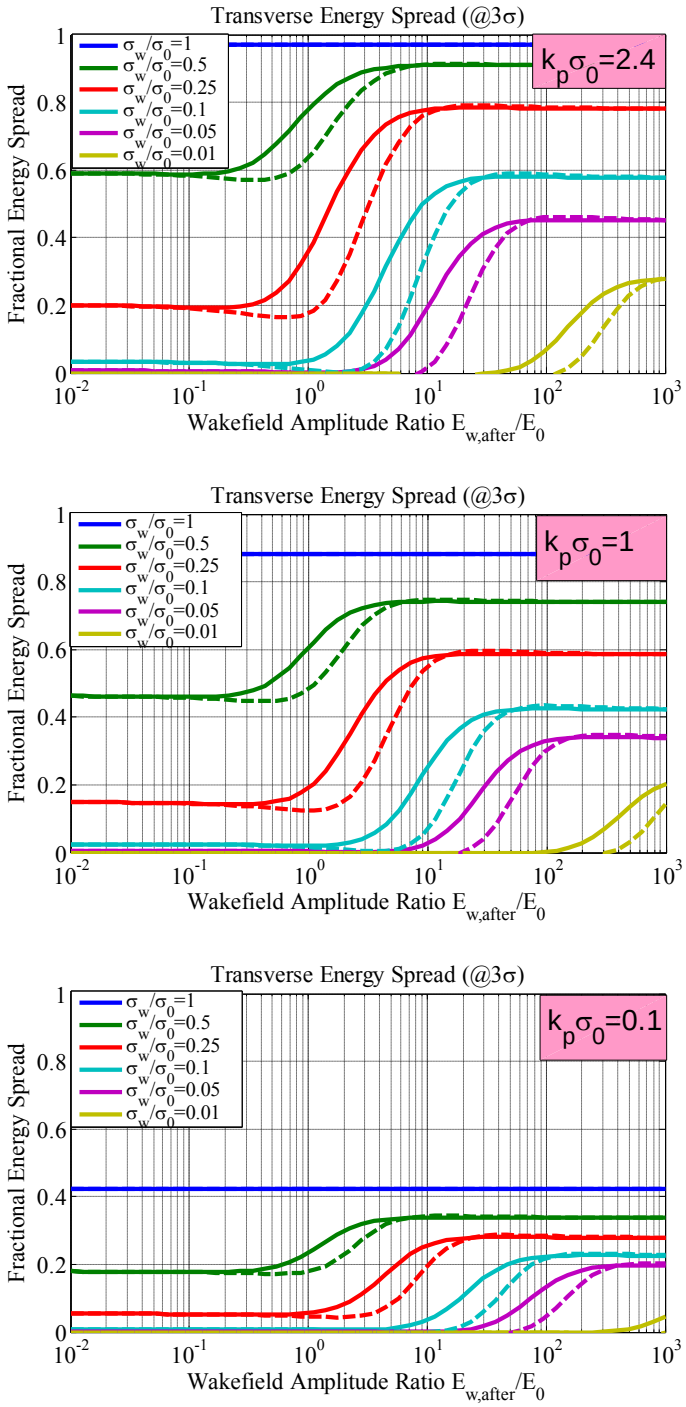

Figure 2.8: Fractional transverse energy spread for a longitudinally square (of width $k_p w$) and transversely Gaussian witness bunch (of spot size σ_w) in the presence of an external wave of amplitude E_0 created by transversely Gaussian bunches of spot size σ_0. The wake amplitude left behind by the witness bunch alone is $E_{w,after} = E_w$. The differently colored curves correspond to narrower witness bunches. The dashed curves correspond to bunch width $k_p w = \pi/4$, while the solid curves correspond to $k_p w = \pi/8$.

2.6 Chapter Conclusions

The following items are concluded from this chapter:

- The transformer ratio can be greater than 2 in the linear regime if either non-symmetric or multiple bunches are used.

- The electron bunches suffer from nonlinear focusing forces in the linear regime, which can be approximately tuned out by adjusting the emmitance of the individual bunches.

- The beam to plasma longitudinal energy transfer efficiency is maximized (for single bunches) when all particles lose energy at the same rate, i.e. the field is constant under the beam. The transverse efficiency is maximized for narrow beams. Regularly shaped single bunches have maximum efficiencies around 60 – 70%.

- Efficiency and transformer ratio are maximized almost simultaneously, however high efficiency schemes transfer more energy to the plasma over shorter distances even if the transformer ratio is smaller.

- There are certain tradeoffs between efficiency, energy spread and accelerating gradient when the wake is loaded with a trailing beam. The resulting energy spread can be reduced either at the expense of the accelerated charge (unless the beam is specially shaped), or at the expense of the gradient (by placing the beam earlier than the peak accelerating wakefield).

Science is facts; just as houses are made of stones, so is science made of facts; but a pile of stones are not a house and a collection of facts is not necessarily science.

- Henri Poincare

Chapter 3

Plasma Sources

3.1 Overview

In order for the plasma accelerators to operate optimally, reliable plasma sources are required. These sources must be able to produce high density (10^{16} - 10^{19} cm^{-3}), low temperature (< 10 eV[1]) and longitudinally uniform plasmas over relatively long distances (> 1 cm) in a controllable, repeatable and consistent manner.

3.1.1 Gas Jets and Metal Vapors

In some occasions the driver (either laser or electron beam) is intense enough to ionize a neutral gas and create the plasma, inside which the wakefields are excited [45]. Such was the case in the recent LWFA experiments by Malka et al., Faure et al., Geddes et al., and Mangles et al. [58, 59, 63, 90, 119], where they managed to systematically produce relatively monoenergetically accelerated electron bunches of good quality (low emmitance and energy spread) using gas jets.

[1] What is usually quoted when we refer to a plasma temperature T is, by convention, the corresponding energy $k_B T$.

In these setups there is typically a tank that holds a gas such as helium or hydrogen in very high pressure. This gas is released into vacuum through a valve and a small nozzle. The front of the focused laser pulse ionizes the gas, while the rest of the pulse expels the electrons and initiates the plasma oscillations. For instance, Faure et al. used a helium gas jet that had a nozzle diameter of 2 mm. The 10^{18} W/cm^2 titanium-doped sapphire laser was focused 800 μm away from the nozzle, generating a longitudinally flat plasma density on the order of 10^{18} – 10^{19} cm^{-3} over a 1.5 mm length with 400 μm density ramps on each side. However in those gas jet systems the acceleration length is limited by the length of the longitudinal plasma density plateau which in turn is limited either by the small nozzle sizes, by the length that can be ionized by the laser or by the dephasing length, thus it cannot be straightforwardly extended to multi-cm-scale lengths.

In a similar fashion, a lithium vapor inside a heat-pipe oven [171] was used as a plasma source in the SLAC energy doubling PWFA experiment [20]. The SLAC 42 GeV electron bunch is 50 fs long, carries 1.8x10^{10} electrons and can be focused down to a 10 μm spot size, thus being intense enough (electric field > 5 GV/m) to ionize the lithium gas[1]. The meter-long plasma density (on the order of 10^{17} cm^{-3}) was adjusted with better than 10% accuracy by tuning the neutral gas pressure and assuming 100% ionization [131].

3.1.2 Capillary Discharge Plasmas

The plasma sources that are the focus in this dissertation are capillary discharges. As opposed to gas jets and metal vapors, capillary discharges do not require an external strong driver to ionize a neutral gas. Rather, the plasma is produced by applying a high voltage (typically in the several kV range) along a capillary tube, which typically have lengths anywhere from a few mm to

[1] Lithium has very low first ionization energy for a metal, equal to 5.4 eV.

several cm and transverse lengths up to couple of mm. The plasma electrons originate either from the ionization of a gas that has pre-filled the capillary tube (gas-filled capillaries [65, 95, 159]) or from the evaporation of the capillary wall material (ablative capillaries [143, 158, 164, 180]). Currents in the kA range may be required to break down the materials, so capillary discharges need to be supported by high voltage circuits that deposit enough energy to the capillary.

Capillary discharges have many favorable characteristics for plasma wakefield acceleration. They can be used to extend the acceleration lengths, especially in LWFA experiments because the typically cylindrical symmetry can create a near-parabolic in the radial dimension profile, which favors laser channeling [52, 65, 84, 107, 159]. Capillaries are also great plasma sources for weak driving electron beams or lasers that are not intense enough to ionize the gas. In addition, the extra parameters introduced, such as the diameter or the initial gas pressure, allow for better control of the selected plasma density. Since the discharges may last for several μs before they die out and the relativistic beams travel close to the speed of light, a beam will transverse the capillary length in a matter of *ps*. The proper timing between a beam and the discharge also allows for a choice in the plasma density. Typically densities on the order of $10^{14} – 10^{19}$ cm^{-3} can be obtained.

On the other hand, the density produced at a capillary may be sensitive to parameters that are not easy to reproduce widely, such as the exact material composition, the shape of the discharging electrodes and the internal impedance of the power supply along with the current pulse it can produce. Since each experiment usually builds its own capillary and power supply, there are difficulties in the reproducibility of the results among the researchers and there seems to be a lack of common knowledge in the literature. In addition, due to the complexity and the

violent nature of the discharges there exists no solid theory that predicts the produced plasma densities with accuracy and only recently a few simulation codes have been published [21, 24, 25, 109, 181] in an attempt to validate experimental results.

The goal of this chapter is to present experimental data for capillaries that were taken at the Pulsed Power Lab at the University of Southern California and at the Accelerator Test Facility at the Brookhaven National Lab. We examine how the various parameters of the capillary geometry (size, length and diameter) and discharge characteristics (charging voltage, gas pressure and electrode shape) affect the generated plasma density. In addition, the evolution of the plasma density with time, which is critical for the experiments described later in this dissertation, is also analyzed.

3.2 Spectral Diagnostics

Plasmas emit light; the light emitted at different wavelengths is a signature of the plasma and carries information about the processes that occur inside it. By collecting that light one can work backwards and estimate the plasma parameters such as the density and the temperature. There are a number of spectroscopic techniques available for analyzing plasmas, and we will review both standard used methods [76] as well as methods used specifically in the experiments described later in the dissertation.

3.2.1 Typical Spectroscopic Methods

A popular method for diagnosing both the plasma density and temperature is Thompson Scattering, which is based on the interaction between an electromagnetic wave and charged particles [156]. The diagnostic setup requires an external laser source that is focused into the plasma. The electromagnetic field of the laser will cause the plasma electrons to start oscillating,

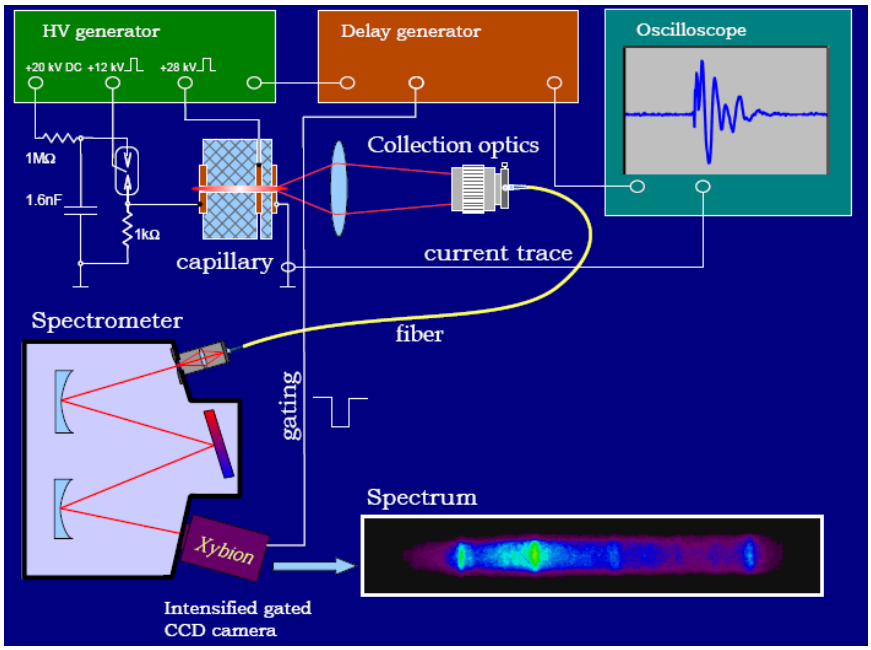

Figure 3.1: Experimental setup layout for the collection of the plasma light for the ablative discharges. Source: Daniil Stolyarov, BNL.

and as the electrons quiver they emit radiation which is strong around the wavelength of the incident field (scattered wave). Since the interaction cross section is on the order of 10^{-13}, this radiation is much weaker than the incident radiation. As a result a powerful laser needs to be used (such as the Ruby at $\lambda = 0.694\ \mu m$) and the scattered radiation needs to be collected and imaged carefully.

More relevant to capillary discharges, a widely implemented method for diagnosing the plasma density is laser interferometry [150, 158, 159]. In these setups typically a Mach – Zender interferometer is built with one of its arms passing through the plasma. The plasma's index of refraction will depend on its density and will cause a phase shift in the incoming laser pulse. This method has the advantage that it provides full time-dependent evolution of the density during the plasma discharge; its main drawback is that the laser light may be deflected or absorbed by the plasma and pollute the interference signal, thus the density has to be extracted from the

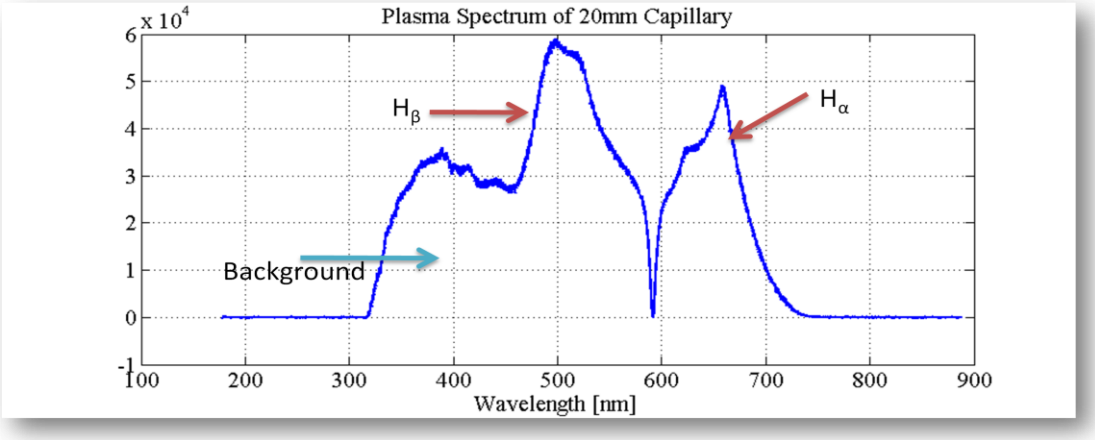

Figure 3.2: High-density time-integrated hydrogen plasma discharge spectrum. The absorption line around 590 nm is attributed to the molybdenum ends of the electrodes.

number of fringe shifts with extra care. For example, using a He-Ne laser over 3 mm of plasma a full phase shift of 360^0 will occur for every $1.2\text{x}10^{18}$ cm^{-3} change in the plasma density[1]. Another advantage of this method is that when a 2D spatial detector is used to record the interferometer signal, then information about the transverse profile of the plasma can be also gained [47, 65].

3.2.2 Stark Broadening of Hydrogen Lines

The principle diagnostic utilized in this work is Stark Broadening on hydrogen plasmas [6, 22, 26, 53, 54, 61, 62, 64, 172, 173], which emit light largely in the optical wavelengths. The main physical principle is that transitions of electrons between atomic levels that would normally produce a spectral line almost at a single wavelength, now occur between perturbed levels and as a result the spectral line broadens [2]. The widening of the lines is caused by the electric fields[2] generated by the free plasma electrons, therefore in general a larger plasma density will

[1] The phase shift over a plasma length L with index of refraction η_p is roughly $\Delta\phi \simeq k_{laser} \cdot L \cdot \eta_p$, and the corresponding plasma density $n_e \simeq \left(4\pi\varepsilon_0 m\Delta\phi\right) / \left(e^2 \lambda_{laser} \cdot L\right)$, assuming that $\eta_p = \sqrt{1-n_e/n_c} \simeq 1-n_e/2n_c$.

[2] The Stark Effect is the electric field analog of the Zeeman Effect, where a magnetic field is applied to perturb the energy levels.

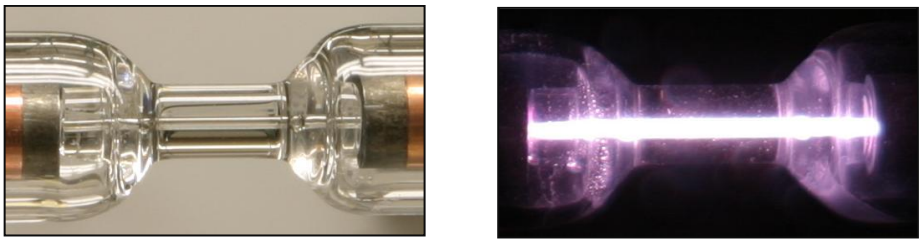

Figure 3.3: Photograph of the hydrogen capillary discharge at USC. Source: Jessica Hao Chen.

cause a larger widening and a bigger Stark broadening [140, 141]. A sample spectrum is shown in Figure 3.2, and a typical hydrogen plasma discharge in Figure 3.3.

Three different spectral techniques were used. First, the Stark broadening of the Balmer H_α (656.3 nm) and H_β (486.1 nm) lines: The width of the lines yields information on the density and the temperature of the plasma[1]. Second, the line intensity ratio between those two lines can provide information on the temperature. Finally, the temperature can be estimated from the background light that is emitted from hydrogen[2] [80].

A typical experimental setup is shown in Figure 3.1 [29, 164]. The plasma light was collected from the side of the capillary through a series of lenses, it was fed into an optical spectrometer with a resolution of approximately 1 nm, and the resulting spectrum was imaged onto a CCD camera. In other setups one or more optical fibers were inserted transversely directly into the center of the capillary body to capture the plasma light at the center of the capillary.

The plasma spectrum is post-processed and the FWHM linewidths $\Delta\lambda_{1/2}$ of the Balmer lines are measured by fitting the theoretically-predicted Lorentzian shapes under the lines (most often H_α). The plasma electron temperature T is measured either from the ratio of the Balmer

[1] The Balmer α (red) and β (blue-green) lines originate from electron transitions from the third (n=3) and fourth (n=4) atomic shells, respectively, to the second (n=2) shell. The α line gives to the famous Orion Nebula its reddish color.

[2] This light originates mostly from bremsstrahlung radiation.

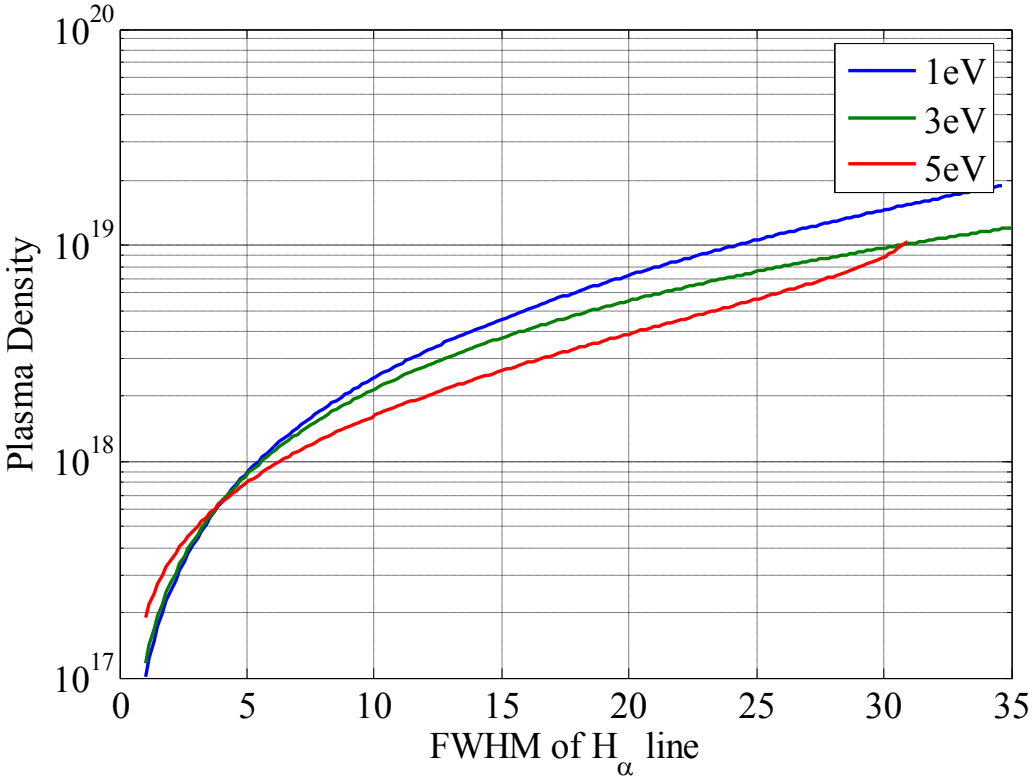

Figure 3.4: The plasma density as a function of the linewidth of the H_α line for different temperatures. The plasma density is in units of cm^{-3} and the linewidth in units of nm.

line intensities [16] or from the line to background ratio under one line [66]. Then, using the theory developed by Griem [66, 67, 68, 69, 70, 94, 160], the plasma density is estimated with a 30% accuracy [16] using the nonlinear equation [7, 67]

$$n[cm^{-3}] = 8.02 \times 10^{12} \left(\frac{\Delta\lambda_{1/2}[\text{Å}]}{\alpha_{1/2}(n,T)} \right)^{3/2} \tag{48}$$

Here $\alpha_{1/2}$ is a parameter that depends on the plasma density, the temperature and the spectral line observed. The above formula is based on a number of assumptions on the state and behavior of the plasma, such as local thermal equilibrium (LTE) for the plasma and validity of the quasistatic approximation, which assumes that the spectral broadening is dominated by the effect of the electrons and that the ions remain static during that time. The theory seems to be

reliable for plasma densities up to 10^{19} cm^{-3} and temperatures up to 5 eV. In Figure 3.4 the dependence of the plasma density on the measured linewidth for different temperatures is plotted for the case of the H_α line.

3.3 Dependence of the Plasma Density on the Capillary Parameters

The goal of this section is to investigate the dependence of the plasma density and temperature on the various parameters controlling a capillary discharge. These data are important because they allow design flexibility when a certain plasma source is to be designed for a plasma wakefield experiment. Most of the work described in this section was performed at the Pulsed Power Lab of the University of Southern California using transparent glass capillaries filled with Hydrogen gas. Unless otherwise noted, the charging voltage was set at 60 kV. The plasma light was collected by imaging the light onto a lens-to-fiber coupler, which was then fed through an optical fiber to an optical spectrometer with resolution of 1 nm. Every possible measure was taken so that only one parameter was varied at any given time, everything else remaining constant[1].

3.3.1 The Effect of Neutral Gas Pressure

In this section we present a comparison of the spectra recorded for different neutral hydrogen pressures, up to 2 atm. The data are presented in Figure 3.5, where the spectra are normalized to the peak of the Balmer H_α line.

[1] Unfortunately the energy transferred from the power supply to the plasma cannot be independently controlled externally since it depends on the impedance of the plasma, which in turn depends on the discharge conditions.

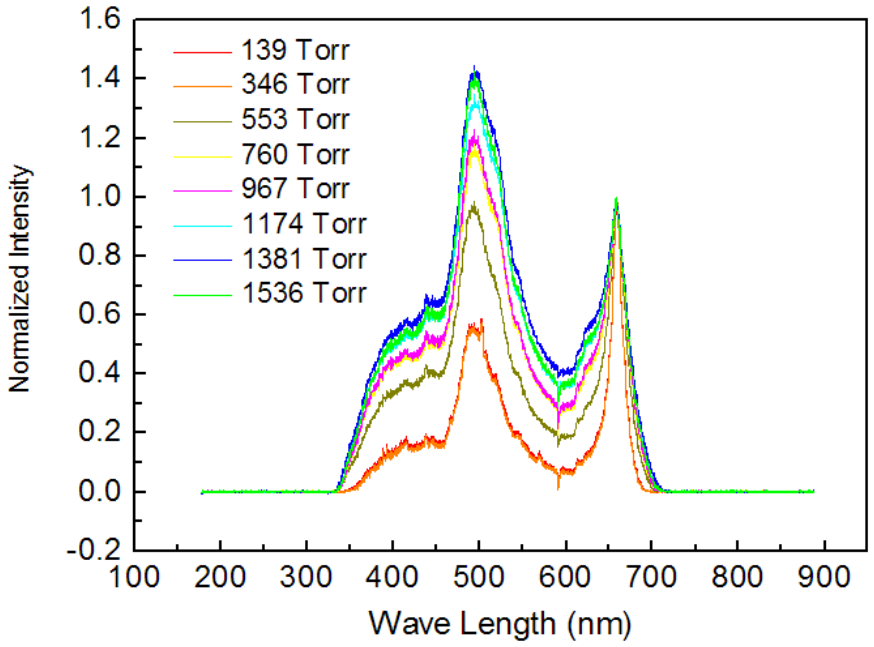

Figure 3.5: Normalized spectra recorded for increasing neutral hydrogen pressures. The right peak is the H_α line and the left peak is the H_β line.

It is evident from this figure that higher plasma densities (wider linewidths) and stronger light emission can be obtained for higher pressures. The linewidths of both lines increase, suggesting an increase in density. This is also accompanied by a change in the ratio of the two line intensities since we observe that the H_β/H_α ratio increases with pressure, suggesting an increase in the plasma temperature with pressure, according to the line-ratio technique that was mentioned previously. Quantitative measurements of the density and temperature are presented in the following sections.

For low pressures and densities the line shape of the H_α line remains mostly Lorentzian, which strengthens the validity of the density calculations. For larger pressures the shape is not purely Lorentzian; however the right side of the H_α line is still Lorentzian enough and in those cases the twice of the right-side half width at half maximum was used to estimate the density.

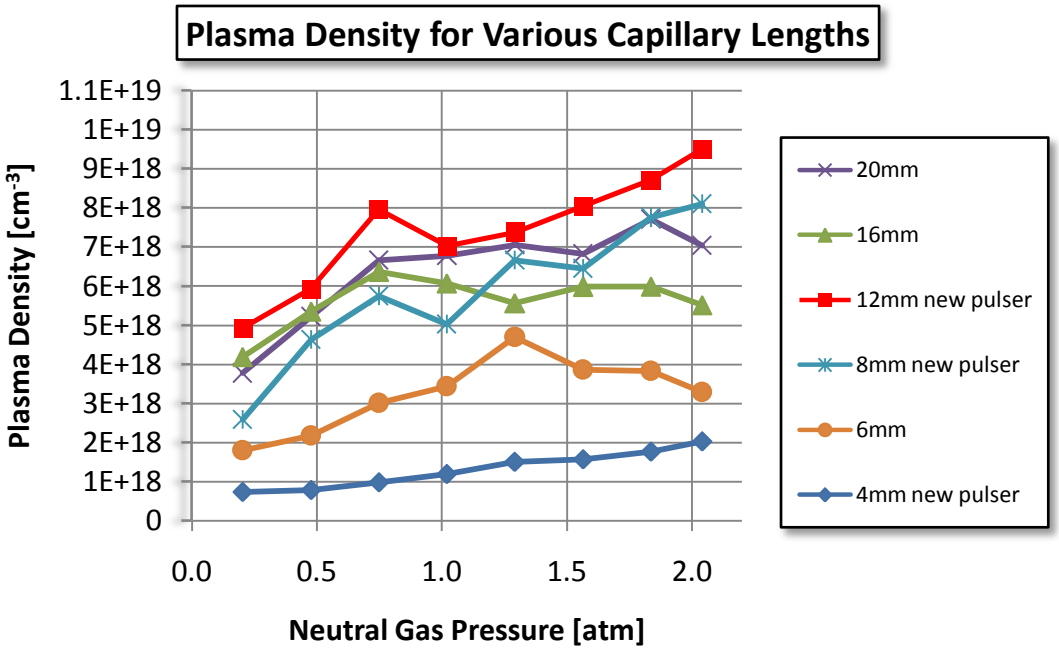

Figure 3.6: The plasma density for different capillary lengths as a function of pressure. "New pulser" refers to shots made after some slight modifications to the power supply unit. The charging voltage was 60 kV and the capillary diameter 0.6 mm.

3.3.2 The Effect of the Capillary Length

Figure 3.6 presents a set of data that depicts the plasma density dependence for different capillary lengths. Each data point is an average of 3 – 5 consecutive discharge shots with the error bar (min – max) being on the order of 10% (not shown). The inaccuracy due to the density extraction from linewidth and temperature uncertainty is higher than this shot to shot variation.

It was observed that in general the density increases with pressure and initially increases with the capillary length, with a maximum density of 9.5×10^{18} cm^{-3} at a length of 12 mm and pressure of 2 atm. For larger lengths (> 12 mm), the density drops and capillaries that had more than 30 mm of length did not always breakdown for fixed voltage settings due to the Paschen curve limitations.

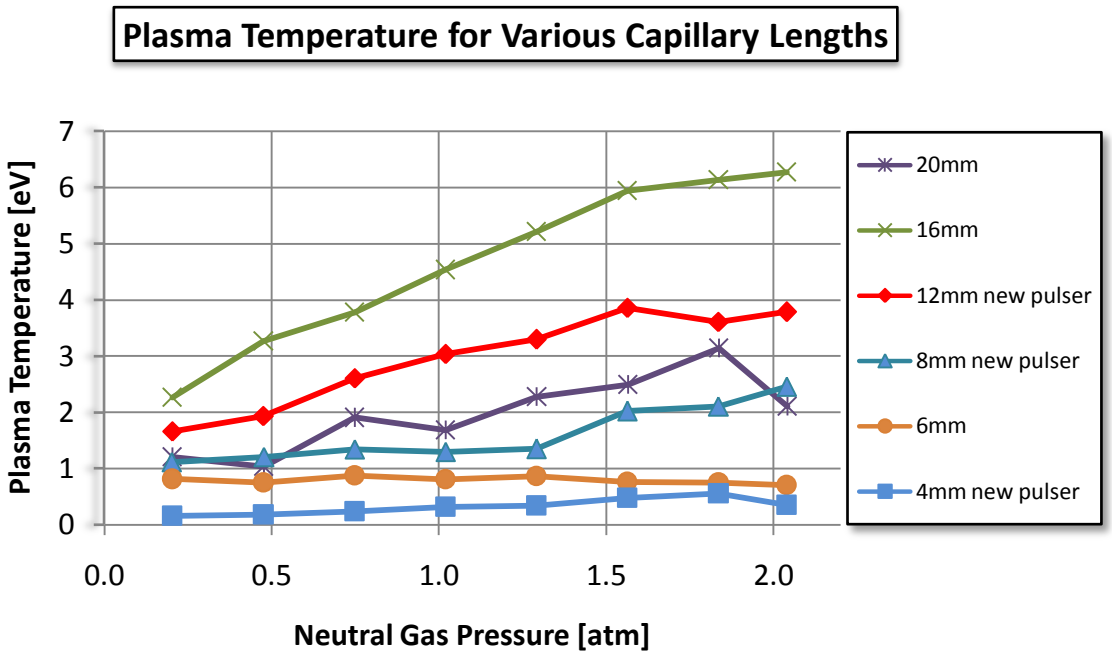

Figure 3.7: The plasma temperature for various capillary lengths. "New pulser" refers to shots made after some slight modifications to the power supply unit. The charging voltage was 60 kV and the capillary diameter 0.6 mm.

A possible explanation for the observed increase in density vs. increasing length could be the following. Since the discharge is based on an avalanche effect, where each electron suffers a number of collisions along its path from one electrode to the other, a lengthier capillary would imply that each individual electron is involved in more collisions. In a short capillary the electrons diffuse out quickly before colliding with enough other particles to increase the plasma density. Then, after some optimal length is crossed, it is tougher to ionize the same number of particles *per unit volume* because the acceleration and speed of the electrons die out before they reach from one electrode to the other.

Figure 3.7 shows the temperature dependence for the same capillary lengths as the previous graph. The temperature was extracted from line to background intensity ratio of the H_α line. It is interesting to observe that the temperature also increases with length, and the

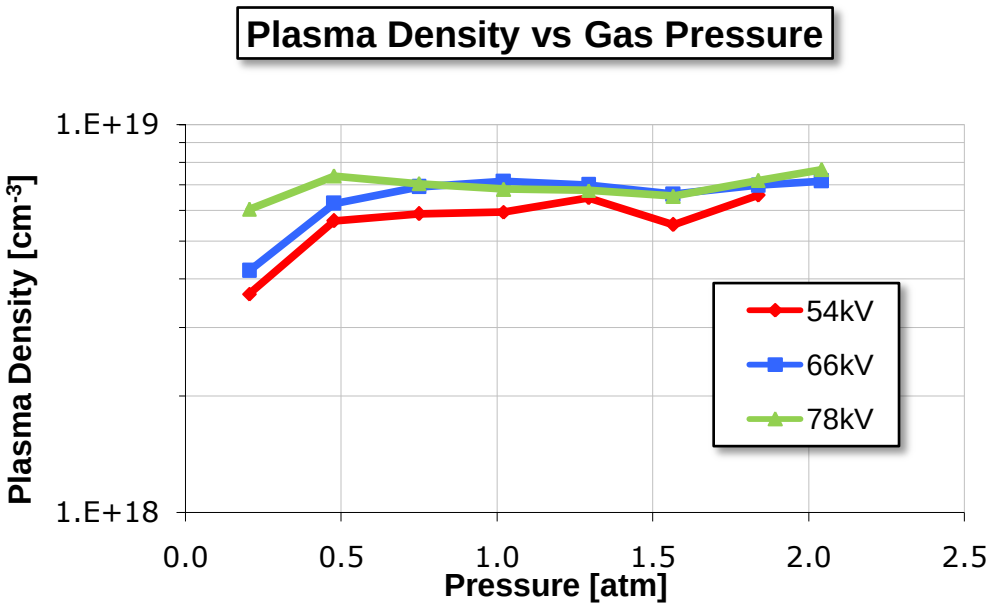

Figure 3.8: The plasma density as a function of the neutral gas pressure for three different charging voltages. The capillary length is 20 mm and the diameter 0.6 mm.

maximum temperature is reached at 16 mm, while the maximum density was reached at 12 mm. In fact, the absolute linewidth was larger for the 16 mm capillary, but according to these results the large linewidth was related to a large temperature increase as opposed to a plasma density increase. Since these plasma densities are close to 10^{19} cm^{-3}, the temperature affects the linewidth more strongly as compared to low densities where the temperature effect is not as important.

3.3.3 The Effect of the Charging Voltage

Figure 3.8 shows plasma density vs. pressure for different charging voltages, 54 kV, 66 kV and 78 kV, for a 20 mm long capillary with 0.6 mm diameter.

The plasma density for a given pressure is slightly higher when the charging voltage is increased from 54 kV to 66 kV, but there is no significant increase when the voltage is further increased to 78 kV (except at low pressures). The extra energy that is deposited into the plasma

in the latter case is most likely distributed into the kinetic energy of the plasma electrons. This conclusion is drawn because the plasma temperature was measured to increase from an average of 2 eV to an average of 4 eV as the voltage was increased from 66 kV to 78 kV (not shown here). Thus further increasing the charging voltage in this case is not expected to yield analogous increased plasma density.

It should be noted here that the energy that is deposited to the plasma during a discharge is not controlled solely from the external power supply. The plasma has its own impedance which is variable depending on the initial pressure, the plasma density and the plasma temperature. The energy transfer would be maximized if the internal impedance of the power supply was adjusted to match the resulting plasma impedance. A mismatched circuit is identified by the large number of oscillations in the current that flows in the system as a function of time.

3.3.4 The Effect of the Capillary Tube Diameter

Figure 3.9 shows plasma density vs. pressure for 3 different capillary diameters (0.6 mm, 1.2 mm and 3 mm). The capillaries were 20 mm long and the charging voltage was set to 60 kV.

The data shows that narrower capillaries greatly enhance the plasma density. When the diameter decreases 2.5 times from 3 mm down to 1.2 mm the density increases 3.25 times, from 0.8×10^{18} cm^{-3} to 2.6×10^{18} cm^{-3}. Then, when the diameter is decreased further by a factor of 2, the density jumps to 7×10^{18} cm^{-3} which is an increase by 2.7 times. This is probably due to the enhanced current density. Assuming that the current supplied is approximately same over those discharges, ideally the current density should be inversely proportional to the square of the diameter of the capillary. The enhancement observed in density is not linear to the current

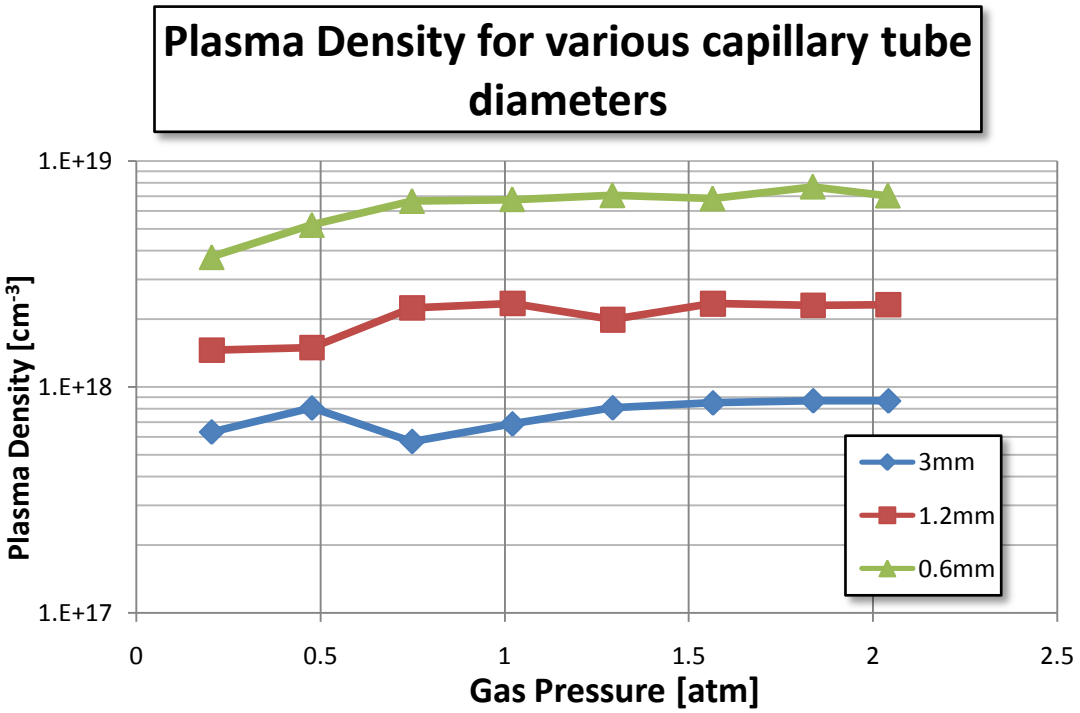

Figure 3.9: The dependence of the plasma density as a function of pressure for 3 different capillary tube diameters. The capillary lengths are 20 mm and the charging voltage 60 kV.

density but it is still very strong, suggesting that in order to achieve high one must minimize the capillary diameter (while preserving the breakdown).

Additionally, when a 0.3 mm diameter capillary of the same length was tested, it was found that the spectrum was radically different with a very large spectral background and no clear H_α line visible. This was attributed to the very high temperature of the plasma caused by the mismatch in the impedances between the high-voltage pulser and the plasma. Only when a 50 Ω load was added in series to the capillary did the temperature drop and the H_α line reappeared (see also the data in the next section).

3.3.5 The Effect of the Hollow Electrode Inner Diameter

In this setup we tested two pairs of electrodes, one pair with 0.6 mm hole diameter (equal to the diameter of the capillary in most cases) and one pair with no holes at all (flat). The purpose

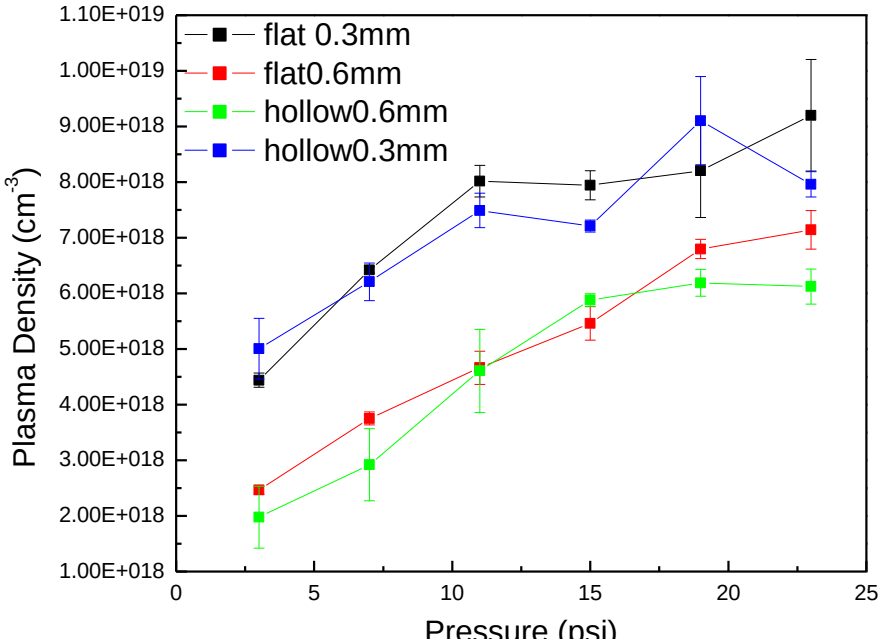

Figure 3.10: Plasma density in a 16 mm capillary as a function of pressure for two different capillary diameters. Two different types of electrodes (flat and hollow) were also tested. 15 psi≈1 atm.

of this experiment was to test for any hollow cathode effects that may enhance the plasma density in the capillary. The capillary that was tested was 16 mm long. We observed that the plasma density is relatively insensitive to the electrode shape, as the differences never exceeded the shot-to-shot statistical variation. Temperature measurements similarly showed that the plasma temperature is also not affected significantly by the choice of the electrode.

3.4 Variation of the Plasma Density along the Length of the Capillary

For the resonant experiments described later in this dissertation, a major requirement for the plasma source is that the plasma remains uniform at a constant density over the length of the capillary. The tolerance in the uniformity of the plasma is determined by the number of bunches

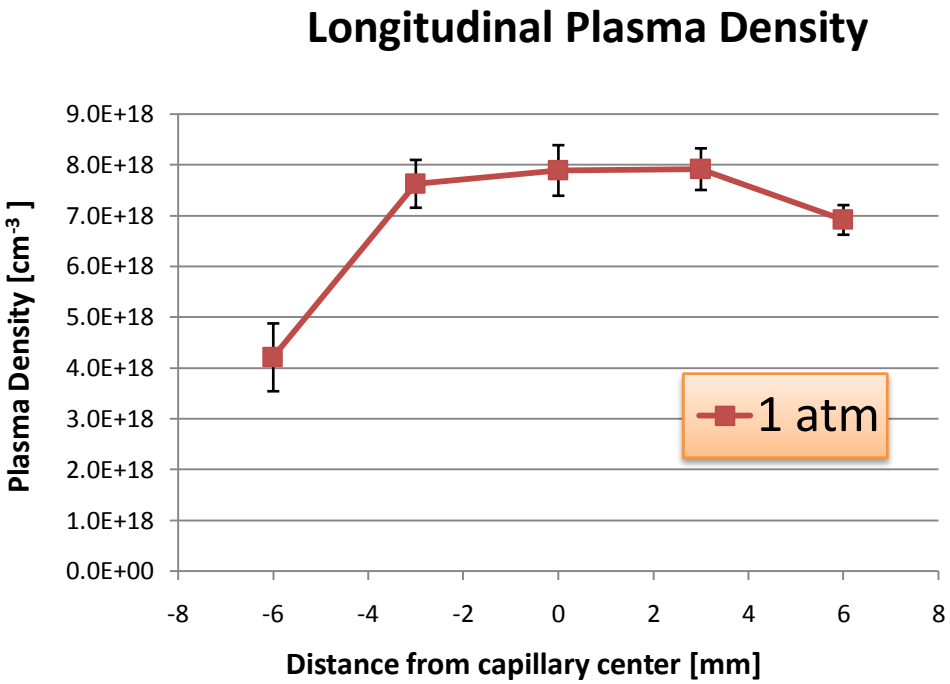

Figure 3.11: Plasma density along the capillary axis for a 60 kV discharge in a 17 mm long capillary at 1 atm of pressure. The error bars indicate 1-σ variations over 10 discharges.

N that drive the wakefields, and scales roughly as $1/N$. For example, for $N=5-10$ drive bunches (typical for the experiments under consideration) the plasma density needs to be constant within 10 – 20%, otherwise the excited wakefields from each bunch will be out of phase and cancel each other before the bunches leave the plasma. Therefore, it was important to establish whether the capillary discharges can produce longitudinally uniform plasmas.

In order to measure the longitudinal dependence of the plasma density an optical fiber was mounted in a 2 dimensional translation stage and it was placed directly against the outer side of the glass capillary walls. The time-averaged plasma light was collected in successive discharges by tuning the position of the fiber along the length of the capillary.

It was measured that for the given 17 mm capillary shown in Figure 3.11, the plasma density over a length of 8 mm near the center of the capillary did not vary more than 10% from

the average value. However near the cathode side the density differs by a factor of two compared to the center of the capillary. This suggests that the resonant interaction length is shorter than the quoted length for the capillary. The plasma temperature behaves similarly along the capillary, having a flat region near the center and dropping fast near the electrodes. Similar results that show reduction in the plasma density and temperature near the electrodes were reported by Levin et al. in [108].

3.5 Variation of the Plasma Density with Time

The time-integrated measurements presented in the previous two sections highlight the effects of the various capillary and discharge parameters, yet they are expected to yield smaller plasma densities than the actual ones because they are not sensitive to high densities that occur for only a short period of time – those peaks are averaged out. Therefore, since in many cases the exact plasma density is selected by tuning the arrival of the electron beam with respect to the discharge, it is important to resolve the plasma density in time.

The time-dependence of the plasma density was investigated in the course of the multibunch experiments at ATF. We tested a 10 mm long hydrogen-filled capillary with 1 mm inner diameter using the following technique. The light during the discharge was collected by an optical fiber inserted directly into the capillary center, which was then fed into an optical spectrometer equipped with a 1,200 gr/mm grating. The entrance and exit slits were adjusted such that a 0.5 – 1 nm spectral window could be imaged onto a Photo Multiplier Tube and yield the signal recorded at that wavelength range as a function of time. By varying the central wavelength of that window, the profile of the H_α line versus time could be reconstructed after successive shots. By fitting a Lorentzian distribution to each set of wavelengths for every point in time the plasma density could then be extracted.

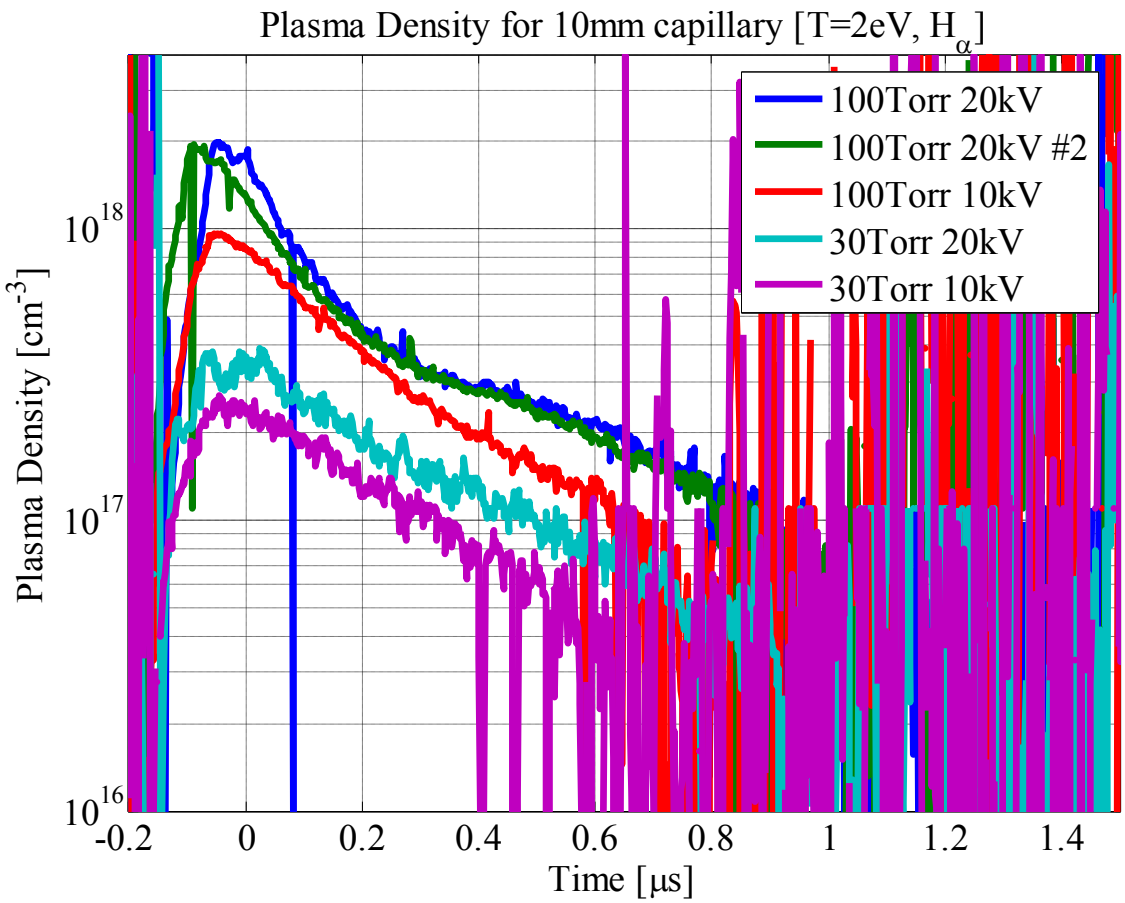

Figure 3.12: Plasma density as a function of time for different discharge parameters. The plasma temperature is assumed fixed at 2 eV for this density range. Two different data sets where collected for 100 Torr pressure and 20 kV charging voltage, separated by one day in time. The measurements become noisy at later times where the light emitted from the plasma is weak.

The success of this method relies on the reproducibility of the discharge among the shots (which needs to be monitored by collecting the light emitted in all wavelengths), and it is limited by the resolution of the spectrometer and the Signal-to-Noise ratio which decreases with narrower spectral windows. Figure 3.12 shows typical results for the evolution of the plasma density for different discharge parameters. The maximum density was obtained for 100 Torr of neutral gas pressure and 20 kV of charging voltage (two successive sets of measurements are

shown here). The peak density dropped by a factor of 2 when the charging voltage was reduced to half its initial value, 10 kV.

For 30 Torr of gas pressure, the peak voltage is even lower, near the 10^{17} cm^{-3} range. Several hundred nanoseconds after the peak, the density is seen to drop linearly which indicates exponential diffusion. The plasma current typically peaks 50 – 100 ns before the density and vanishes 200 – 400 ns after that peak.

In those sets of data the spectral window was 1 nm in the 100 Torr cases and 0.5 nm in the 30 Torr cases. This change allows smaller densities to be measured (narrower linewidths), yet the method becomes unreliable earlier in time due to the decrease in the light recorded. It can be improved though if a higher-resolution spectrometer is utilized while the optical sensitivity is preserved. For the spectra shown in this graph, the maximum single-to-noise ratio was 10, which implies that the density is known with 20% accuracy or better[1] at densities down to 10^{17} cm^{-3}.

3.6 Chapter Conclusions

The following items are concluded from this chapter:

- Capillary discharges are a favorable option for PWFA experiments that require pre-ionized plasmas. The density can be tuned through the initial neutral gas pressure, the capillary geometry or by tuning the arrival of the beam with respect to the discharge.

- The Stark Broadening of the Hydrogen line H_α is a good diagnostic for plasma densities in the range 10^{17} cm^{-3} – 10^{19} cm^{-3}. The plasma temperature also needs to be known at the high densities by measuring the line-to-continuum spectral ratio.

[1] Higher densities than 10^{17} cm^{-3} are known more accurately and lower densities are known less accurately, since higher densities produce more light.

- The density increases with increasing gas pressure, albeit less than linearly proportional. It becomes harder to ionize the plasma unless more energy is deposited.

- The maximum plasma density initially increases with the capillary length up to an optimal of 12 mm length and a density of 9.5×10^{18} cm^{-3} for 2 atm of pressure. The density decreases for longer capillaries and eventually it becomes hard to even break down.

- Increased charging voltage increases the amount of light emitted but this is attributed to temperature increase and not due to density increase.

- The density increases between linearly and quadratically with decreased capillary tube diameter due to higher current density.

- The hollow cathode effect is insignificant at the pressure range measured here (> 100 Torr).

- The plasma density varies less than 10% longitudinally near the center of the capillary (for about half the total length), but it decreases by as much as a factor of 2 near the electrodes.

- As a function of time the density has a peak shortly after the discharge current peak and then eventually starts dropping exponentially, probably due to diffusion as the plasma recombines at the capillary walls.

The things we know best are the things we haven't been taught.

- Marquis de Vauvenargues

Chapter 4

High-gradient Acceleration of a Trailing Electron Bunch

Plasma waves can sustain extremely large electric fields that are orders-of-magnitude larger than those in conventional radio-frequency accelerators, which are limited by vacuum breakdown to accelerating gradients of up to 150 MV/m [23]. Such large amplitude electron density waves, or wakes, can be excited in plasmas by a laser pulse (laser wakefield acceleration – LWFA), or a relativistic particle beam (plasma wakefield acceleration – PWFA). Recent LWFA experiments demonstrated quasi-monoenergetic acceleration of self-trapped plasma electrons [58, 63, 106, 120]. Further scaling of LWFA to higher energies, by using higher laser power but larger spot sizes and lower density plasmas, will probably require injecting relativistic electron bunches into a plasma wave rather than starting with plasma electrons at zero energy (in order to maintain small emmitances). So far, this approach to potentially monoenergetic particle acceleration using plasmas has not been explored.

Experiments using PWFA methods similarly face the challenge of producing low-energy-spread acceleration of an injected relativistic particle bunch. In previous PWFA experiments (see for example Refs. [12, 20, 179]) a single relativistic electron-bunch both drove the wake and provided the electrons to be accelerated. Using this scheme at SLAC, a record-high energy gain of 42 GeV over 85 cm of plasma was demonstrated [20], albeit with an undesirable ≈100% spread of the electron energy spectrum. To realize a future collider, such as one incorporating the PWFA afterburner concept [105], a well-defined bunch is required that is suitably phased on the plasma wake of a preceding drive bunch thereby to achieve high efficiency and a small energy spread (≈0.1% which is typical for conventional accelerators). In the following sections a double-bunch PWFA experiment is detailed which demonstrates controllable high-gradient acceleration of a witness relativistic electron bunch injected into a plasma wave.

4.1 Previous Work

Earlier double-bunch PWFA experiments [14, 100, 128, 134, 148] utilized relatively long, picosecond electron bunches in low-density (10^{13} cm^{-3}) plasmas; wakefields of only up to ≈4 MV/m were inferred. This experiment differed substantially from these studies. First, the driver and witness bunches had subpicosecond lengths ($\sigma_z \sim 100\ fs$), and both were shorter than the plasma wavelength. Consequently, the energy shift of both bunches could be directly observed rather than mathematically extracted[1], as was required in earlier works. Second, the shorter bunch lengths and the higher plasma densities employed (up to 10^{17} cm^{-3}) resulted in generated wakefield amplitudes that were two orders-of-magnitude larger compared to those studies.

[1] The wakefield in some of these works was extracted by evaluating the shifts of the bunch centroid after background signal subtraction.

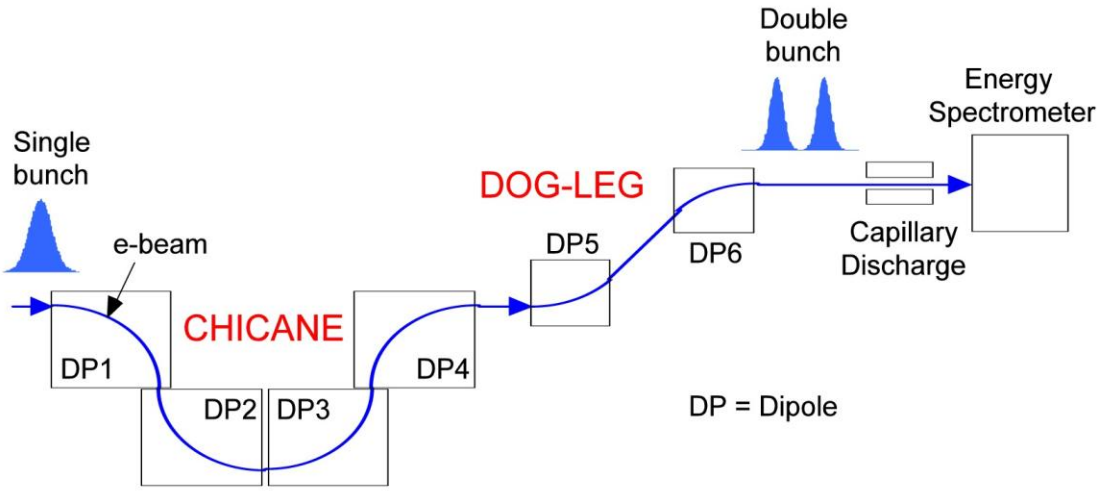

Figure 4.1: Layout of the double-bunch PWFA experimental setup. Figure by W. Kimura.

In this experiment, the plasma density could be chosen such that energy lost by the drive electron bunch was transferred through the plasma wave to the second bunch, which, in turn, gained energy with minimum energy spread. The drive bunch lost about 1.0 MeV over 6 mm propagation in a plasma of 10^{16} cm^{-3} density, and the witness bunch, delayed by 500 fs, gained ≈0.9 MeV corresponding to an average loaded accelerating gradient of ≈150 MV/m, while the beam loading efficiency was estimated to be approximately 77%. The measured energy gain and loss agree well with 2D linear theory calculations. This experiment was the first to generate and directly probe large plasma accelerating gradients (> 100 MV/m) utilizing a trailing electron bunch [85].

4.2 Experimental Setup and Diagnostics

The experiment was performed at Brookhaven National Laboratory's (BNL's) Accelerator Test Facility (ATF). A photocathode rf gun followed by a conventional 2.856 GHz (S-band) accelerator produced a 1.5 ps-long (rms), 500 pC, 60 MeV single electron bunch [28] that was compressed and split into two distinct (in time and energy) subpicosecond bunches after traveling through a

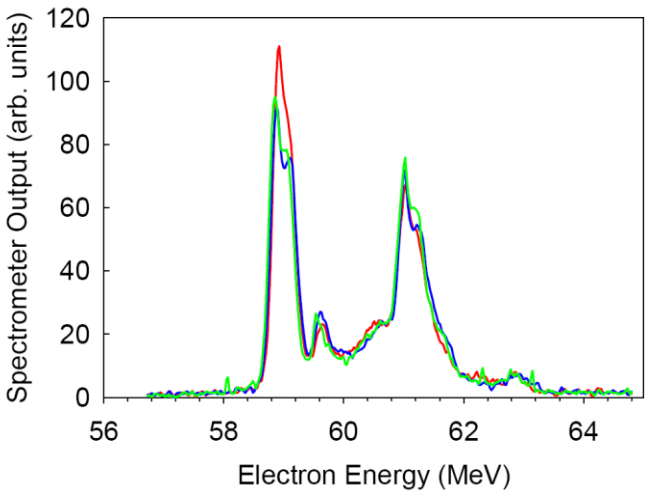

Figure 4.2: Example of three different double bunch energy spectra taken many minutes apart, indicating the stability of the beam break-up.

chicane compressor and "dog-leg" dipoles downstream from the linac (see Figure 4.1). These two bunches were focused transversely to $\sigma_r \simeq 100\,\mu m$ at the entrance of a 10^{14} – 10^{17} cm^{-3} density plasma produced by an ablative capillary discharge [83]. A magnetic spectrometer at the end of the beamline recorded the energy change imparted to the bunches by the plasma.

4.2.1 Coherent Transition Radiation Diagnostics

Production of subpicosecond driver-witness electron bunch pairs separated by a distance appropriate for PWFA experiments in high-density plasmas (10^{16} – 10^{17} cm^{-3}) is challenging [155]. The breakup of the electron beam into two distinct bunches at ATF was attributed to the combination of a nonlinear energy chirp introduced by the linac, over-compression of the bunch in the chicane, and coherent synchrotron radiation effects in the chicane and the dog-leg dipole magnets.

Therefore, although the breakup of the bunch is repeatable and consistent [98, 165], control of its characteristics is limited. The two bunches were separated by approximately 1.8 MeV in energy and had a typical full-width-at-half-maximum (FWHM) of 0.4 MeV, thus allowing

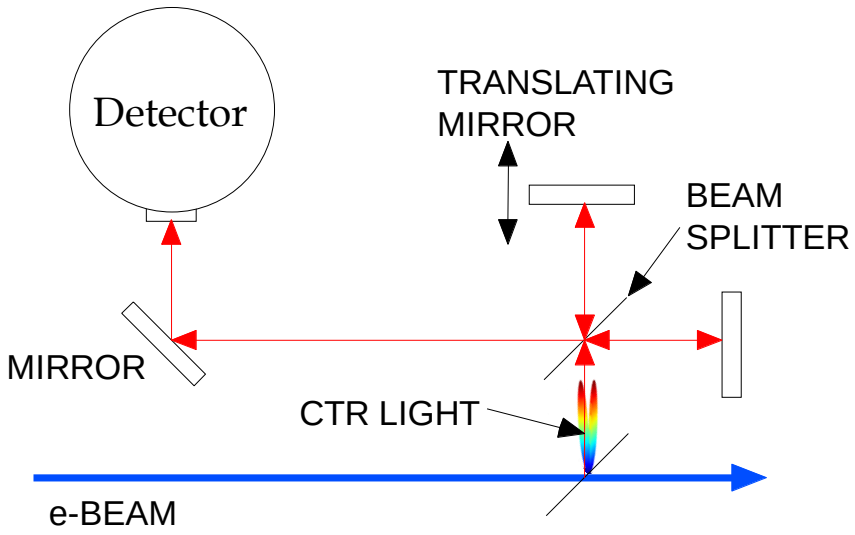

Figure 4.3: Experimental setup of the CTR interferometry diagnostic for the double-bunch experiment. Figure by W. Kimura.

direct observation of their energy shifts caused by their interaction with the plasma. Figure 4.2 shows three double-bunch energy spectra recorded many minutes apart, demonstrating the stability of the break up.

In addition, coherent transition radiation (CTR) interferometry [125, 157] was used to diagnose the two bunches in time (see details in Appendix C.4). The experimental setup for this diagnostic is shown in Figure 4.3. Figure 4.4 shows the CTR signal recorded as the position of the mirror in one of the interferometer arms was varied, for the cases of a single bunch and both bunches. The dips observed in the signal are attributed to the frequency limitations of the systems which act as a high-pass filter and neglect frequencies below a certain threshold[1]. Assuming that each bunch has a Gaussian shape, by fitting the observed signal traces to the model it was found that the high-energy and the low-energy bunches, respectively, were roughly 45 μm (150 fs) and 27 μm (90 fs) long (rms), and were separated by $\Delta z = 150\,\mu m$ (500 fs). Beam-position monitors and a Faraday cup also indicated that the total charge was

[1] This frequency cutoff was included in the CTR model.

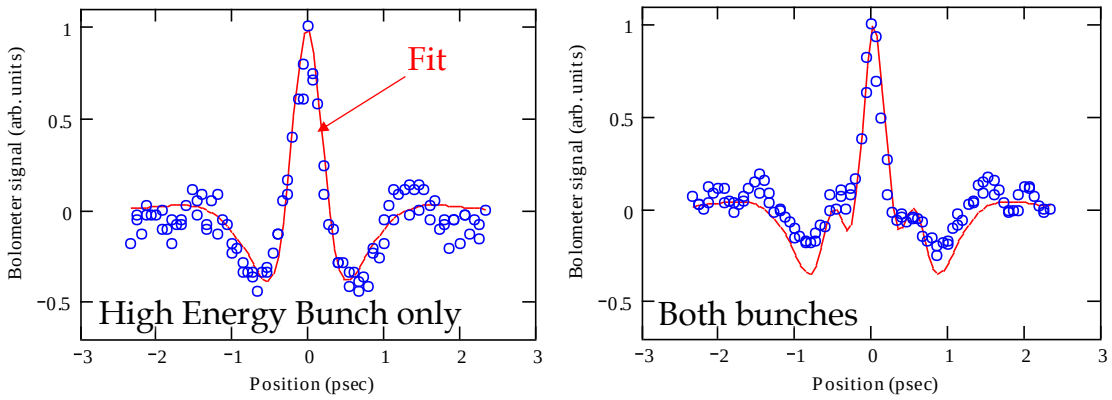

Figure 4.4: CTR interferometry diagnostic for the single bunch (left) and for both bunches (right). The blue circles indicate experimental data, while the solid red line indicates the model fit. Figure by W. Kimura.

preserved during the break up, with the low-energy bunch having about 60% (180 pC) of the charge of the high-energy bunch (300 pC). Finally, observations of the interaction between the bunches and the plasma showed that the high-energy bunch lost energy in the plasma independently of the presence of the low-energy bunch, thus implying that the former preceded the latter, which acted as the witness bunch.

4.2.2 Plasma Density Diagnostics

The plasma source was a 16.5 kV pulsed electrical discharge through a readily available 6 mm long polypropylene capillary with a 1 mm inner diameter. It should be noted that there is no fundamental limitation in using a longer, centimeter-scale, capillary to reach a larger energy gain. The breakdown in the vacuum ablates the capillary walls creating a carbon-hydrogen plasma. The discharge light was collected and guided by an optical fiber into a spectrometer that measured the hydrogen Balmer H_α linewidth, and the plasma density was derived from the well-tabulated Stark broadening [7] (see section 3.2). An intensified time-gated camera collected spectral measurements with a resolution of 300 ns.

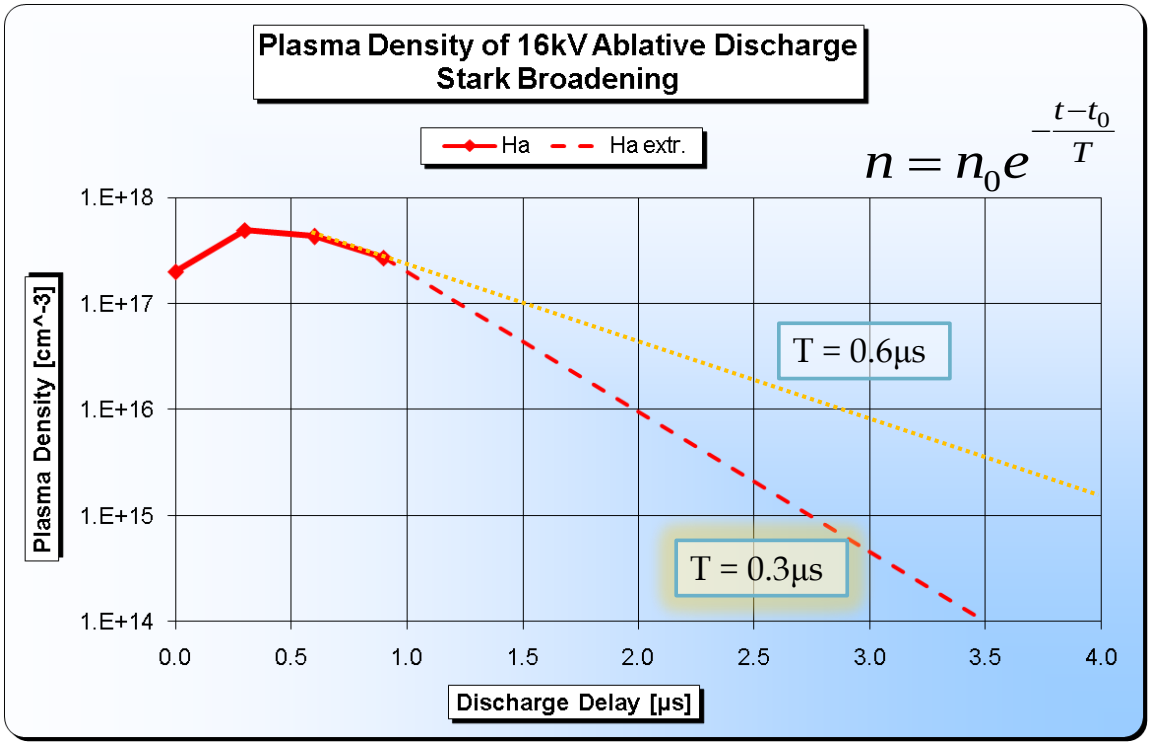

Figure 4.5: Plasma density diagnostic for the double-bunch experiment. The Stark broadening of the H_α line was used to identify the density in the first μs (solid line), after which the density was extrapolated assuming exponential diffusion. The two dashed lines indicate the density dependence for two different time constants.

Those measurements are plotted in Figure 4.5 for the first μs, after which the density was extrapolated due to insufficient plasma light reaching the camera. The data show that the plasma reaches a maximum density of approximately 5×10^{17} cm^{-3}, after which it is assumed to exponentially decay due to diffusion through the capillary openings [21, 179], according to the formula $n(t) = n_0 e^{-\frac{t-t_0}{T}}$. The diffusion constant chosen was estimated to be equal to $T = 0.3\mu s$ for the data sets in this experiment, which corresponds to a nominal diffusion rate of one order-of-magnitude per 1.5 μs. Therefore, the required plasma density, n_p, could be selected by tuning the time-delay of the *e*-beam after the discharge started. The peak electric field of the discharge was about 3 MV/m (16.5 kV over 6 mm), which was much smaller than the typical

plasma wakefields in this experiment (> 80MV/m), and did not affect the energy spectra of the electron bunches significantly.

4.3 Plasma Interaction Results

4.3.1 Double Bunch Interaction

The peak beam density, n_b, of the two compressed bunches was approximately 10^{14} cm^{-3}, so placing the physics of the beam-plasma interaction mostly in the linear overdense regime ($n_b < n_p$) for the range of plasma densities used in these experiments [116]. In this regime, each bunch independently creates a wakefield with a spatial period equal to the plasma wavelength. While the drive bunch only loses energy due to its own wakefield, the witness bunch samples the superposition of the two fields, and loses or gains energy depending on its relative phase in the wakefield driven by the first bunch. This phase was controlled by tuning the plasma density (and hence, the plasma wavelength). Specifically, energy gain was expected at plasma densities such that the witness bunch samples the second half-period of the plasma wave driven by the first bunch, i.e., when approximately $\frac{\lambda_p}{2} < \Delta z < \lambda_p$; here, $\lambda_p = \frac{2\pi c}{\omega_p}$ with $\omega_p = \sqrt{\frac{n_p e^2}{\varepsilon_0 m}}$.

In order to model the behavior of the witness bunch, a 2D numerical program was developed to calculate the linear wakefields driven by two Gaussian-shaped bunches [86] with the aforementioned experimental parameters (see Appendix D on ThemOsiris code). The validity of the modeling was verified by comparing the findings with the fully-explicit 2D particle-in-cell code OSIRIS [71]. The amplitudes of the wakefields simulated by both methods agreed within 10%, thus justifying the use of the thousand-times-faster numerical calculation.

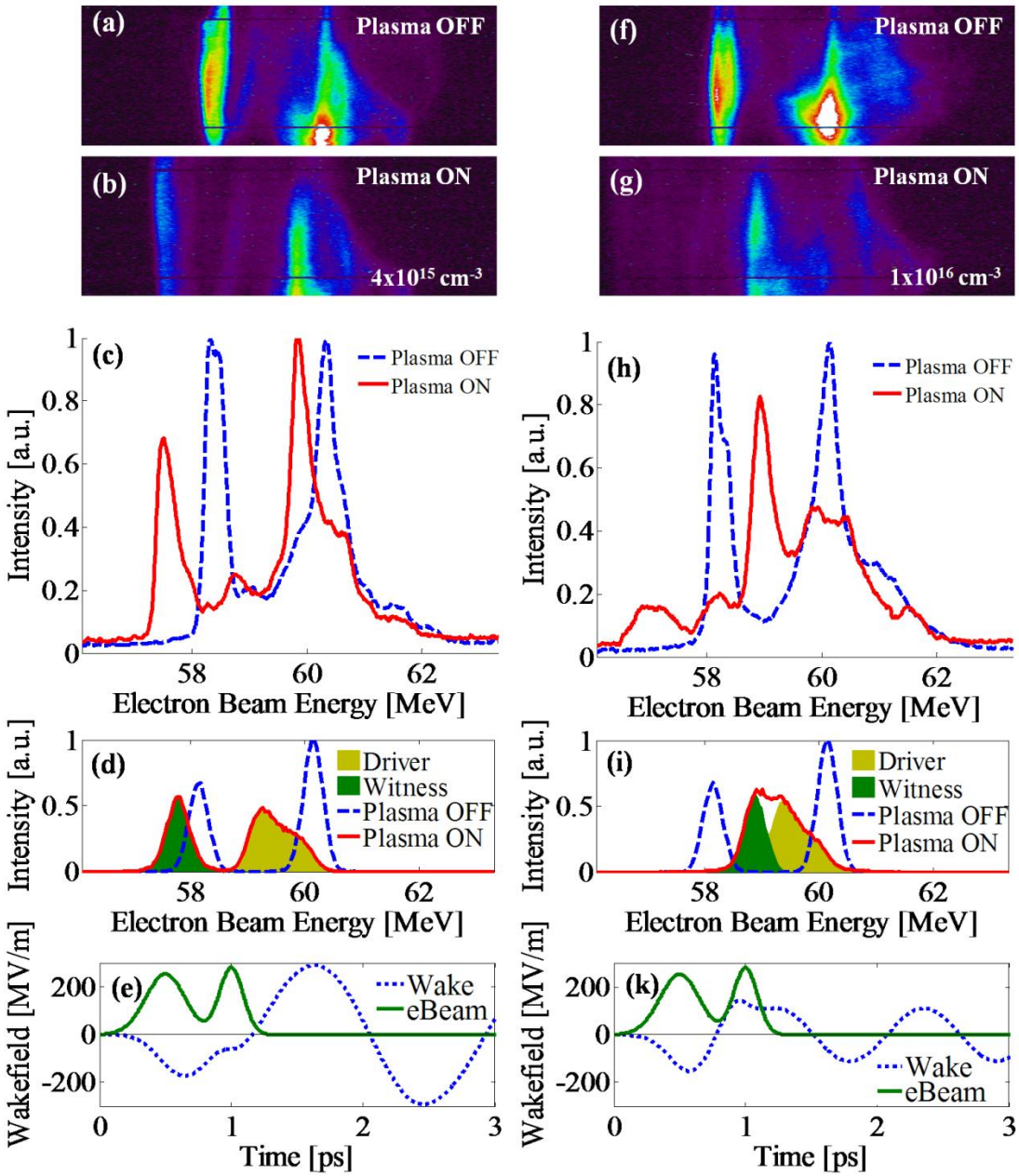

Figure 4.6: Experimental and simulated energy spectra of the double-bunch beam after the 6 mm-long capillary discharge at 4×10^{15} cm^{-3} plasma density (left column), and at 1×10^{16} cm^{-3} density (right column): a,f) raw energy spectrum without plasma; b,g) raw energy spectrum with plasma on; c,h) experimental energy profiles; d,i) simulated energy profiles; e,k) simulated plasma wakefield and position of the bunches inside the wake.

Comparison of the double-bunch interaction at two different densities is shown in Figure 4.6. The left-hand side column presents experimental energy spectra of the *e*-beam with the plasma discharge turned off [Figure 4.6(a)] and as measured after the 4×10^{15} cm^{-3} density plasma [Figure 4.6(b)], together with plots of the area-normalized line profiles integrated vertically (across the beam's profile) in Figure 4.6(c). At this plasma density, both bunches clearly lost energy, since the plasma wavelength is longer than the separation between the bunches ($\lambda_p = 529\mu m > 2\Delta z \simeq 300\mu m$). The drive bunch lost ≈0.5 MeV, and the witness bunch lost ≈0.8 MeV, corresponding to average wakefield amplitudes (over the 6 mm capillary length) of 83 MV/m, and 133 MV/m. Figure 4.6(d) plots the simulations of the predicted energy spectra before and after the plasma interaction; they confirm that both bunches should lose energy. Figure 4.6(e) shows simulated combined plasma wakefield and longitudinal phasing of the two bunches in this field.

The right-hand side column in Figure 4.6 shows the experimental energy spectra recorded when the plasma density was increased to 1×10^{16} cm^{-3}, therefore reducing the plasma wavelength to $\lambda_p = 334\mu m \simeq 2\Delta z$. The witness bunch in this case mainly gained ≈0.9 MeV in energy [Figure 4.6(g-h)]. The simulation illustrates that the observed peak in the energy spectrum around 59 MeV resulted from the superposition of both accelerated electrons from the witness bunch and decelerated electrons from the drive bunch (which only lost energy) [Figure 4.6(i-k)]. Some residual charge of the drive bunch was recorded around 60.5 MeV, probably reflecting the non-Gaussian initial energy distribution in the experiment.

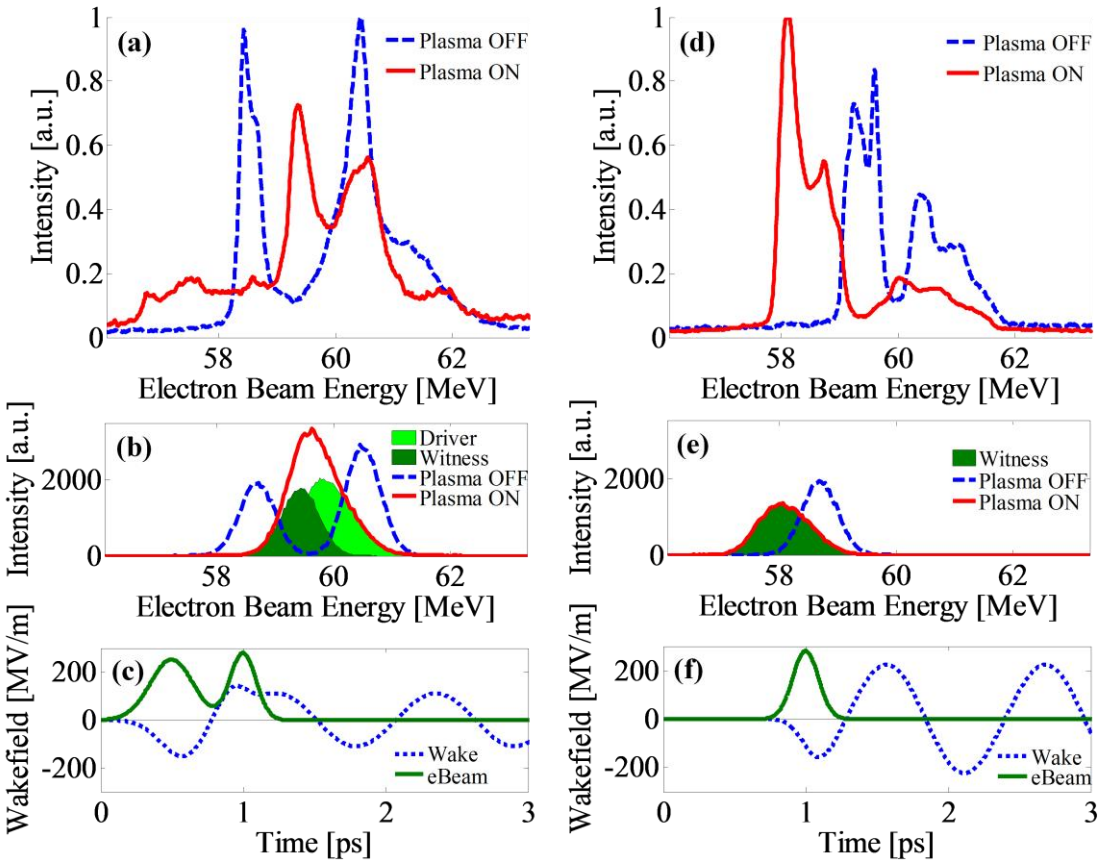

Figure 4.7: Experimental and simulated energy spectra after the 6 mm-long capillary discharge at 1×10^{16} cm^{-3} plasma density for the double-bunch beam (left column), and for the witness bunch only (right column): a,d) experimental energy profiles; b,e) simulated energy profiles; c,f) simulated plasma wakefield and position of the bunches inside the wake.

4.3.2 Single Bunch Interaction

In order to confirm that the witness bunch was indeed affected by the drive bunch, the higher-energy bunch was partially blocked by closing a slit located at the dispersion plane inside the dog-leg. Side-by-side comparison of the double-bunch and single-bunch interaction is shown in Figure 4.7. When the plasma density remained at 1×10^{16} cm^{-3}, the witness bunch had an average energy loss of ≈1 MeV [Figure 4.7(d)]. Since the witness bunch lost 1 MeV due to its own wake and gained 0.9 MeV in the presence of the drive bunch, we conclude that the net energy shift due to the drive bunch was 1.9 MeV, corresponding to a ≈315 MV/m unloaded accelerating

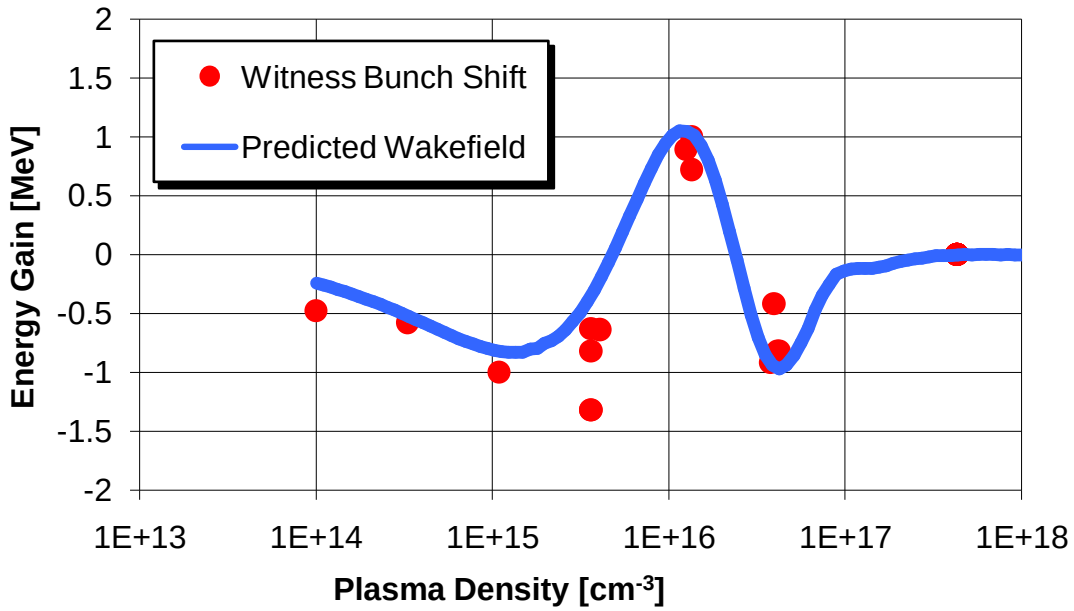

Figure 4.8: Experimental data points for the energy shift of the witness electron-bunch centroid for a range of plasma densities. The solid curve represents 2D numerical calculations for the centroid energy shift.

wakefield amplitude driven by the first bunch. This value agrees with the numerical calculation and therefore the beam-loading efficiency is estimated approximately $\eta_b \simeq 1-\frac{150^2}{315^2} \simeq 77\%$ for this interaction[1].

4.3.3 Plasma Density Scan

Figure 4.8 depicts the measured energy shift of the witness-bunch centroid as the plasma density was scanned from 1×10^{14} cm^{-3} up to 4×10^{17} cm^{-3}. Comparison of the recorded shifts with the 2D numerical calculation of the corresponding predicted energy shifts demonstrates good agreement with the simulation for the chosen plasma density decay profile. The experimental points show that the witness bunch progressively lost more energy as the plasma density was

[1] That would be the fraction of the energy transferred if the bunches were let to propagate over long distance while preserving their wakes. See section 2.5.

increased from its minimum value, provided that the plasma wavelength remained longer than the bunch separation ($\lambda_p > \Delta z$) and both bunches reside at the decelerating phase of the wake [see Figure 4.6(e)]. As the density was increased further near the 10^{16} cm^{-3} range, the plasma wavelength decreased and the witness bunch now sampled the second, accelerating half of the plasma wave period [$\lambda_p \simeq 2\Delta z$; see also Figure 4.7(c)], and therefore it gained energy while simultaneously loading the wake since its charge was comparable to that of the drive bunch. Energy loss was observed again at an even higher plasma density (> 4×10^{16} cm^{-3}) where the witness bunch sampled the decelerating first half of the second period of the excited plasma wake ($\lambda_p < \Delta z$).

On the low plasma density side the wakefield eventually drops when the transverse beam size of the bunches ($\sigma_r \sim 100\mu m$) becomes shorter than a plasma wavelength because the total charge in the bunches is not enough to excite a plasma oscillation with the corresponding large plasma wavelength. On the high plasma density side, the wakefield also drops because the longitudinal size of the bunches ($\sigma_z \sim 30\mu m$) becomes long when compared to the plasma wavelength and thus the wakefields cancel out inside the bunches. For the plasma densities in between these two extreme cases, the wakefield excitation is optimal and its amplitude is determined by the relative phase at which the wakefields excited from each bunch add together.

In summary, it was demonstrated that by adjusting the plasma density tunable energy gain or energy loss of a short ($\sigma_z < \lambda_p$) witness bunch that samples the wakefield generated by a leading subpicosecond drive bunch is possible. The measured energy gain of 0.9 MeV over a 6 mm long, 10^{16} cm^{-3} density plasma corresponds to an unloaded average accelerating gradient

of 315 MV/m. The loaded gradient measured was 150 MV/m and the extrapolated beam loading efficiency of 77%. This work demonstrates that short-pulse accelerated trailing electron beams can be produced with a double-bunch PWFA scheme, and hence, the method constitutes a promising step forward towards producing monoenergetic bunches in next-generation ultra-high gradient plasma accelerators.

4.4 Chapter Conclusions

The following items are concluded from this chapter:

- Two ≈100 fs long 500 pC bunches could be generated at ATF, distinct in both energy and time (as diagnosed through CTR). Both bunches are shorter than half plasma wavelength for densities 10^{16} cm^{-3} and below.

- By tuning the plasma density, the second bunch could be made to sample the accelerating phase of the wakefield driven by the first bunch. Loaded accelerating gradients of 150 MV/m were measured for the first time for a trailing short bunch.

- When the drive bunch was blocked the witness bunch lost 1 MeV energy at the same density it gained 1 MeV before, thus implying a 315 MV/m unloaded accelerating gradient and an estimated 77% beam loading efficiency.

- The energy shift of the witness bunch as a function of the plasma density (selected through the timed arrival of the beam with respect to the plasma discharge) agrees well with a simple 2D linear theory model.

For every complex problem there is an answer that is clear, simple, and wrong.

- Henry Louis Mencken

Chapter 5

Multibunch Schemes and Simulations

In this chapter the theoretical framework of designing a multibunch PWFA accelerator will be analyzed. The difference compared to previous chapters is that now the wakefield is driven by more than one bunches (a witness bunch is still required to sample the generated wakefield). When using multiple bunches, by controlling their position and charge the accelerator can be tuned to either maximize the wakefield, the transformer ratio or the efficiency of the system. Specifically of interest for future PWFA-based colliders are schemes where the energy of the incoming witness beam is multiplied. In section 5.1 the various schemes will be analyzed in the linear regime, and particle-in-cell simulations using OSIRIS will be shown in section 5.2. In section 5.3 we will simulate an example of multiple drive bunches in the nonlinear regime.

5.1 Multibunch Schemes

In this section the basic principles of multibunch PWFA will be analyzed. Specifically, we will explore how, by adjusting the bunch spacing and the charge per bunch, that the plasma

accelerator can be tuned to maximize the wakefield, the transformer ratio or the efficiency. In the models we will utilize transversely Gaussian and longitudinally square bunches of the same width (with the exception of the witness bunch which may be shorter). Although longitudinally Gaussian shapes are more realistic, the square bunches do not have significantly different behavior (see Figure 2.4) yet they are much more tractable analytically and provide quick and easy physics insight in the process.

So let us assume a series of M drive bunches with the same width w. The $m-th$ bunch has N_m particles, is placed at a position ξ_m and has a transverse spot size σ_r. This corresponds to the following beam density profile:

$$n_b(\xi,r)=\sum_{m=1}^{M}\underbrace{\frac{N_m}{2\pi\sigma_r^2 w}}_{n_{bm}}rect\left(\frac{\xi-\xi_m}{w}\right)e^{-\frac{r^2}{2\sigma_r^2}} \tag{49}$$

The function $rect$ has a value of 1 for $|\xi-\xi_w|<w$, ½ for $|\xi-\xi_w|=w$ and 0 otherwise. The total longitudinal electric field is simply the superposition of the fields created by the individual bunches, which was given in equation (27), and is equal to

$$\begin{aligned}E_z(r,\xi)=&+\frac{e}{\varepsilon_0 k_p}\sum_{j=1}^{M}n_{bj}\sin\left[k_p\left(\xi-\xi_j+w/2\right)\right]\cdot rect\left(\frac{\xi-\xi_j}{w}\right)\cdot R(r)+\\&+\frac{e}{\varepsilon_0 k_p}2\sin\left(\frac{k_p w}{2}\right)\sum_{j=1}^{M}n_{bj}\cos\left[k_p\left(\xi-\xi_j\right)\right]\cdot U\left(\xi-\xi_j-w/2\right)\cdot R(r)\end{aligned} \tag{50}$$

The transverse wakefield can be found from equation (10):

$$\begin{aligned}W_\perp(r,\xi)=&-\frac{e}{\varepsilon_0 k_p^2}\sum_{j=1}^{M}n_{bj}\cos\left[k_p\left(\xi-\xi_j+w/2\right)\right]\cdot rect\left(\frac{\xi-\xi_j}{w}\right)\cdot\frac{dR}{dr}+\\&+\frac{e}{\varepsilon_0 k_p^2}2\sin\left(\frac{k_p w}{2}\right)\sum_{j=1}^{M}n_{bj}\sin\left[k_p\left(\xi-\xi_j\right)\right]\cdot U\left(\xi-\xi_j-w/2\right)\cdot\frac{dR}{dr}\\&-\frac{e}{\varepsilon_0 k_p^2}\sum_{j=1}^{M}n_{bj}U\left(\xi-\xi_j-w/2\right)\cdot\frac{dR}{dr}\end{aligned} \tag{51}$$

In the next few sections we will explicitly describe what can be achieved with different setups.

5.1.1 Enhancing the Wakefield

In order to create the maximum possible wakefield, the individual wakefields from each bunch need to be added in-phase. This occurs when the bunches are separated by one plasma wavelength[1], placing each bunch in the decelerating phase of the wake created by previous bunches. This means that

$$\xi_m = (m-1)\lambda_p \tag{52}$$

The wakefield left after the bunches ($\xi > \xi_M + w/2$) is then equal to (from (50))

$$E_z(r,\xi) = +\frac{e}{\varepsilon_0 k_p} 2\sin\left(\frac{k_p w}{2}\right)\cos(k_p\xi)\cdot R(r)\cdot\sum_{j=1}^{M} n_{bj} \tag{53}$$

It is interesting to observe in this case that the number of particles per bunch does not affect the wakefield, as it simply adds together and the total wake is proportional to the total number of particles in all bunches. The focusing force at the center of bunch m ($\xi = \xi_m = (m-1)\lambda_p$) is equal to

$$W_\perp(r,\xi_m) = -\frac{e}{\varepsilon_0 k_p^2}\left[n_{bm}\cos\left(\frac{k_p w}{2}\right) + \sum_{j=1}^{m-1} n_{bj}\right]\cdot\frac{dR}{dr} \tag{54}$$

We observe that in addition to its own focusing force, each bunch will experience the force due to all the previous bunches. Thus, later bunches are focused stronger.

The tradeoff for the enhanced wakefield in this scheme is the reduction in the transformer ratio, which approaches unity as the number of bunches increases. For identical bunches ($N_m = N_0$) with transformer ratio R_0 , the total transformer ratio R_{tot} is equal to

[1] More general, the separation can be any integer number of plasma wavelengths.

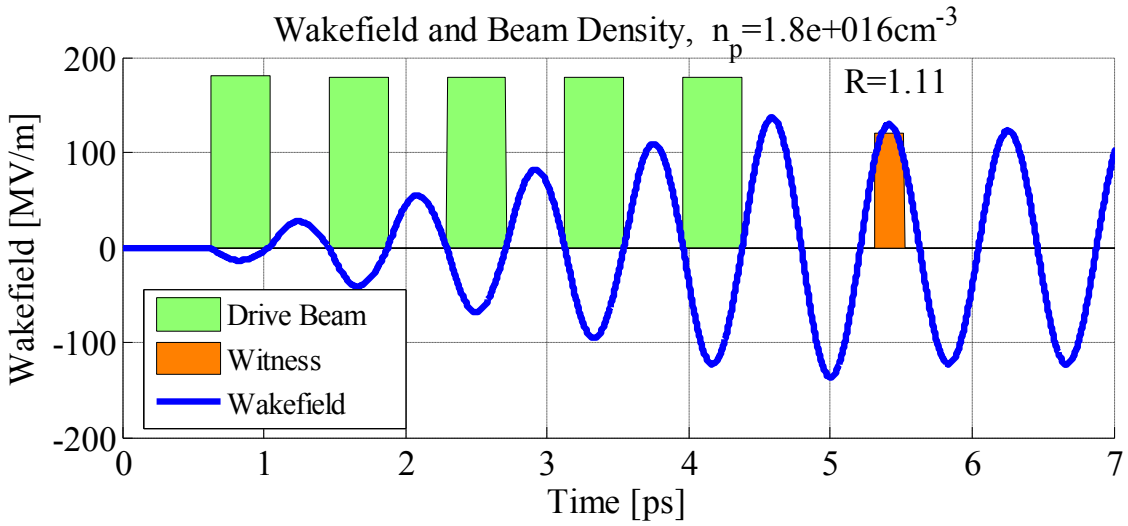

Figure 5.1: Example of a multibunch plasma accelerator in a maximum wakefield setup. The bunches are identical with $k_p w = \pi$ and are separated by one plasma wavelength apart. A witness bunch 180° out of phase samples the accelerating wakefield. In this example $\lambda_p = 250 \mu m$ and $\sigma_r = 100 \mu m$.

$$R_{tot} = \frac{M}{M - \left(1 - \frac{1}{R_0}\right)} \tag{55}$$

An example of a PWFA under such a setup is presented in Figure 5.1 where the on-axis beam density and wakefield of a 5+1 bunch system (5x30 pC drive bunches and 1 witness bunch) is shown. In this example $k_p w = \pi$, and the bunches are separated by 250 μm at 1.8×10^{16} cm^{-3} plasma density ($\lambda_p = 250 \mu m$). A relevant experiment that creates the bunches through IFEL using a laser is analyzed later in section 6.1.

The reason why the transformer ratio and the efficiency are not enhanced is because the last bunch feels the almost full decelerating field, while the early bunches feel a smaller decelerating field. In this example the transformer ratio is $R = 1.1$ and the efficiency is only 13% (as defined in section 2.4.1). In order to increase the transformer ratio each bunch needs to feel the exact same decelerating field, and this is explored in the next section.

5.1.2 Enhancing the Transformer Ratio

In order to maximize the transformer ratio, each bunch needs to be placed in the accelerating phase of the wake created by the preceding bunches, and its charge needs to be increased such that the total decelerating wakefield under each bunch is the same for every bunch. This scheme was suggested first by Laziev et al. [104] and more recently by Power et al. for a dielectric wakefield accelerator [144] and was demonstrated experimentally in a proof of principle experiment in 2006 by Jing et al. using two drive bunches [78, 79].

The total wakefield under the $m-th$ bunch is given by equation (50)

$$\begin{aligned} E_z(r,\xi) &= \frac{e}{\varepsilon_0 k_p}\left[n_{bm}\sin\left[k_p\left(\xi-\xi_m+w/2\right)\right] + 2\sin\left(\frac{k_p w}{2}\right)\sum_{j=1}^{m-1} n_{bj}\cos\left[k_p\left(\xi-\xi_j\right)\right]\right]\cdot R(r) \\ &\triangleq \frac{e}{\varepsilon_0 k_p} n_{b1}\sin\left[k_p\left(\xi-\xi_m+w/2\right)\right]\cdot R(r) \end{aligned} \tag{56}$$

The last equality is set such that the wakefield under each bunch is equal to the wakefield under the first bunch (shifted by the location of the bunch center). By requiring the above expression to hold true for every ξ, a solution for the number of particles N_m for the $m-th$ bunch and its center ξ_m can be found. For example, for an arbitrary bunch width $k_p w$, a solution for the number of particles and the location for the second bunch is

$$\begin{aligned} N_2 &= N_1\left[1+2\sin\left(\frac{k_p w}{2}\right)\right] \\ k_p\xi_2 &= k_p\xi_1 + \frac{5\pi}{2} + \frac{k_p w}{2} \end{aligned} \tag{57}$$

Under an arbitrary bunch width the bunches are not equidistant and their charge may not scale in a simple way – those values need to be evaluated numerically from equation (56).

The most interesting case though is the one that maximizes the transformer ratio of the single bunch, i.e. $k_p w = \pi$ for which $R_1 = 2$. In this case the wake around each bunch is

symmetric with respect to its center and the equations are greatly simplified. In that special scenario it is found that the number of particles per bunch and their location scale in a simple way:

$$N_m = N_1(2m-1)$$
$$k_p\xi_m = k_p\xi_1 + m\cdot 3\pi \tag{58}$$

The decelerating wakefield under each bunch is now the same, and the envelope of the beam density of the bunches is a linear ramp, much like the continuous single-bunch linear ramp that is analyzed in Appendix B.2 . Equation (58) implies that the bunches must be placed 1.5 plasma wavelengths apart from each other[1] and their charge must scale as $N_1\times[1:3:5:\ldots]$.

The total wakefield left after the drive bunches in the case where equations (58) is satisfied for the $k_p w=\pi$ case is

$$E_z(r,\xi) = M\cdot\frac{2en_{b1}}{\varepsilon_0 k_p}(-1)^{M-1}\cos(k_p\xi)\cdot R(r) \tag{59}$$

Note that the phase of the wakefield resets after each drive bunch. Using equation (56), the transformer ratio of the system is then

$$R_{tot} = 2M = M\cdot R_1 \tag{60}$$

The last equation summarizes the ultimate advantage of this scheme, since the transformer ratio of the system is proportional to the number of bunches used to drive the wakefield.

The transverse wakefield at the center of the $m-th$ bunch is in this scenario equal to (from equation (51))

[1] They can also be any half-integer number of plasma wavelengths apart.

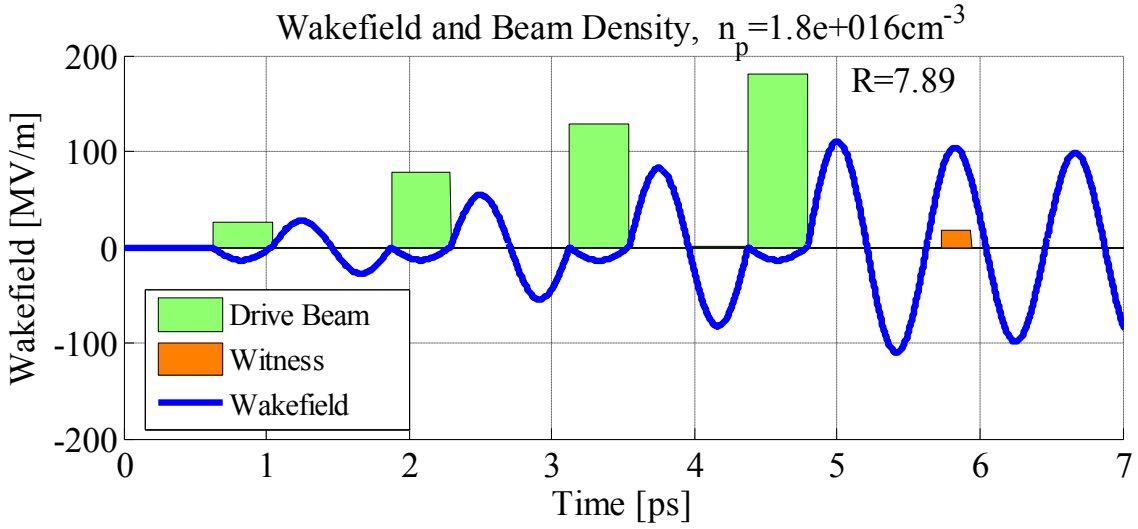

Figure 5.2: Example of a multibunch plasma accelerator in a maximum transformer ratio setup. The bunches are identical with $k_p w = \pi$ and are separated by 1.5 plasma wavelengths apart. The total charge is 500 pC and in each bunch is increased linearly. A witness bunch equidistant to the other bunches samples the accelerating wakefield. In this example $\lambda_p = 250\mu m$ and $\sigma_r = 100\mu m$.

$$W_\perp(r,\xi_m) = -\frac{en_{b1}}{\varepsilon_0 k_p^2}\cdot\left[(m-1)^2 + \sin\left(k_p(\xi-\xi_m)\right)\right]\cdot\frac{dR}{dr} \tag{61}$$

Here $|\xi-\xi_m| \le w/2$. It is interesting to observe that although the system is designed such that the longitudinal wakefield is identical under each bunch, as equation (56) suggests, on the other hand the transverse wakefield is not the same for each bunch but it scales at their center quadratically with the number of drive bunches instead. This is a consequence of the fact that the total charge fed into the system scales also quadratically with the number of bunches, i.e. $N_{tot} = M^2 \cdot N_1$. As a result, later bunches experience stronger focusing force.

Figure 5.2 illustrates an example where a ramped bunch train of 4 drive bunches is fed into a 1.8×10^{16} cm^{-3} plasma. The bunches are separated by 1.5 plasma wavelengths apart and have a total charge of 500 pC, while their charges scale as $31pC\times[1:3:5:7]$. The transformer

ratio is 7.9 and the 1D driving efficiency of the system is 64%, equal to the efficiency of a single bunch.

Several things need to be pointed out in this figure. Although the total wakefield increases linearly with the number of bunches, similar to the maximum wakefield scheme of section 5.1.1, this occurs here by supplying quadratically more charge (as opposed to linearly more). The total wakefield amplitude per total unit charge put into the system scales inversely proportional with the number of bunches in the ramped bunch train scheme described here [87]. In addition, from an energy perspective, each particle is depositing into the plasma as much energy as the particles in the first bunch do, and the rest of its energy is being transferred to the following bunch in the train to prevent it from decelerating faster. In this way all the particles deposit their energy at the same rate (on average along the bunch), and the last bunch in the train releases this net energy into the plasma.

Note that the efficiency of the system is limited by the efficiency of a single bunch, which is achieved when the charge in each bunch is adjusted properly such that the wakefield under each bunch is the same. Even so, the variation of the wakefield inside each individual bunch sets an upper bound for the efficiency. This limit can be overcome (at the slight expense of the transformer ratio) if the positions and number of particles per bunch are fine-tuned, as we will show in the following section.

5.1.3 Enhancing the Efficiency

Gaussian, square and other realistically-shaped bunches have maximum single bunch efficiencies around 60% - 70%, depending on their width relative to the plasma density. This is the maximum fraction of their energy that can be transferred to the plasma. Even if the

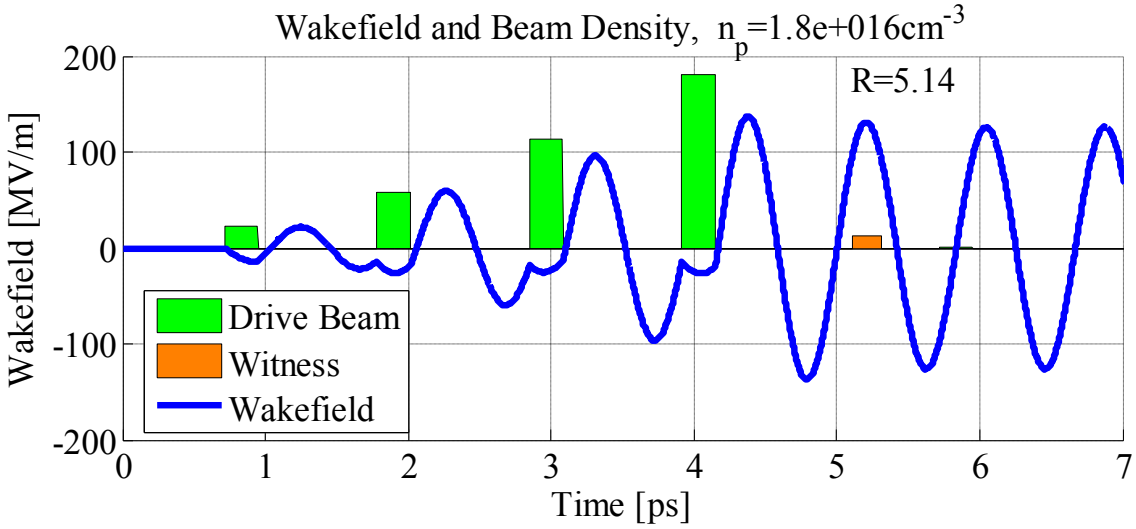

Figure 5.3: Example of a multibunch plasma accelerator in a maximum efficiency setup. The bunches are identical with $k_p w = 0.56\pi$ and are separated by 1.28 plasma wavelengths apart. The charge in each bunch is $17.5pC \times [1:2.70:5.20:8.22]$. A witness bunch samples the accelerating wakefield. In this example $\lambda_p = 250\mu m$ and $\sigma_r = 100\mu m$. The driving efficiency of this system is 84% and the transformer ratio is 5.14.

transformer ratio is maximized, as was explored in section 5.1.2, the efficiency is never larger than the single bunch efficiency for those setups.

It is possible however using multiple drive bunches to obtain a total system efficiency that is larger than the individual bunch efficiency, without a need to specially shape the bunches. This is achieved by placing the bunches at those phases of the wakefields such that the total wakefield under each bunch is most flat (thereby depositing energy more efficiently), even if the wakefield is not exactly the same between bunches. Notice in Figure 5.2 for example, there are particles inside each bunch that experience an almost zero wakefield (near the edges), while other particles near the center of the bunches experience the full decelerating field. This can be avoided if the bunches are placed earlier in the wakefield such that they sample both a portion of the decelerating phase of the wakefield and a portion of the accelerating phase as

well, with the number of particles per bunch is adjusted accordingly. Such an example using 4 drive bunches is shown in Figure 5.3.

In this scenario the bunches are equidistant and separated by 1.28 plasma wavelengths apart, and the total charge is 300 pC and scales as $17.5pC\times[1:2.70:5.20:8.22]$ in each bunch. Those optimal values are found numerically by running an optimization routine for the efficiency as a function of the bunch separation and the bunch charges. Further enhancements (few %) can be achieved if the restriction for equidistant bunches is lifted. The 1D driving efficiency of the plasma accelerator shown here is 84%, while the transformer ratio is 5.14 (instead of the theoretical maximum of 8 for 4 bunches).

It is interesting to observe the physics of this interaction. In contrast to the maximum transformer ratio scheme of the previous section, the wake under each bunch is not identical anymore. The first bunch experiences a weaker decelerating wakefield for example. However this is allowed here because from an energy perspective the first bunch is not as important as the later bunches that carry more energy and affect the efficiency more significantly. In essence, the first bunch jump-starts the wake such that the second bunch will sample a more flat portion of it. Shorter bunches increase the efficiency further as they sample narrower portions of the sinusoidal wakes.

5.2 Meter-scale Simulations of a Multibunch Accelerator

So far in this chapter we have been limited to the initial wakes generated by multibunch electron drivers. These waves are valid at time $t=0$, before the beam starts to evolve inside the plasma. In reality though the plasma will generate transverse forces that will act on the beam and unless the beam is matched the longitudinal wakefield structure will be disrupted after a

few mm of propagation in the plasma. In the blowout regime the beam is more stable along the plasma propagation because the lack of electrons creates a radially linear focusing force to which the beam emmitance or thermal spread can be matched, however those longitudinal wakefields excited cannot be efficient for multibunch drivers (see section 5.3). It is the purpose of this section to show that in the linear regime, even though (ironically) the transverse forces are not linear, a high-transformer-ratio wakefield structure can be maintained over long distances. The scenario analyzed in section 5.1.2 under the conditions of equation (58) will be explored.

5.2.1 Multibunch Emmitance Balancing

We seek to find a "matched" or balanced emmitance for each drive bunch such that they remain as stable as possible and the wakefield is not altered significantly as the bunches propagate in the plasma. In the linear regime examined here, and assuming that the bunches have transversely Gaussian shape, the matched emmitance along the bunch was analyzed in section 2.2.2 and is given by equation (18), where the function $Z(\xi)$ is the longitudinal component of the transverse wakefield which was found in equation (61). The matched emmitance along the longitudinal beam profile of the $m-th$ bunch is then

$$\varepsilon_N(\xi) = \sqrt{\gamma}\sqrt{\frac{n_{b1}}{n_0}\left[(m-1)^2 + \sin\left(k_p(\xi-\xi_m)\right)\right]}\cdot\sqrt{I(\sigma_r)}\sigma_r \tag{62}$$

Under realistic terms, one might attempt to match in an average way the emmitance at the center of each bunch, $\xi = \xi_m$:

$$\varepsilon_N(\xi_m) = (m-1)\cdot\sqrt{\gamma}\sqrt{\frac{n_{b1}}{n_0}}\cdot\sqrt{I(\sigma_r)}\sigma_r \tag{63}$$

The value of $I(\sigma_r)$ is given for transversely Gaussian bunches in Figure 2.2. It should be noted that the value given from the above formula is approximate, as the bunch will eventually evolve and the assumptions under which this formula was derived (e.g. transversely Gaussian bunches) will not hold. Still, it serves as a good starting point. Note that all such transverse nonlinear focusing effects can be avoided if a hollow plasma channel is utilized [34], thus avoiding the need to adjust the emmitances.

5.2.2 Simulation Results

The parameters of the multibunch accelerator that is modeled in 2D OSIRIS are as follows. The plasma has a neutral density of 2×10^{17} cm^{-3} and a length of 50 cm. $M=4$ drive bunches have longitudinal widths of $k_p w=\pi$ (37.5 μm), transverse spot sizes of $k_p\sigma_r=2.4$ (28.6 μm), initial energy of $\gamma=2\times10^5$ (102.25 GeV), and are separated by 1.5 plasma wavelengths or 112.5 μm. Their charge scales as $62pC\times[1:3:5:7]$ for a total of ≈1 nC of drive charge, which corresponds to normalized beam densities of $n_{bm}/n_0=0.01\times[1:3:5:7]$, thus placing the interaction into the linear regime. The transverse emmitances of the drive bunches where tuned according to equation (63) to the values $\varepsilon_N/\sigma_r=22:22:45:67$ [1]. A short and narrow test witness bunch with 5 pC charge, width $k_p w_w=\pi/4$ (9.4 μm), transverse spot size $k_p\sigma_w=0.2$ (2.4 μm) and same energy is placed another 1.5 plasma wavelengths after the last drive bunch, at the peak of the accelerating phase of the wake ($n_{bw}/n_0=0.3$ for that bunch).

[1] Realistic thermal spread was added to the first bunch to prevent its tail from collapsing under its own focusing force.

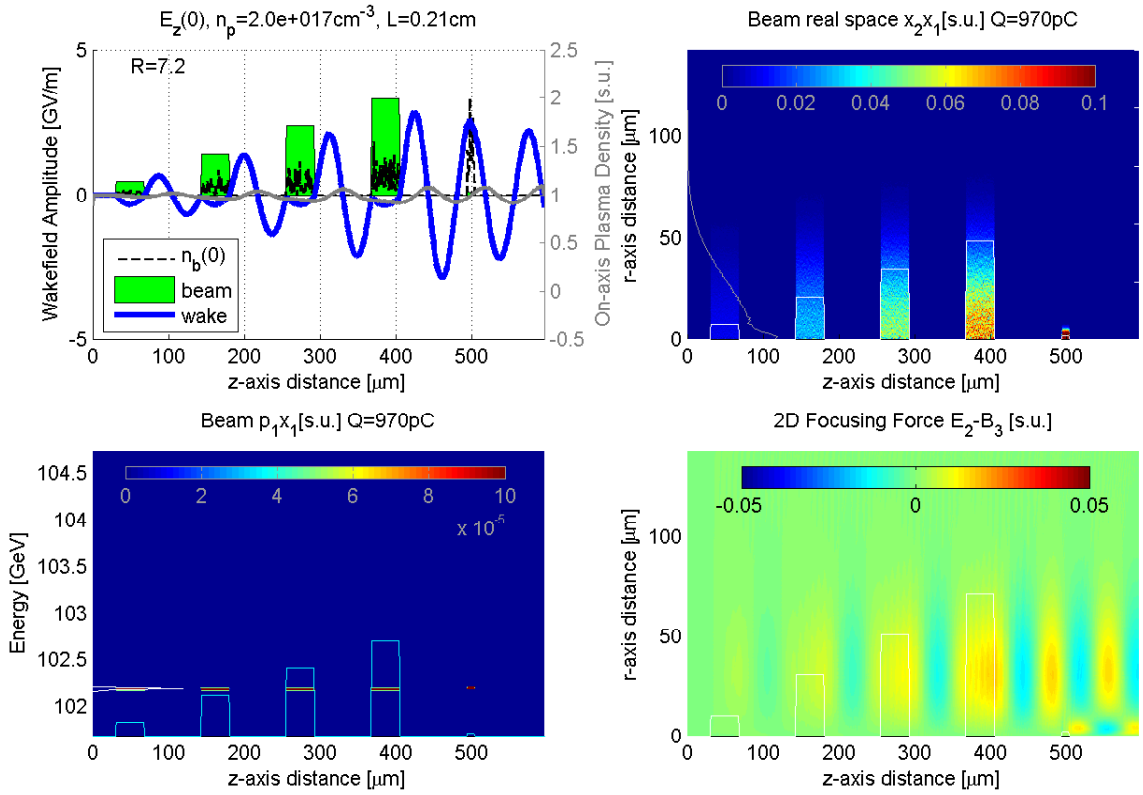

Figure 5.4: Simulation of 4 drive bunches in the linear regime at the entrance of the plasma. Top left panel: On-axis electron beam density (green area), longitudinal on-axis electric field (blue line), on-axis beam density (black line) and on-axis plasma density (gray line). Top right panel: 2D dependence of the electron beam density (in units of n_0). The white line shows the on-axis longitudinal position of the drive bunches, and the gray line (on the left) the summed transverse profile. Bottom left panel: Beam phase space p-z (in units of mc). The blue line shows the longitudinal position of the bunches. Bottom right panel: The 2D dependence of the focusing force of the plasma.

The results of the simulation at the entrance of the plasma are shown in Figure 5.4. Using now the theoretical background that was detailed in the previous chapters of the dissertation we can make estimations for the system and compare them with the simulations. The theoretically predicted transformer ratio is 8 (from equation (60)), the driving efficiency is $\eta = \eta_{\parallel} \cdot \eta_{\perp} = 64\% \cdot 55\% = 35\%$ (from equation (28) and Figure 2.3) and the wakefield amplitude after the bunches is equal to 2.8 GV/m (from equation (59)). In the simulation the transformer ratio is 7.2, and the on-axis wake amplitude 2.9 GV/m. We also observe that the focusing force

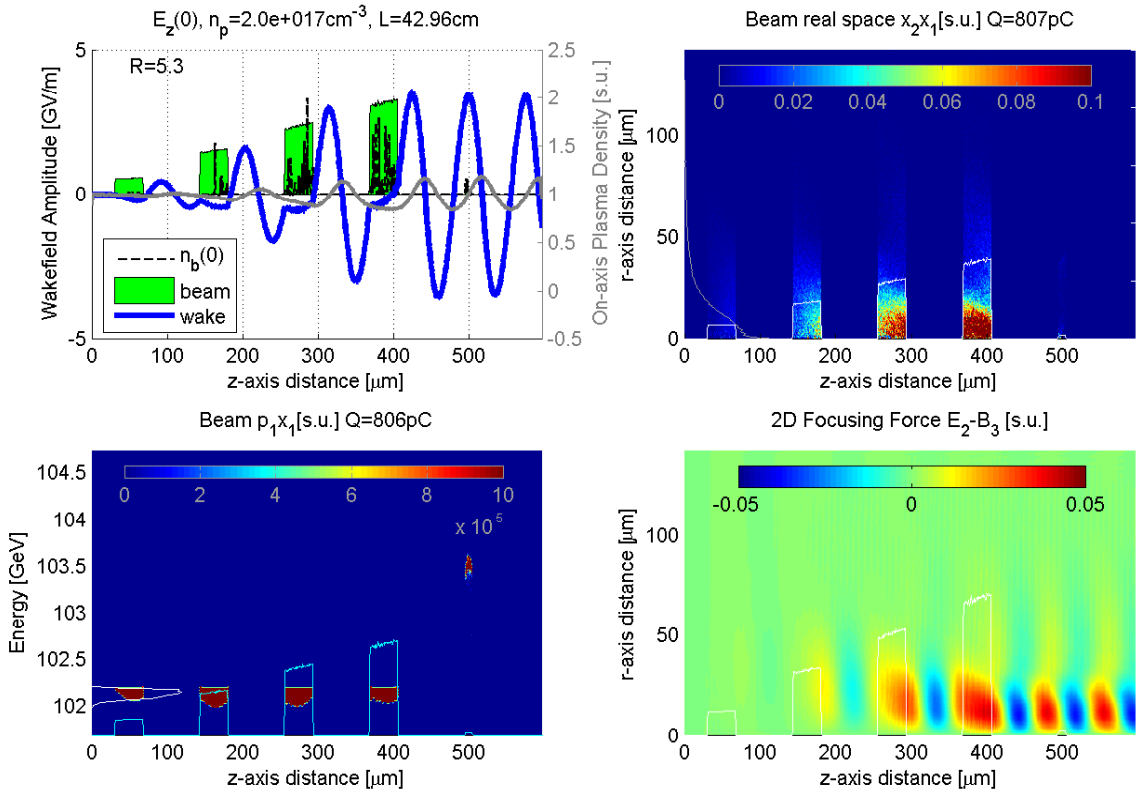

Figure 5.5: Simulation of 4 drive bunches in the linear regime after a 43 cm long plasma. Top left panel: On-axis electron beam density (green area), longitudinal on-axis electric field (blue line), on-axis beam density (black line) and on-axis plasma density (gray line). Top right panel: 2D dependence of the electron beam density (in units of n_0). The white line shows the on-axis longitudinal position of the drive bunches, and the gray line (on the left) the summed transverse profile. Bottom left panel: Beam phase space p-z (in units of mc). The blue line shows the longitudinal position of the bunches. Bottom right panel: The 2D dependence of the focusing force of the plasma.

(in the bottom left panel) increases with each bunch and also varies within each of them, as predicted by equation (61). Overall the agreement between theory and simulation is very good.

The simulation results after 43 cm of plasma are shown in Figure 5.5. The wakefield and the transformer ratio oscillate during the length of the plasma but on average they remain stable, probably a result of the chosen emmitances for the bunches. In the snapshot shown here the transformer ratio is 5.3 and the wakefield amplitude is 3.5 GV/m, since the bunches have slightly focused (especially near the tails). The most intriguing result of course is shown in the

bottom left panel which depicts the energy of the bunches, where we observe that the witness bunch has gained $3GeV/m \times 0.5m \simeq 1.5GeV$, while the drive bunches have lost only $1.5/6 \simeq 0.25GeV$ each, thus demonstrating the high-transformer ratio scheme.

The beam loading was kept light in this simulation in order to preserve the energy spread of the witness bunch. For the given witness bunch parameters, we can calculate the ratio

$$\frac{E_w}{E_0} = \frac{n_{bw} \cdot r_w}{n_{b1} \cdot R_{tot}} \simeq \frac{0.3 \cdot 0.77}{0.01 \cdot 8} \simeq 2.9 \tag{64}$$

Here E_w and E_0 are the longitudinal components of the wake amplitudes left behind by the witness bunch and drive bunches alone, respectively (defined in equations (40) and (41)), and $r_w = 2\sin\left(k_p w_w / 2\right)$ & $R_{tot} = 2 \cdot M$ are their corresponding transformer ratios. Then, using Figure 2.7 we can estimate the total beam loading efficiency to be $\eta_b \simeq 10\%$ (since $\sigma_w / \sigma_0 \simeq 0.1$). The longitudinal energy spread is estimated through the ratio

$$p_0 = \frac{E_{0w} R_w(0)}{E_0 R_0(0)} = \frac{n_{bw} \cdot k_p w_w \cdot R_w(0)}{n_{b1} \cdot R_{tot} \cdot R_0(0)} \simeq \frac{0.3 \cdot \frac{\pi}{4} \cdot 0.07}{0.01 \cdot 8 \cdot 0.8} \simeq 0.26 \tag{65}$$

The parameters shown here are defined in section 2.5.1. From Figure 2.5, the 3-σ longitudinal energy spread is estimated $f_{w\|} \simeq 25\%$ and the transverse energy spread (from Figure 2.8) is negligible since the witness bunch was made 10 times narrower than the drive bunches.

5.3 Multiple Drive Bunches in the Blowout Regime

In this section we will explore the possibility of using multiple drive bunches to enhance the transformer ratio and the efficiency in the highly nonlinear regime, where the bunches are strong enough to blowout all the electrons near them. Attempting to extend the techniques used in the linear regime, we place each subsequent drive bunch in the accelerating phase of

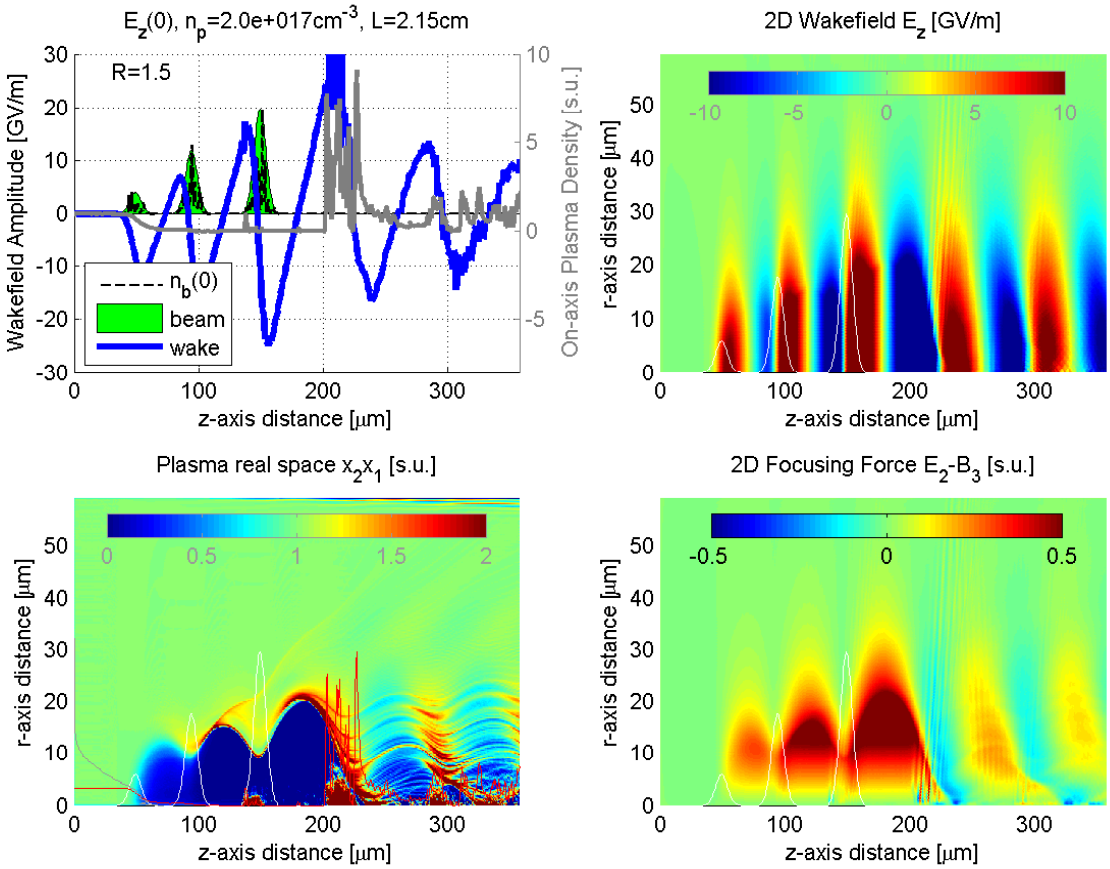

Figure 5.6: Simulation of 3 drive bunches in the blowout regime. Top left panel: On-axis electron beam density (green area), longitudinal on-axis electric field (blue line), on-axis beam density (black line) and on-axis plasma density (gray line). Top right panel: 2D dependence of the longitudinal electron field. The white line shows the longitudinal position of the drive bunches. Bottom left panel: Plasma density real space (in units of n_0). The white line shows the longitudinal position of the bunches, and the gray line (on the left) shows the transverse profile of the bunches. The red line shows the plasma density on-axis. Bottom right panel: The 2D dependence of the focusing force of the plasma.

the wakefield driven by the previous bunch, while at the same time ramping its charge so that the total wakefield in the center of the bunch is the same for all bunches, and the bunches deposit their energy at the same rate.

This scheme is examined through OSIRIS simulations only, since it is an analytically intractable scenario. The plasma density is set to $n_0 = 2.0\times10^{17}$ cm^{-3}. There are 3 drive bunches that have bi-Gaussian shapes with 6.7 μm spot sizes (in either dimension), and their charge

scales as 135:405:675 pC. This corresponds to normalized beam densities of $n_{b0} / n_0 = 2.5 : 7.5 : 12.5$. The second bunch is placed 45 μm after the first, and the third bunch is placed 55 μm after the second bunch. This non-equidistant placement was found empirically and it is necessary because of the frequency shift that increases with higher drive charges in the nonlinear regime, which results from the electrons being blown out at larger radii from the axis, thus increasing the wavelength of the oscillation. The results from the simulation after 2 cm of propagation in the plasma are shown in Figure 5.6.

We observe (top left panel) that although the on-axis wakefield at the center of each bunch is the same (blue line), it varies greatly along the length of each bunch. This is because in the nonlinear regime, the wakefield from highly-accelerating becomes highly-decelerating inside each bunch, resulting in the front of each bunch gaining energy and the tail of each bunch depositing energy. This sharp dichotomy is clearly observed when looking how the 2D r-z dependence of the longitudinal wakefield (top right panel) varies inside each bunch, thus reducing the driving efficiency and the transformer ratio which is only 1.5 in this example. This is in stark contrast with the linear regime where the wakefield inside each bunch is always linear, i.e. a section of a sinusoidal function, which at worse has a slope of k_p [1].

The bottom left panel of Figure 5.6 shows the plasma density real space r-z. The blowout region is clearly visible, and it is interesting to notice the electrons that are expelled away from the first bunch, which are then returning to the axis but they are blown out again at a greater radius by the second bunch. When the ions still attract them back, they are blown away for a third time by the third (and strongest) bunch. Only after that last bunch do the electrons have a chance to return back to the axis creating a density spike and a peak electric field of

[1] This occurs near the zero-crossing of the wakefield.

30 GV/m. Finally, the bottom right panel shows the 2D transverse focusing wakefield along the bunch dimensions.

We conclude that because of the nonlinearities in the blowout regime the wakefield inside each drive bunch cannot be made flat and thus the efficiency and the transformer ratio are not enhanced in the same way they do in the linear regime using simply unshaped bunches. The most probable workaround to resolve this is to utilize shaped bunches, such as a single long triangular bunch or multiple properly shaped drivers. Those drivers will most likely require a delta-function-like front in order to bring the wakefield from accelerating to decelerating inside the rest of the bunch. However, for regularly shaped bunches (e.g. Gaussians, flat-tops) the linear regime is more favorable. Finally, a combination of the two regimes where the driving of the wakefield occurs in the linear regime and the beam loading in the mildly nonlinear regime may also be optimal.

5.4 Chapter Conclusions

The following items are concluded from this chapter:

- By placing multiple drive bunches separated by an integer number of plasma wavelengths apart the wakefields add resonantly and the amplitude is maximized and increases linearly with the total charge in the beam. The transformer ratio and efficiency are minimized.

- By placing multiple drive bunches at the accelerating phase of the wakefield driven by preceding bunches, then by adjusting the charge in each bunch the wakefield under each bunch can be made equal, thus increasing the transformer ratio beyond two which now scales linearly with the number of bunches. Single bunch efficiencies are obtained.

- By fine-tuning the position and charge in each bunch the system can be more efficient than a single bunch system without shaping the bunches, at a slight expense of the transformer ratio. An example with efficiency 85% and transformer ratio 5.1 is presented using 4 drive bunches.

- By linearly increasing the emmitance on each subsequent bunch, 4 bunches are tuned to balance the transverse focusing force of the plasma and propagate over 43 cm of 2×10^{17} cm^{-3} density plasma while maintaining a transformer ratio of 6 in a 2D OSIRIS simulation.

- These schemes cannot simply be extended into the nonlinear regime because the wakes change very abruptly and each drive bunch experiences both energy loss and energy gain. This may be circumvented by shaping the bunches.

In theory, there is no difference between theory and practice; in practice, there is.

- Chuck Reid

Chapter 6

Multibunch Experiments

The use of multiple drive electron bunches to excite plasma waves has been limited to only two notable sets of experiments, mainly due to the unavailability of multiple ultra-short drivers. Berezin et al. in the 1970s have reported the use of a series of 2 MeV electron bunches in 10^{11} cm^{-3} density 1 m long plasma and observed gradients of 0.25 MV/m [17, 176]. Similar experiments were conducted in the KEK 500 MeV linac in Japan, where 6 drive bunches were fed into a 1 m long 5×10^{12} cm^{-3} plasma and up to 20 MV/m gradients were recorded [126, 132, 133]. In both cases there was very poor agreement between the results and the theoretical predictions. The bunches were separated by the linac RF electric field, which corresponds to several hundred picoseconds period. The goal of those experiments was to excite resonantly wakefields in the plasma. Such strategies can have interestingly high gradients only when high-density plasmas are used, which is not possible using the above mentioned technique to generate the bunches.

In this chapter, we will investigate two methods to excite large wakefield resonantly. The first uses ≈100 ultra-short bunches in 10^{19} cm^{-3} plasmas created through the use of the

Inverse Free Electron Laser (IFEL) bunching technique. This method will be analyzed in section 6.1. The second method for creating subpicosecond bunches uses a mask technique to selectively block portions of the initial beam profile. This method offers the advantage of creating adjustable charge per bunch and adjustable spacing between the bunches (along with the creation of a witness bunch), thus bypassing the IFEL method limit which is restricted to bunch separations fixed to the laser wavelength only. Beam diagnostics and beam-plasma interactions results using this method will be presented in sections 6.2 and 6.3, respectively.

6.1 Resonant Wakefield Excitation with IFEL

The experimental setups described in this section explore the possibility of creating GV/m wakefields by modulating a single electron beam through IFEL and then feeding the created bunches into a high-density plasma [88]. The motivation and beam-plasma simulations along with diagnostics of the microbunched beam will be presented here. The experiments took place at the Accelerator Test Facility (ATF) of the Brookhaven National Lab.

6.1.1 Motivation and Theoretical Background

Given an electron beam with a fixed charge and transverse dimensions, what is the optimal beam distribution that will excite the strongest wakefield in the plasma? Since the plasma operates as a simple harmonic oscillator in the linear regime, the wakefield amplitude will be maximized when the plasma is driven to its resonance by a periodic force with a frequency equal to the natural oscillation frequency of the system, i.e. the plasma frequency. This suggests that the use of a series of microbunches separated by a distance equal to the plasma wavelength λ_p to be driven into such a plasma. For M Gaussian drivers, the beam density would be then given by

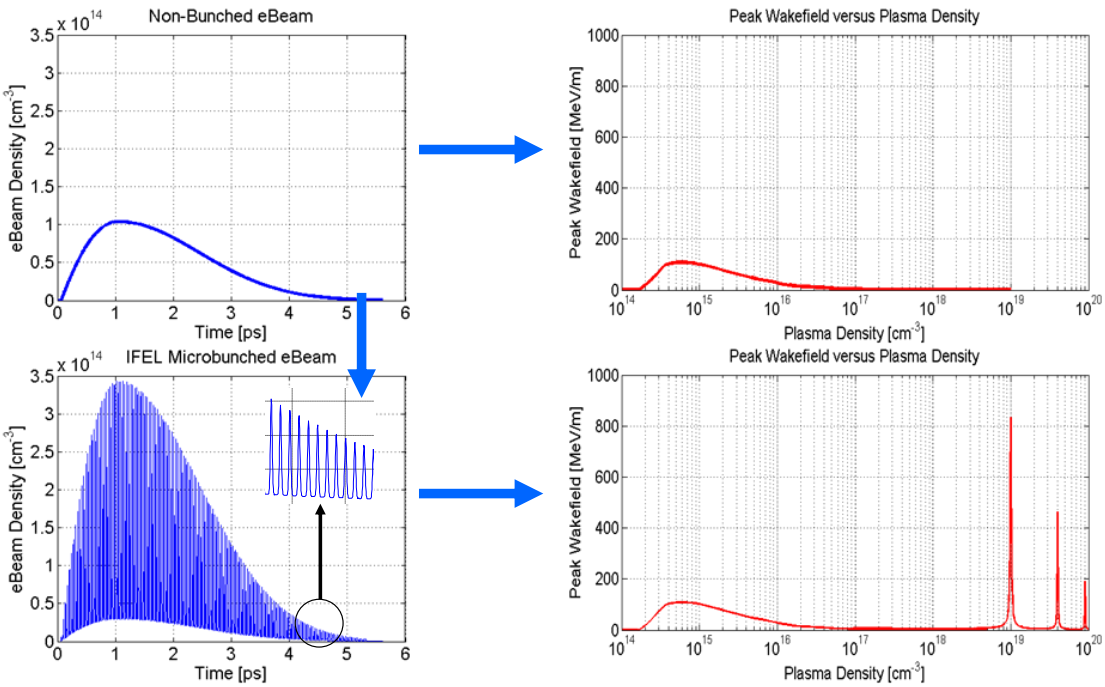

Figure 6.1: The plasma wakefield amplitude response of a non-bunched beam (top) and of a corresponding microbunched beam (bottom) of equal charge. The bunch separation is 10.6 μm and the microbunch length 1 μm FWHM.

$$n_b(r,\xi) = \frac{N}{2\pi\sigma_r^2} e^{-\frac{r^2}{2\sigma_r^2}} \cdot \sum_{j=1}^{M} \frac{A_j}{\sqrt{2\pi}\sigma_z} e^{-\frac{(\xi-\xi_j)^2}{2\sigma_z^2}} \quad , \quad \sum_{j=1}^{N} A_j = 1 \qquad (66)$$

Here A_j is the normalized amplitude of each microbunch and $\xi_j = j\lambda_p$ for resonant interaction. The response of the plasma to such a driver is shown in Figure 6.1, an example modeled after the beam parameters at ATF.

The initial broad Gaussian-like beam distribution is shown on the top left panel, along with its plasma response in the top right panel for various plasma densities. For a 1×10^{14} cm^{-3} peak beam density, the plasma wakefield excited is around 100 MV/m. In the bottom left panel, the same total charge of the beam is distributed into a series of microbunches, separated by a distance 10.6 μm. The plasma response on the bottom right panel shows some new interesting features. Although the beam envelope response remains at the low densities (since the plasma

wavelength is too large to resolve the microbunches), when the plasma density is such that the plasma wavelength matches the separation of the bunches (here this happens at a 1×10^{19} cm^{-3} density) then each bunch creates a wakefield which adds constructively and drives the total wakefield in a resonant manner. The amplitude is now almost an order of magnitude larger, more than 800 MV/m, limited by the finite size of the microbunches and the residual charge between the peaks.

Also visible are the harmonics of the interaction, appearing at densities 4×10^{19} cm^{-3}, 9×10^{19} cm^{-3} etc, where the plasma wavelength is an integer multiple of the resonant wavelength and there is now a microbunch placed every two, three or more periods of the plasma wave. The decreasing amplitudes of those resonances reflect the finite width of the microbunches and are determined by the Fourier transform of the microbunch Gaussian-like shape (a series of delta functions would create harmonic responses of equal amplitude).

6.1.2 Experimental Setup and Simulations

The idea of resonantly generating an enhanced wakefield is sought after experimentally at ATF[1]. There are two main parts in achieving the goal, 1) create equally spaced microbunches and 2) generate the corresponding resonant plasma density. A proposed experimental setup is shown in Figure 6.2.

The process for creating the microbunches is the Inverse Free Electron Laser (IFEL) , whereby an unmodulated electron beam and a long laser pulse are fed co-propagating into a magnetic wiggler [27, 101, 137]. The longitudinally sinusoidal-dependent static magnetic field inside the wiggler causes a perpendicular force on the beam electrons and initiates electron motion in the transverse plane. Using this transverse motion the electron beam can be coupled

[1] This idea was initially suggested by Ilan Ben-Zvi.

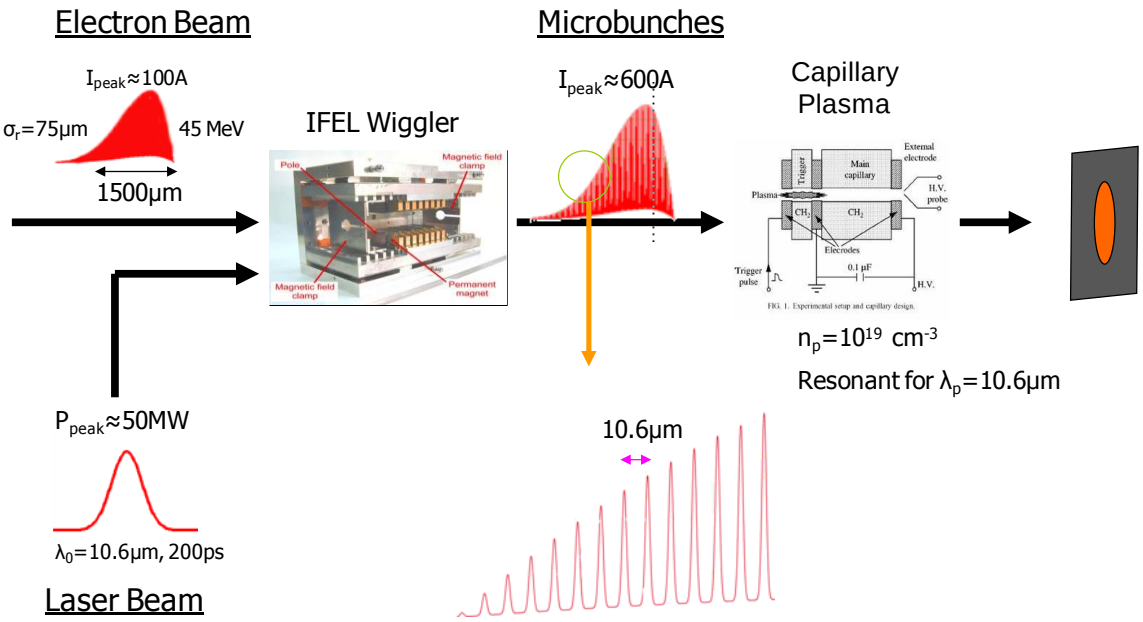

Figure 6.2: Experimental setup of resonant multibunch experiment at ATF. The unmodulated electron beam is inserted co-propagating with a CO_2 laser in the IFEL wiggler microbuncher. The output modulated beam is then fed into a high-density plasma, and the energy change imparted onto the beam is imaged with a spectrometer on a phosphor screen.

to the laser pulse (by tuning the wiggler field period) such that some electrons feel the decelerating electric field of the laser and some other the accelerating field [38]. This picture of half-acceleration and half-deceleration repeats over every laser period along the beam length and results in a velocity modulation of the beam electrons [162]. After the exit of the wiggler the beam is left to propagate in vacuum over some specific distance, after which the low-velocity electrons have caught up with the high-velocity electrons thus creating microbunches, separated at the laser's wavelength [111]. In this experimental setup a 10.6 μm CO_2 laser at 50 MW power is used [96, 97, 163].

The required optimal bunching distance s_0 for an electron beam with a given γ is determined by the condition that electrons compress but never outrun each other, i.e. their

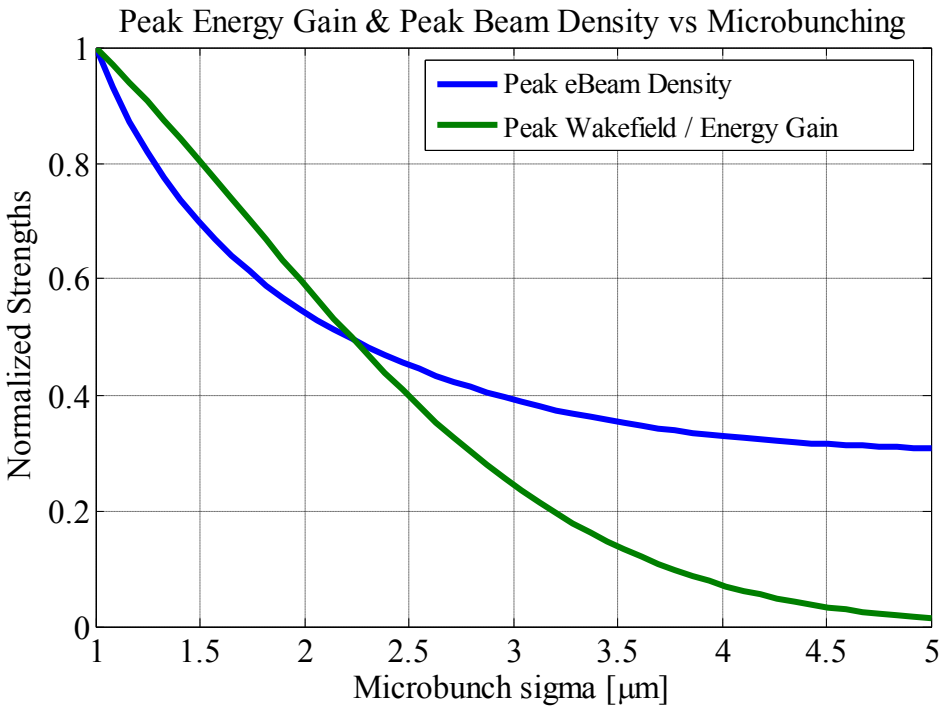

Figure 6.3: Dependence of the relative resonant wakefield amplitude on the microbunch longitudinal spot size for a plasma with a 10.6 μm wavelength.

relative drift distance within a laser period Δs is less than a quarter of the plasma wavelength. This is described by the formula

$$\frac{\Delta s}{s_0} = \frac{\sqrt{\gamma^2 - \frac{1}{(1+q)^2}}}{\sqrt{\gamma^2 - 1}} - 1 \simeq \frac{q}{\gamma^2} \tag{67}$$

Here q is the fractional initial energy modulation imparted on the electrons at the exit of the wiggler, determined by the laser electric field. The approximate expression above holds true for small modulations and large γ's. For the 45 MeV ATF electron beam ($\gamma \simeq 100$) the required drift distance for $q = 1\%$ modulation is estimated at $s_0 \simeq 2.7\,m$ for the given laser parameters.

As we will present in the next section, such microbunches have been successfully created and measured at ATF. The relative dependence of generated plasma wakefield

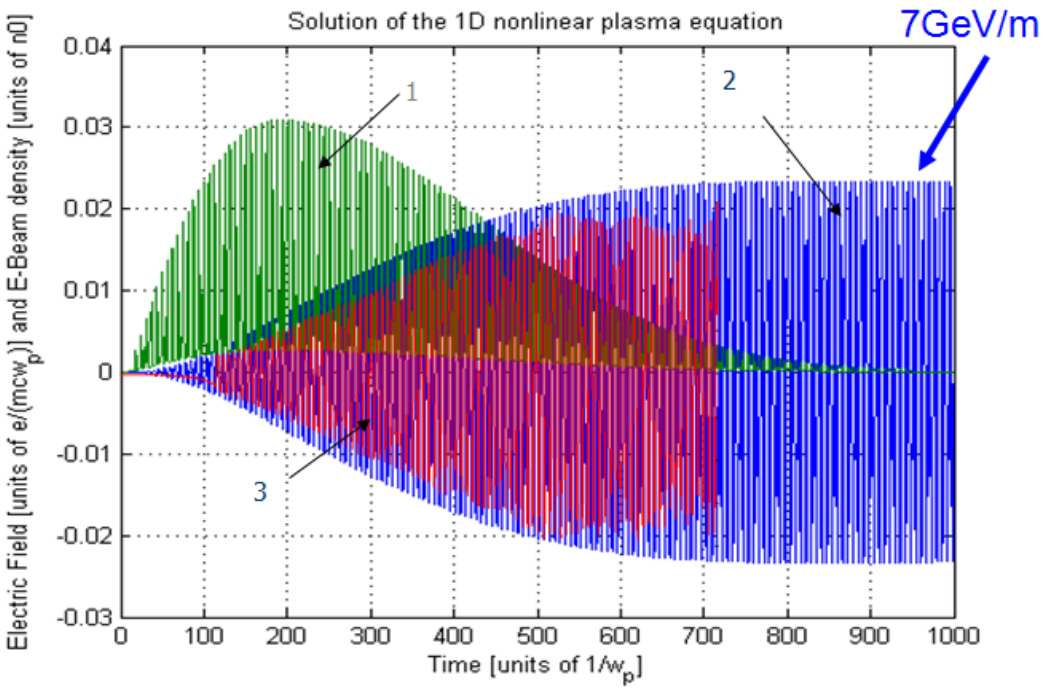

Figure 6.4: Simulated plasma wakefield amplitude response on-axis after the beam has fully entered the plasma. 1) Multibunched beam density 2) ThemOsiris calculated wakefield 3) OSIRIS calculated wakefield. For a transverse spot size 35 μm (shown here) and 500 pC of total charge, the generated wakefield amplitude is 7 GV/m. The plasma density is 1×10^{19} cm^{-3} .

amplitude on the Gaussian microbunch quality (i.e., their width) is shown in Figure 6.3 for a 10.6 μm plasma wavelength and bunch separation distance.

The simulated wakefield response on-axis for the multibunched ATF beam is shown in Figure 6.4 when the plasma density is exactly on resonance, 1.0×10^{19} cm^{-3}. The wakefield amplitude versus time is calculated using the fully explicit code OSIRIS, as well as the much faster quasi-2D code ThemOsiris, and they are shown to agree well. The wakefield amplitude resonantly excited from the 500 pC 35 μm spot size beam is 7 GV/m in this scenario. Since the individual wake from each bunch is added constructively, only the total charge that is fed into the plasma is important and not the charge distribution per bunch. Therefore, the wakefield amplitude at a given time is proportional to the integral of the charge up to that time.

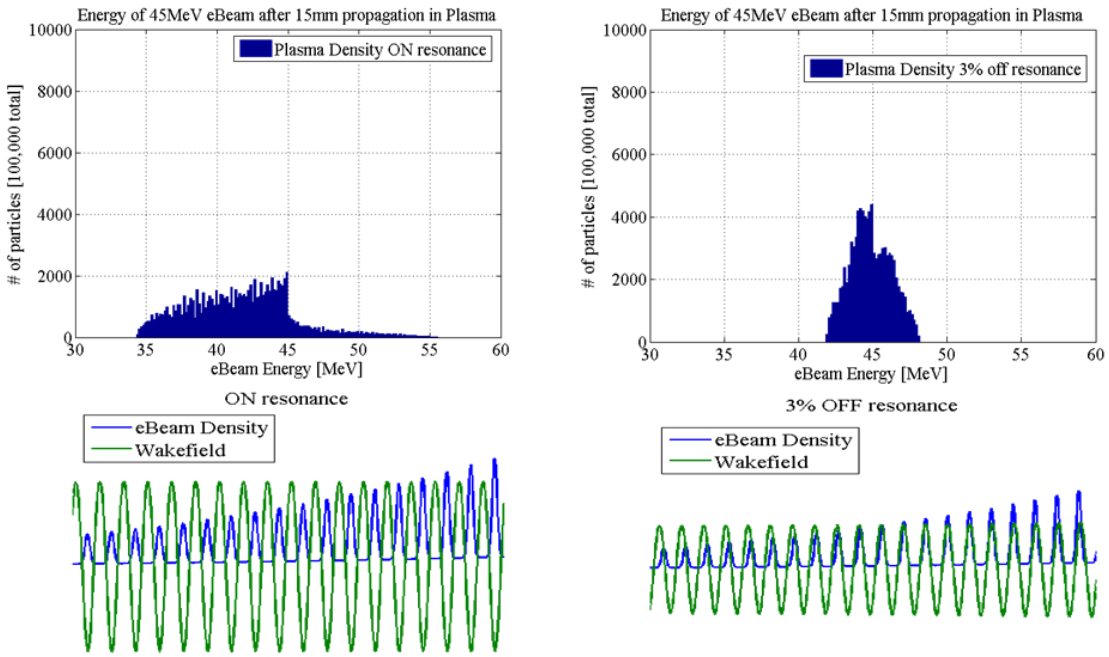

Figure 6.5: Energy spectra of the 45 MeV microbunched beam for a plasma density exactly on resonance (left) and 3% off resonance (right). The initial energy spread is 0.1 MeV. The bottom of the figure shows the relative phasing between the bunches and the wakefield near the tail of the beam (the charge is too low to enhance the wakefield visibly).

It is interesting to look at the electron energy spectra after a 15 mm long plasma interaction, both on and off resonance. This is shown in Figure 6.5, for a case exactly on resonance and for a case with a plasma density 3% off resonance, along with the relative phase of the wakefield with respect to the beam microbunches.

We observe that the energy shifts drop sharply even slightly off resonance, as is apparent also from Figure 6.1: the resonance width is inversely proportional to the number of microbunches. For $M = 100$ or more bunches seen here, the resonance width is on the order of $1/M \simeq 1\%$, and the higher wakefield is obtained at the cost of a narrower resonance. In addition, in Figure 6.5 (left panel) we observe that the accelerating wakefield occurs only in between the bunches, thus the accelerated electrons are the residual particles outside the microbunch peaks (roughly 10% of the total charge using this IFEL scheme). In the slightly off

resonance case though (right panel), the energy gain is much larger and comparable to the energy loss since the wakefield now partially cancels out in each bunch, resulting in larger number of accelerating particles compared to the on-resonance case. This may be a welcome tradeoff for the experimenter.

Ultimately, the crucial item in such an experiment is to obtain a reliable high plasma density with very high accuracy (1% or better). This is not straightforward since in typical plasma sources such as capillary discharges (see Chapter 3) the density varies by several orders of magnitude in microsecond timescales.

6.1.3 Diagnostics of the Multibunched Electron Beam

In order to diagnose the quality of the microbunching of the IFEL modulated electron beam, we collected the CTR emitted when the microbunches traverse two 1 μm thick titanium foils [177]. CTR is emitted because the electric fields of the electrons in the beam displace violently the free electrons in the metal surfaces, which in turn radiate due to the acceleration they suffer.

In the experiment, the first metal foil was placed perpendicular to the beam direction of propagation and served the purpose of blocking the CO_2 radiation used to drive the IFEL, since it could interfere with the CTR signal measurement. The second foil was placed at 45^o with respect to the direction of propagation and emitted radiation through a window out of the beamline. The sum of the radiation emitted from both foils was collected.

In contrast to the CTR interferometry technique used in the experiment described in Chapter 4 (see section 4.2.1 and Appendix C.4), the microbunch spacing here was too short to be resolvable using interferometry. The spectrum of the CTR radiation was recorded instead, since it contains information about the longitudinal current profile of the electron beam. Specifically, the on-axis spectrum is proportional to the amplitude-squared of the Fourier

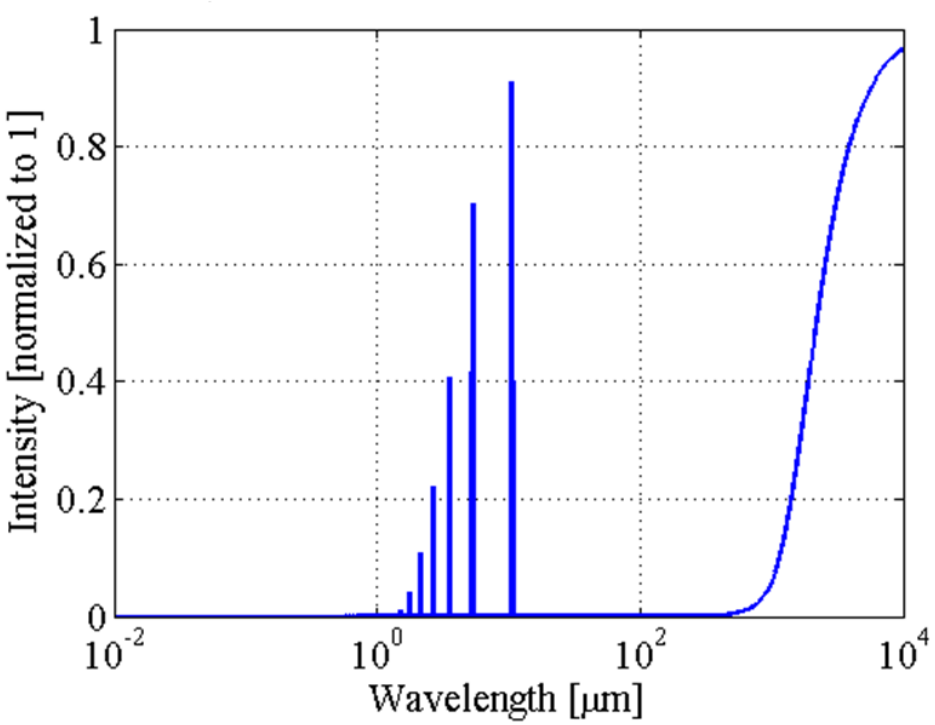

Figure 6.6: The spectrum of the CTR emitted when the microbunched electron beam passes through a metal foil.

transform of the current profile of the beam (see Appendix C.3). For a beam density defined in equation (66), the bunch form factor (which determines the CTR spectrum) is given by the formula

$$f\left(k;\theta\right)=e^{-\sigma_r^2k^2\sin^2\theta}e^{-\sigma_z^2k^2\cos^2\theta}\left|\sum_{j=1}^{M}A_je^{+ik\cos\theta\xi_j}\right|^2 \tag{68}$$

Here $k=2\pi/\lambda$ is the wavenumber of the radiation, θ is the radiation angle with respect to the radiation propagation direction[1], σ_r is the radial spot size of the beam, σ_z is the longitudinal spot size of each microbunch, M is the total number of microbunches, A_j are their relative charge amplitudes, and $z_j=j\lambda_p$ are their longitudinal locations.

[1] The detector has a surface area large enough to capture the radiation emitted at most of the angles.

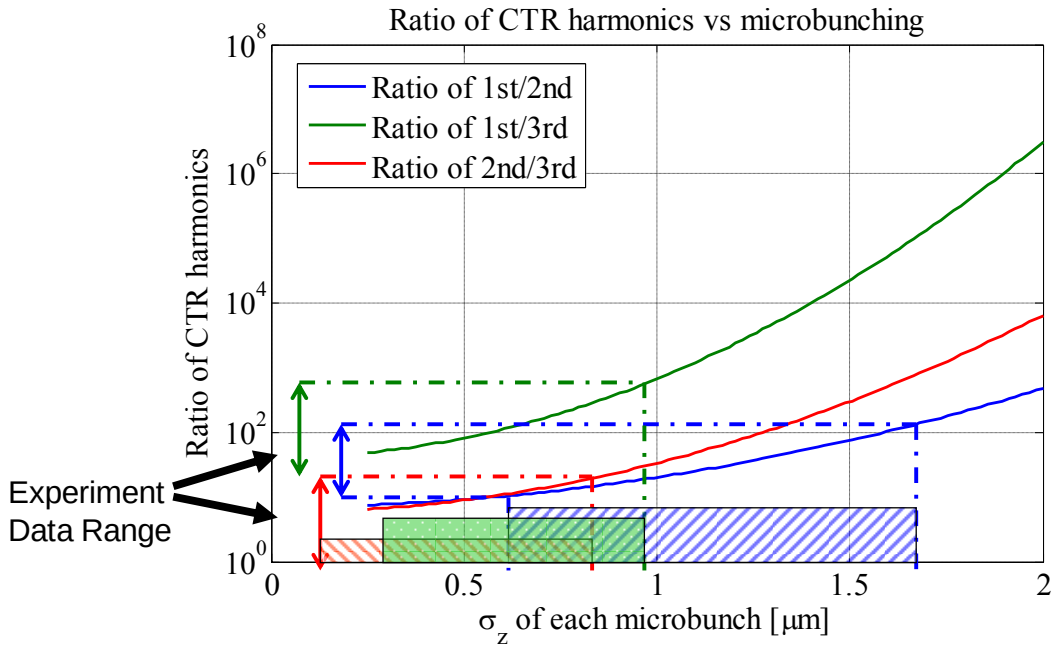

Figure 6.7: Ratio of energy collected in each harmonic of the CTR spectrum for various microbunch widths. The solid colored curves correspond to the theoretical predictions. The arrows on the left depict the experimentally recorded data. The three sets of data agree at the region around $\sigma_z \simeq 0.7\mu m$. These ratios include the response of the detector and the transmission of the filters.

The geometry of the electron beam is uniquely mapped into its CTR spectrum, which is shown on-axis in Figure 6.6 (for the beam profile shown in Figure 6.4). The low frequency (long wavelength) radiation on the right corresponds to the envelope of the beam. For other wavelengths, the radiation in general adds out-of-phase except at the harmonics of the separation wavelength $\lambda_0 = 10.6\mu m$ between the microbunches, $\lambda_m = \lambda_0 / m,\ \ m = 1,2,\ldots$. The existence of radiation at each harmonic is therefore the result of the periodicity of the microbunch train. Finally and most importantly, the amplitudes of these harmonics are modulated by the Fourier transform of each microbunch, which is assumed to be a Gaussian profile. Therefore, the measurement of the amplitude ratio between these harmonics provides a direct way of estimating the microbunches' width.

In order to collect the CTR, a helium-cooled bolometer detector sensitive between 3 μm – *20* μm wavelengths is used. Furthermore, narrow Gaussian band-pass filters with roughly 0.5 μm FWHM transmission were used to isolate the radiation of the first, second and third laser frequency harmonics, in successive measurements. After recording about 100 events at a roughly constant IFEL laser pulse energy (within a factor of 2) at all three harmonics, we calculated the three possible ratios of the signals. The data range for each ratio is shown on the vertical axis in Figure 6.7.

Using equation (68) for small angles ($\theta \simeq 0$) and after accounting for the response of the detector and the filters, we calculated the expected theoretical ratio between the energy radiated under each of the harmonics as a function of the microbunches' widths. These three predicted ratios are also plotted in Figure 6.7. The data show that the measured ratios indicate a microbunch width around $\sigma_z = 0.7 \pm 0.1 \mu m$, in good agreement with the predicted value of 0.5 μm. Although the microbunch width was inferred using CTR before [111], this is its first direct measurement that also utilizes the information from different harmonics.

In order to confirm the 10.6 μm separation between the microbunches, the IFEL drive laser was tuned to 10.2 μm, while still using the same narrowband 10.6 μm filter to detect the CTR. In that case the signal recorded was at least 100 times less than when the IFEL was driven at 10.6 μm and very close to the noise level of the detector, thus confirming the periodicity of the bunching at the laser wavelength only.

6.2 Generation of Microbunch Trains by Masking Chirped Beams

In this section we will describe a method for creating subpicosecond microbunches with adjustable spacing, which are required for most of the experiments described in this chapter.

Previous multibunch PWFA experiments relied on the different bunches to be created by very long beams being placed and bunched over different RF buckets in the linac [17, 79, 135]. Since those fields are in the microwave range, very low plasma densities had to be used (10^{11} cm^{-3} – 10^{13} cm^{-3}) in order for the plasma wavelength to be comparable with the bunch spacing, thus reducing the accelerating gradient significantly (which depends on the square root of the plasma density – see equation (2)). A future PWFA collider will require GeV-scale wakefields, which can only be achieved at high densities (10^{16} cm^{-3} and above). The plasma wavelength at those densities is on the order of 1 ps or less, and as a result a multibunch PWFA accelerator requires bunches separated at subpicosecond-scale spacing, a challenging process [155].

One method to create such microbunches is outlined in section 6.1.2 using velocity bunching after an IFEL interaction. However, in this case the spacing is not adjustable because it is fixed by the laser's wavelength. The method illustrated in the following section 6.2.1 uses a metal mask in a high-dispersion plane of the accelerator to create microbunches and does away of those limitations. CTR diagnostics of the output microbunches will be then presented from proof of principle experiments in section 6.2.2.

6.2.1 Mask Method

The principle of generating a train of microbunches is shown schematically in Figure 6.8. The electron beam enters the "dog-leg" portion of the beamline having a correlated energy spread along its length. In the case shown here, the front of the beam ("F") has a lower energy than the back of the beam ("B"). The first dipole disperses the different energies of the beam in space, and thus the energy-time correlation becomes also energy-space correlation. Subsequently, the metal mask that consists of a periodic set of metal wires is placed along the path of the beam, thus spoiling the emmitance of the particles that hit upon the solid parts of the mask which are

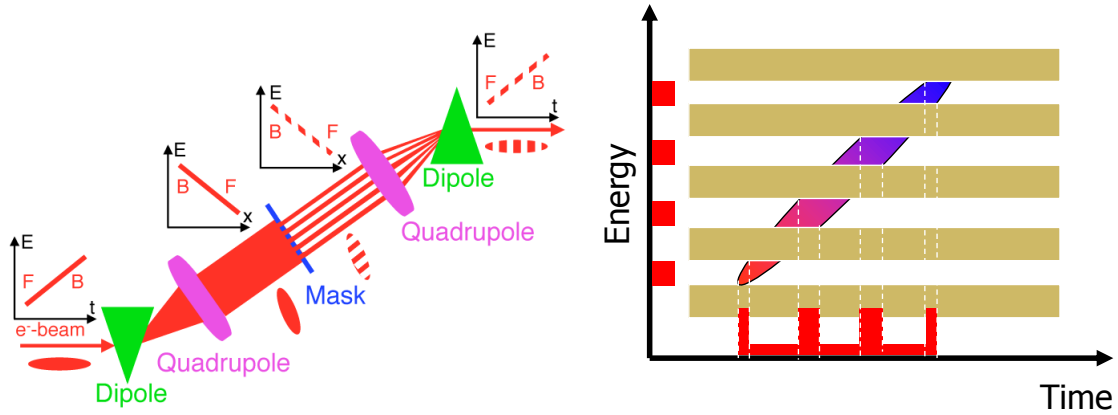

Figure 6.8: Left panel: Simplified schematic of the microbunch generation technique using the mask. The beam with a correlated energy spread enters the dog-leg on the left, is dispersed in space, goes through the mask, and then is brought back to energy-time correlation. The letters "F" and "B" stand for the front and back of the beam, respectively. Right panel: microbunch structure created by the wire mask in both time and energy. Source: P. Muggli.

then lost along the beam transport line. The energy-space microbunches then become energy-time microbunches when passing through a second dipole that removes the energy-space correlation of the beam.

The advantage of this technique is that the mask is fixed in space and therefore the microbunches are extremely stable, affected only by the incoming beam variations. The initial correlated energy spread can be introduced by accelerating the beam off the crest of the linac RF wave. The number of bunches can be selected by tuning the width of a limiting energy slit aperture, thus selectively blocking some parts of the initial beam. The width of the bunches can be selected by tuning the width of the wires on the mask. Note that a fraction d/D of the initial beam charge is lost after hitting the mask, where D is the separation between the wires on the mask and d their individual width. In addition, the shadow that is cast by the mask is crisp as long as the finite transverse size of the beam at the mask, σ_x, which is determined by its emmitance ε_N, is much smaller than the individual wire width:

$$\sigma_x = \sqrt{\frac{\beta_x \varepsilon_N}{\gamma}} \ll d \tag{69}$$

Here β_x is the beam beta function at the location of the mask, ε_N is the normalized emmitance of the beam, and γ is its relativistic parameter.

The distance between the microbunches is selected through the fractional energy spread imparted on the beam, $\Delta E / E_0$, with E_0 being the mean beam energy, for a given dispersion of the beam at the mask $\eta_{x,mask}$. Specifically, the longitudinal length of the beam at the exit of the dog-leg is $\sigma_z' = \sigma_z \pm R_{56} \Delta E / E_0$, where R_{56} is the dog-leg longitudinal dispersion function and σ_z is the beam length before the dog-leg. The transverse size L_x of the beam at the mask is a combination of its intrinsic beam size $\sigma_x = \sqrt{\beta_x \varepsilon_N / \gamma}$ and the dispersion width added by the magnets, $\sigma_\eta = \eta_{mask} \Delta E / E_0$. The mask is placed at a high-dispersion and low β_x plane along the beamline such that $\sigma_x \ll \sigma_\eta$ and thus

$$L_x = \sqrt{\sigma_x^2 + \sigma_\eta^2} \overset{\sigma_x \ll \sigma_\eta}{\simeq} \sigma_\eta \tag{70}$$

Therefore the number of microbunches is $N_b = \sigma_\eta / D$ and thus the bunch separation is given by the formula

$$\Delta z = \frac{\sigma_z'}{N_b} = D \frac{\sigma_z \pm R_{56} \left(\frac{\Delta E}{E_0} \right)}{\eta_{x,mask} \left(\frac{\Delta E}{E_0} \right)} \tag{71}$$

Although the mask here is periodic and the bunches are equidistant, a non-periodic mask with properly designed solid parts can be used to generate bunches at any position and with different

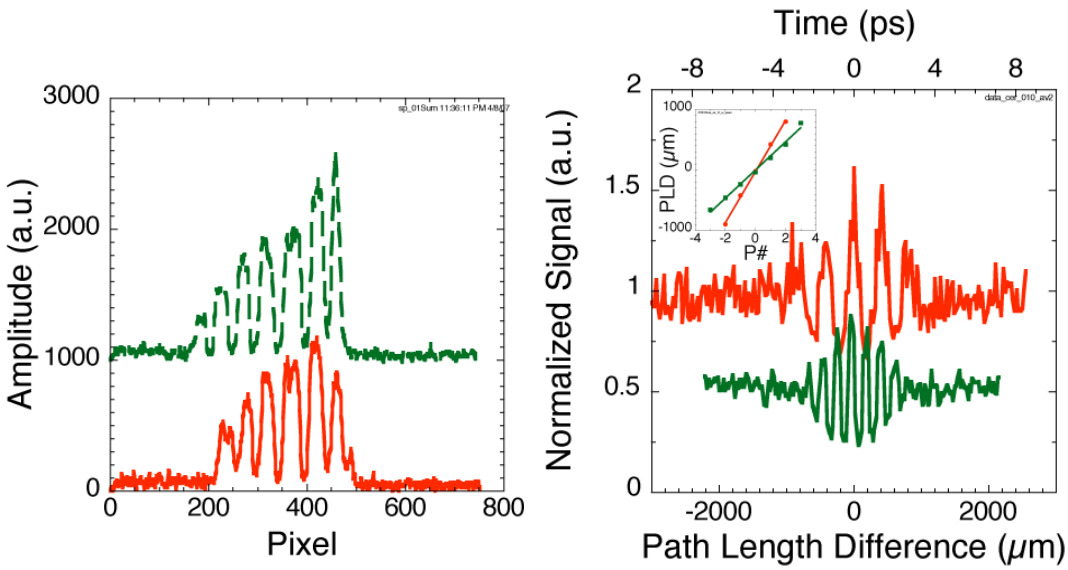

Figure 6.9: Left panel: Microbunches generated with the mask method dispersed in energy, for two cases with different number of bunches. Right panel: Auto-correlation time-integrated CTR traces as a function of the interferometer arms path length. N=3 bunches with 1.4% energy spread and N=4 bunches with 3.4% energy spread are shown. Source: P. Muggli.

mount of charge in each bunch. This is ideal for the multibunch setups explored in this chapter, especially for the creation of out-of-phase witness bunches.

6.2.2 Beam Diagnostics

In order to experimentally verify the generation of microbunches, CTR interferometry was employed in proof-of-principle setups at ATF [124]. This is similar to the technique described in section 4.2.1 that was used to diagnose the bunches in the double-bunch experiment, and is analyzed more in Appendix C.4. The CTR signal that is emitted when the bunches pass though a copper mirror is collected and sent through an interferometer that auto-correlates the signal in time. This auto-correlation time-integrated trace is recorded for different path lengths inside the interferometer by a liquid helium cooled silicon bolometer detector. A train of N equidistant bunches is expected to yield a symmetric trace with $2N+1$ peaks.

For the experimental setup at ATF, the mean beam energy was $E_0 = 58 MeV$, the dispersion of the beam at the mask was $\eta_{x,mask} = 1.4 m$, the initial envelope bunch length was $\sigma_z = 1650 \mu m$ (or 5.5 ps full width at half maximum), and the dog-leg dispersion was $R_{56} = -4 cm$. The total beam charge was $500 pC$, the typical energy spread on around 1% and the beam emmitance was $\varepsilon_N = 2 mm - mrad$. The mask was made of circular steel wires of diameter $d = 500 \mu m$ and separation period of $D = 1270 \mu m$. For this beam $\sigma_x \simeq 140 \mu m$ and condition (69) is moderately satisfied, while (70) is easily satisfied.

The left panel on Figure 6.9 shows the energy distribution profile of the beam after dispersed at the spectrometer at the end of the beamline, for $\Delta E / E_0 = 0.5\%$. By changing the width of the limiting slit either 6 or 7 bunches could be selected. The modulation of the number of particles per bunch reflects the initial profile of the incoming beam.

The right panel on Figure 6.9 shows two CTR auto-correlation traces for two incoming bunch parameters with energy spreads 1.5% & 3.4% and $N = 3$ & $N = 4$ bunches, respectively. The number of peaks in the traces is 5 and 7, in agreement with the $2N + 1$ expectation value. The distance between the bunches is measured from the distance between the peaks in the traces (shown in the inset panel), and corresponds to $434 \pm 22 \mu m$ and $216 \pm 60 \mu m$, respectively. Note that because only a portion of the CTR spectrum could be collected (low frequencies), the auto-correlation traces are not ideal and they have values smaller than the average. However this does not affect the bunch separation measurement. The above measured bunch periods are correctly predicted by equation (71) considering that the full width of the beam is a few times the quoted σ_z value.

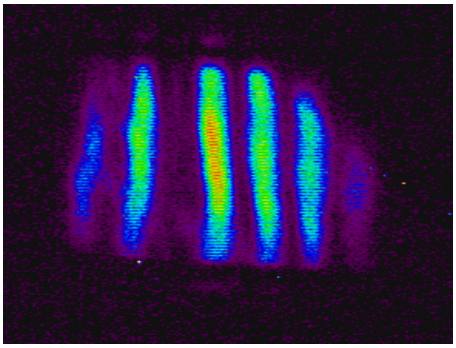

Figure 6.10: Electron energy spectrum of the bunched beam with 3 drive bunches and one strong witness bunch (out of phase) as recorded at the energy spectrometer at the end of the beamline. This is a favorable setup for a PWFA experiment. The horizontal axis is increasing energy to the right, while the vertical axis contains beam transverse profile information.

Finally, an example shot of the energy spectrum of the beam with 3 drive bunches and one witness bunch out of phase is shown in Figure 6.10. The rest of the bunches have been blocked by limiting energy slit. Notice that the separation of the drive bunches in energy ΔE is fixed by the period of the wires D for a given beam energy E_0 through $\Delta E = E_0 \cdot D / \eta_{mask}$.

6.3 Beam-Plasma Interactions Using the Mask

A series of experiments at the ATF have the goal of demonstrating proof-of-principle PWFA accelerators using multiple drive bunches. We will present here some simulations and experimental results specific to the ATF parameters, using the bunch generation technique described in the previous section. In the set presented here the drive bunches and the plasma density are adjusted such that the accelerator works in the maximum wakefield setup (see section 5.1.1) since we wish to first detect the maximum possible effect of the plasma on the bunches, and thereafter increase the transformer ratio in a future second set of experiments.

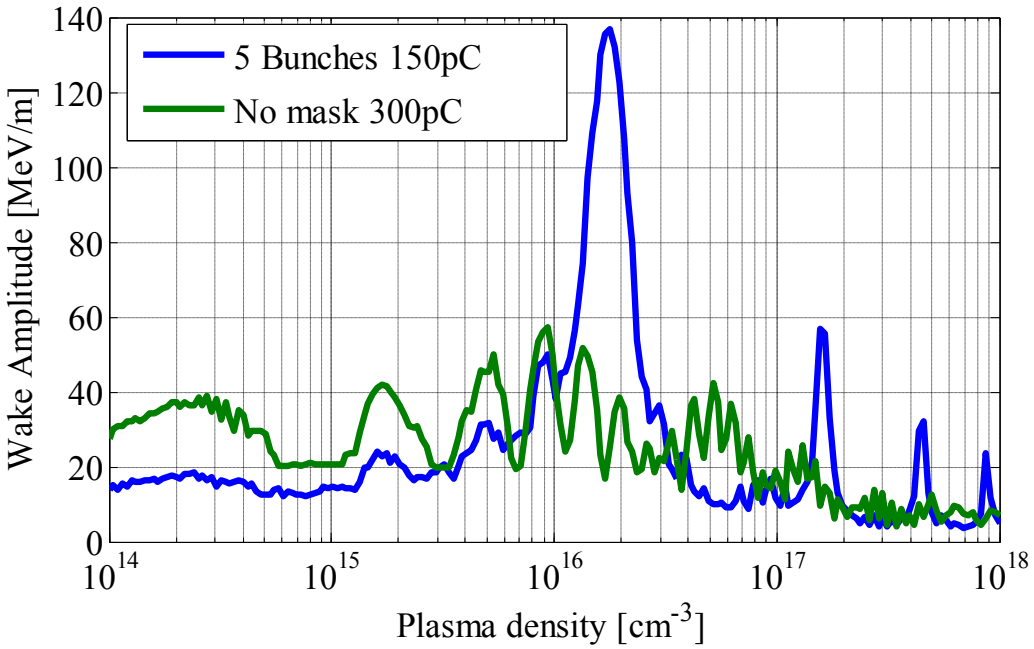

Figure 6.11: Plasma wakefield amplitude response as a function of the plasma density for a bunched and non-bunched square beam. The bunches are separated by one plasma wavelength and their width is half a plasma wavelength.

6.3.1 Predicted Response

The predicted plasma response as a function of the plasma density is shown in Figure 6.11. In the no-mask case the single 300 pC 4 ps long ATF electron beam is fed into the plasma, and the maximum wakefield amplitude is 60 MV/m assuming $\sigma_r = 100\mu m$. The envelope response appears in the 10^{14} – 10^{15} cm^{-3} density range, while the slight beating visible at higher densities relate to the fact that the model of the beam was a square bunch with sharp cutoffs at the edges. In the case where the wire mask was blocking sections of the beam to create the bunches, the total charge is 150 pC and is assumed to be distributed over 5 bunches which have width equal to 125 μm (half the plasma wavelength). The bunches are separated by one plasma wavelength apart. It is observed that the wakefields are very low for most densities, expect for the resonant density at 1.8×10^{16} cm^{-3} (where the wakes of all 5 bunches add in-phase) where the

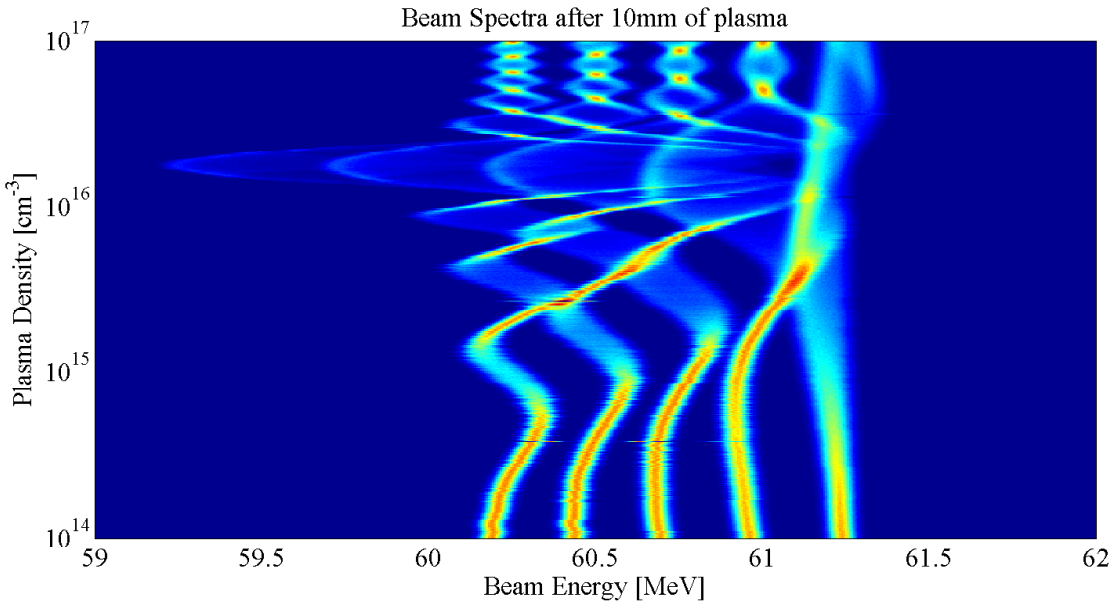

Figure 6.12: Energy spectrum of 5×30 pC drive bunches separated by 250 μm in space and by 0.25 MeV in energy as a function of the plasma density after 10 mm of plasma propagation. In densities above and below resonance the bunches suffer small energy spread, while at the resonance of 1.8×10^{16} cm^{-3} the wakefield is maximum and the energy spread becomes large. The last drive bunches samples the highest wakefield.

wake is expected to peak at 140 MV/m. Weaker wakefield peaks also appear at the plasma frequency harmonics. It is important to notice that the resonance width is around 20%[1], which is the accuracy with which the plasma density must be known in order to operate near it.

Since the bunches are also spaced apart in energy, each bunch samples a different phase of the wakefield and thus it will shift in energy. Those expected shifts in energy as a function of plasma density are simulated in Figure 6.12 using ThemOsiris after 10 mm of propagation in the plasma. The bunches are assumed equidistant in energy between 60 MeV and 61.5 MeV, separated by 0.25 MeV and their individual energy spread is 0.05 MeV. The first drive bunch has the higher energy, and is only experiences its own wake, thus the energy shift is relatively small. Later bunches experience their own wakefield plus the wakefield created from

[1] Inversely proportional to the number of bunches.

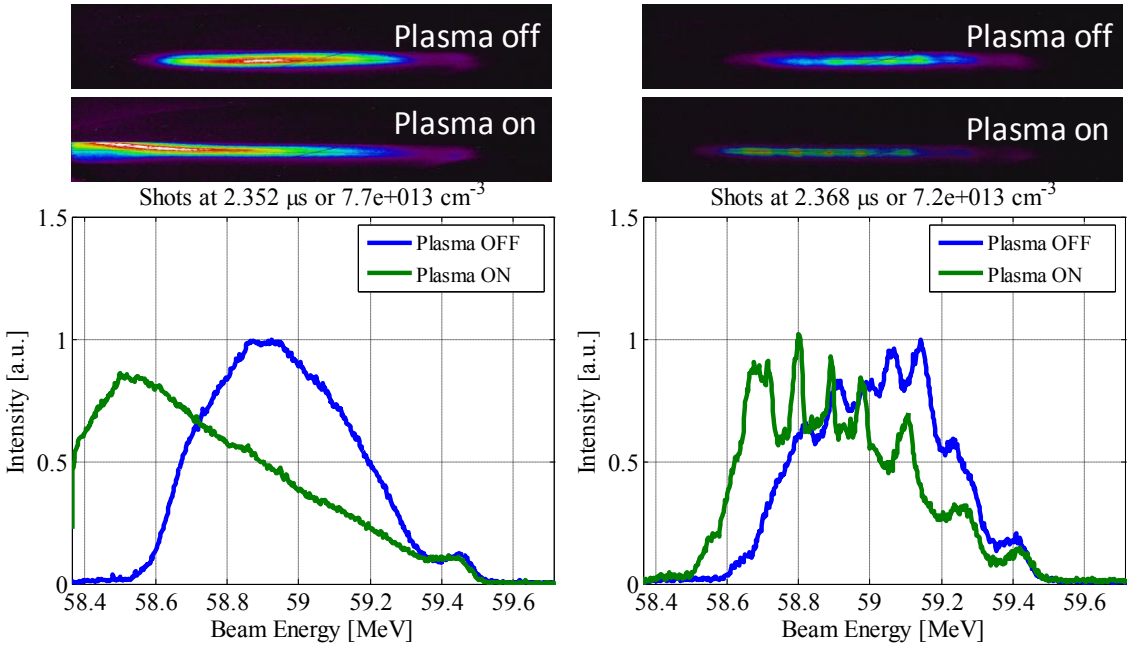

Figure 6.13: Recorded energy spectra of the bunched (right panel) and non-bunched (left panel) before and after a 6 mm long plasma at a low density.

all the previous bunches. At the resonant density of 1.8×10^{16} cm^{-3} the wakefield is maximum and this shows up as a strong spreading in energy, since the bunches are not much shorter than the plasma wavelength and sample half of its phase. In higher densities the bunches suffer small energy spreads.

6.3.2 Experimental Data

The experimentally recorded energy spectra of 7 bunches fed into a 6 mm plasma produced by a 25 kV capillary discharge at 150 Torr gas pressure (see details on the plasma source in Chapter 3) are shown in Figure 6.13 at a low density of 7×10^{13} cm^{-3}, selected by delaying the arrival of the beam with respect to the discharge. On the left panel the effect of the plasma on the full 300 pC – 400 pC beam was recorded, showing energy loss gradient of 35 MV/m compared to the plasma off case (as deduced from the energy loss for the given plasma length). In this setup the beam length is between 0.5 mm – 1 mm and has a transverse spot size close to 100 μm.

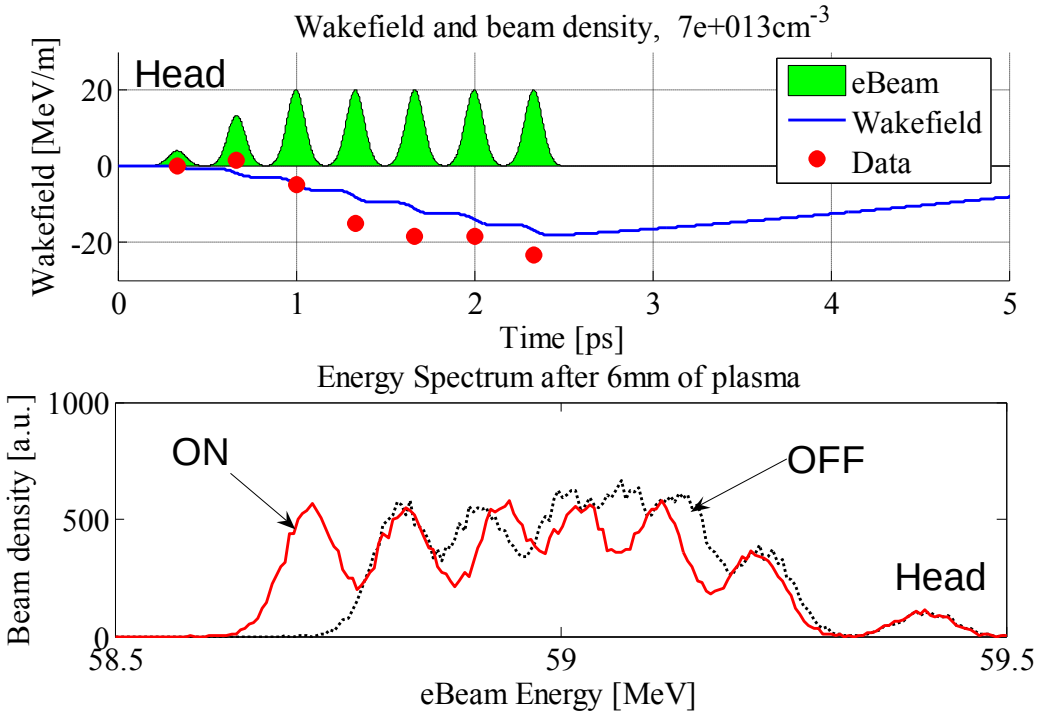

Figure 6.14: Simulated wakefield and energy spectra for the experimental data of the beam plasma interaction of Figure 6.13. The top panel shows the 7 bunches with 200 pC total charge fed into a 7×10^{13} cm^{-3} density 6 mm long plasma. The wakefield under each bunch deduced from the energy shifts is shown with red dots. The bottom panel shows the simulated energy spectra before and after the plasma.

When the mask is inserted the microbunches are now fed into the plasma (right panel), with a measured period (through CTR diagnostics) between 100 μm – 200 μm and width equal to half their period. The first drive bunch has the highest energy, around 59.4 MeV. The total charge now is reduced to roughly 100 pC – 200 pC, which results in a smaller average energy loss of 22 MV/m. This is still envelope interaction at the low density, as demonstrated by the increasingly larger energy loss of the later drive bunches. The simulated excited wakefield and energy spectra for the bunches is shown in Figure 6.14 and compared with the experimentally recorded energy shifts, demonstrating good agreement with the data.

Operation near the resonance is more challenging because the plasma density must be stable within ≈20% for the bunches shown here over the desired plasma length. Plasma

instabilities larger than these values, or non-uniform longitudinally plasmas will result in decreased wakefield. As was shown in Chapter 3, for capillary discharges the density may vary by 3 – 4 orders of magnitude over a few microseconds, and the beam needs to be timed to arrive within this 20% window around the resonance. If the plasma density varies as $n_p(t) = n_{\max} e^{-a(t-T)}$, and the enhanced wakefield is to be observed in a range of densities Δn around a resonant density n_0, then the time scale Δt over which the resonance will evolve is given by

$$\Delta t = \frac{1}{a} \ln \left(\frac{1 + \frac{1}{2}\frac{\Delta n}{n_0}}{1 - \frac{1}{2}\frac{\Delta n}{n_0}} \right) \overset{\frac{\Delta n}{n_0} \ll 1}{\simeq} \frac{1}{a}\frac{\Delta n}{n_0} \tag{72}$$

For example, if there is a $\Delta n / n_0 = 20\%$ wide resonance and the density drops exponentially with a coefficient $a = 2.9 \mu s^{-1}$, then $\Delta t \simeq 70 ns$. This is the time over which the density must be scanned in order for the resonance to be detected. Finally, instabilities in the incoming beam energy distribution may also affect the location of the resonance as the bunch period may drift during a run (see equation (71)).

6.4 Chapter Conclusions

The following items are concluded from this chapter:

- Using the IFEL technique the 5.5 ps long ATF beam can be modulated into ≈100 microbunches separated by 10.6 μm, which is predicted to resonantly excite a 1 GV/m wakefield when fed into a 10^{19} cm^{-3} density plasma.

- By recording the spectral energy under each harmonic of the CTR radiation when the beam traverses a metal foil the length of the individual microbunches was measured close to $0.7 \pm 0.1 \mu m$.

- A method for generating microbunch trains of tunable separation is presented by placing a metal wire mask at a high energy dispersion plane along the beam path and selectively blocking parts of the beam. 3 – 7 bunches with 200 μm – 400 μm separation were measured using CTR.

- Using the mask technique a 140 MV/m wakefield is predicted to be excited if the plasma density is matched to the bunch separation. This is 2 – 5 times stronger than any non-resonant wake, with or without the mask. The mask pattern can also be adjusted to create bunches for a maximum transformer ratio scheme.

- Wakefields around 20 MV/m where measured at low densities where the plasma responds to the envelope of the bunches, by observing the bunch energy shifts which increase with later bunches.

Write a wise saying and your name will live forever.

- Anonymous

Chapter 7

Conclusions

7.1 Summary of the Results

The main goal of this dissertation was to explore the use of multiple bunches as a tool for enhancing the performance of plasma wakefield accelerators. This was done through a unique combination of theory, simulations and experiments. In Chapter 1 we offered an overview of the role of particle accelerators in modern physics and we explained the need for new technologies based on harnessing the fields in waves driven in plasmas. In Chapter 2 the main aspects of plasma wakefield theory were rigorously laid out, and some aspects relevant to the transformer ratio and efficiency (both driving and beam-loading) of plasma accelerators were examined in more detail.

The need for plasma sources was addressed in Chapter 3. The main characteristics of capillary discharges were analyzed and a large volume of data was presented, based on many months of experimental work in ATF at BNL and in the Pulsed Power Lab at USC. We found that densities between 10^{14} cm^{-3} – 10^{19} cm^{-3} can be generated stably using capillary plasma sources, tunable through gas pressure, tube diameter, tube length and also by varying the time-delay of

the arrival of the electron beam during the discharge. The spectral diagnostic of Stark Broadening was found to be an excellent method for measuring the plasma density as long as the light spectra during the discharge are relatively clean such that the spectral lines can be identified.

In Chapter 4 we presented experimental evidence for the acceleration of a trailing witness electron bunch in the wakefields driven by a preceding bunch in a plasma. For the first time the accelerating gradient for such a scenario was above 100 MV/m while the bunch remains shorter than the plasma wavelength, thus being a promising technology for accelerating bunches to high energies while preserving the beam quality. It is most likely that any future plasma-based collider will require the acceleration of a trailing bunch in a similar fashion.

Chapter 5 laid the theoretical framework for creating high-transformer-ratio wakefields in a plasma accelerator through the use of multiple drive electron bunches. We find that it is possible to multiply the energy of an incoming electron beam when the position of the bunches and the charge per bunch are adjusted properly, as long as the beam can be maintained stable over long plasma lengths. The second half of this chapter demonstrates through simulations that indeed a witness beam can propagate over meter-scale plasmas if its emmitance of each bunch is properly matched to the increasing focusing force that each subsequent bunch experiences. Other than those elements the bunches need not be specially shaped, which implies that these ideas could be tested straightforwardly experimentally.

Finally, in Chapter 6 we presented some recent experimental results and diagnostics related to multibunch experiments. Two different techniques for generating multiple bunches were examined, either through IFEL bunching or by using the mask technique to selectively block portions of the incoming beam. Although some charge is inadvertently lost with this

method, it is found to offer great design flexibility, such as the easy creation of a witness electron bunch. Preliminary experimental results of the interaction of multiple bunches with plasmas are also presented in this chapter.

7.2 Future Work

After the exciting possibilities that multiple bunches open up for plasma accelerators, a variety of approaches require experimental testing. The most immediate one would be the acceleration of a trailing witness bunch using SLAC-scale gradients (GV/m) to very high energies. This would be a direct extension of both the energy doubling experiment [20] (which had a single bunch and high energy spread) and the trailing bunch acceleration experiment presented here in Chapter 4 (where the gradient was large but the energy gain was limited by the plasma length). Furthermore, such experiments need to also be conducted for positrons, the equally important other half of a possible PWFA-based future collider.

In addition, there is a lot of room for improvement in the demonstration of resonant plasma wakefields using multiple drive bunches. The wakefields need to be measured thoroughly as a function of the plasma density and the number of bunches in the drive beam. Subsequently, it is extremely important to demonstrate experimentally that multiple drive bunches can provide wakes with high transformer ratio. So far, only a small enhancement of 30% has been verified in dielectric accelerators [79]. Using the mask technique presented here, the required bunches can be designed. Using the plasma source suggestions also presented here, the required plasma source could also be built. ATF could provide the first proof-of-principle results at low energies, but eventually these schemes need to be tested in GeV-scale machines.

Simulations can also help greatly in examining the possibility of using multiple drive bunches over very long plasmas. There is still the question whether plasma instabilities, such as the electron hosing instability, will hinder the acceleration of witness beams. The electron hosing instability arises when the beam accelerates in pure ion channels in the blowout regime of PWFA, triggered by small transverse motions of the tail of the beam. This may not be an issue if the accelerator operates in the linear regime (as examined in this work) since there is no ion channel, yet this needs to be verified.

The work here can be extended in more detail in the nonlinear regime. Although using unshaped bunches does not seem to work directly in the nonlinear regime, simulations can indicate whether properly shaped bunches (such as a step function followed by a linear ramp) can lead to transformer ratio enhancements in the blowout regime as well. Such bunches, although more technically challenging to create, would take advantage of the nice focusing properties of the blowout regime and from the higher acceleration gradients (thus reducing the required plasma length, if also the high transformer ratio can be maintained).

Once high beam loading efficiency and high transformer ratio beams are generated, it will be important to generate them at high quality, starting with low energy spread. Currently this seems to be feasible by shaping the witness bunch in a reverse-ramped fashion that causes a constant wakefield under the bunch, thus reducing the energy spread. Another idea that has not been explored yet is to achieve that using the technique that is popular with conventional accelerators, which is to accelerate the beam on different slopes of the wakefields. By tuning the phase the beam can sample either a negative slope or a positive slope of the accelerating wave, thus on average compensating for the field variation across the beam. A similar effect could also be achieved in a plasma wakefield accelerator by tuning the phase of the witness

bunch. For example, one could implement a transverse magnetic field so that the beam acquires a transverse velocity that results in its dephasing with respect to the wake – this was suggested initially in [91] to actually avoid dephasing. Alternatively, plasma sections with different plasma densities could be placed in an alternating fashion such that the plasma wavelength is different between sections and thus the beam could sample in a similarly alternating fashion two different crests of the plasma wake, averaging out the wakefield variation.

7.3 Epilogue

We have come a long way since the ancient Greek philosopher Thales of Miletus wrote that by rubbing animal fur onto amber[1] a particular attraction was observed, thus providing the very first understanding of the electromagnetic forces. Had he been around Geneva today to see the underground tunnel of the Large Hadron Collider, without a doubt he would have been awed by the intricate ways that we have devised to manipulate these forces in order to probe the fundamental mysteries of Nature. Though the means may have changed, the spirit for discovery has remained unaltered through the ages; it has also inspired the writing of this dissertation in an attempt to allow plasma accelerators to aid the future of particle acceleration.

This dissertation will end in the same way it started, with a quote from Richard Feynman, this time taken from his "Lectures in Physics" to the Caltech undergraduate students in 1962. It is probably the shortest piece of text that I have ever seen to summarize all of the intricate interconnections of science so beautifully.

"A poet once said: *the whole universe is in a glass of wine*. We will probably never know in what sense he said that, for poets do not write to be understood. But it is true that if we look in glass of wine closely enough we see the entire universe. There are the things of physics: the

[1] Amber is "ήλεκτρον" in Greek, hence the name of the electron.

twisting liquid which evaporates depending on the wind and weather, the reflections in the glass, and our imagination adds the atoms. The glass is a distillation of the earth's rocks, and in its composition we see the secrets of the universe's age, and the evolution of the stars. What strange arrays of chemicals are in the wine? How did they come to be? There are the ferments, the enzymes, the substrates, and the products. There in wine is found the great generalization: all life is fermentation. Nobody can discover the chemistry of wine without discovering the cause of much disease. How vivid is the claret, pressing its existence into the consciousness that watches it! And if in our small minds, for some convenience, divide this glass of wine, *this universe*, into parts - physics, biology, geology, astronomy, psychology, and so on - remember that nature does not know it! So let us put it all back together, not forgetting ultimately what it is for. Let us give one more final pleasure: *drink it and forget it all*!"

Bibliography

[1] Large Hadron Collider <http://en.wikipedia.org/wiki/Large_Hadron_Collider>

[2] Stark Effect <http://en.wikipedia.org/wiki/Stark_Effect>

[3] "*ILC draft reference design report*",(2007).

[4] Abramowitz, M. and I. Stegun, *Handbook of Mathematical Functions with Formulas, Graphs, and Mathematical Tables* (Dover, 1964).

[5] Akhiezer, A. I. and R. V. Polovin, "*Theory of wave motion of an electron plasma*", Soviet Physics JETP 3, no.5, 696 (1956).

[6] Alexiou, S., "*Stark broadening of hydrogen lines in dense plasmas: Analysis of recent experiments*", Physical Review E (Statistical, Nonlinear, and Soft Matter Physics) 71, no.6 (2005).

[7] Ashkenazy, J., R. Kipper and M. Caner, "*Spectroscopic measurements of electron density of capillary plasma based on Stark broadening of hydrogen lines*", Physical Review A 43, no.10, 5568 (1991).

[8] Aubert, J. J. *et al.*, "*Experimental Observation of a Heavy Particle J*", Physical Review Letters 33, no.23, 1404 (1974).

[9] Bane, K. L. F., P. Chen and P. B. Wilson, "*On Collinear wakefield acceleration*", IEEE Transactions on Nuclear Science 32, no.5, 3524 (1985).

[10] Bane, K. L. F. and P. B. Wilson, "*Wakefields and Wakefield Acceleration*",SLAC-PUB-3528 (1984).

[11] Barnett, R. M. *et al.*, "*Review of Particle Physics*", Physical Review D 54, no.1, 1 (1996).

[12] Barov, N. *et al.*, "*Ultra high-gradient energy loss by a pulsed electron beam in a plasma*", in Proceedings of the Particle Accelerator Conference (IEEE, 2001), pp. 126.

[13] Barov, N. and J. B. Rosenzweig, "*Propagation of short electron pulses in underdense plasmas*", Physical Review E 49, no.5, 4407 (1994).

[14] Barov, N. *et al.*, "*Observation of plasma wakefield acceleration in the underdense regime*", Phys. Rev. ST Accel. Beams 3, 011301 (2000).

[15] Barov, N. *et al.*, "*Energy loss of a high-charge bunched electron beam in plasma: Analysis*", Phys. Rev. ST Accel. Beams 7, no.6 (2004).

[16] Bekefi, G., *Principles of Laser Plasmas* (John Wiley and Sons, 1976).

[17] Berezin, A. K. *et al.*, "*Wakefield excitation in plasma by a relativistic electron pulse with a controlled number of short bunches*", Plasma Physics Reports 20, no.7, 596 (1994).

[18] Bingham, R., "*Plasma physics: On the crest of a wake*", Nature 445, no.7129, 721 (2007).

[19] Blue, B. E. *et al.*, "*Plasma-Wakefield Acceleration of an Intense Positron Beam*", Physical Review Letters 90, no.21, 214801 (2003).

[20] Blumenfeld, I. *et al.*, "*Energy doubling of 42 GeV electrons in a metre-scale plasma wakefield accelerator*", Nature 445, no.7129, 741 (2007).

[21] Bobrova, N. A. *et al.*, "*Simulations of a hydrogen-filled capillary discharge waveguide*", Physical Review E 65, no.1, 016407 (2001).

[22] Boddeker, S. *et al.*, "*Shift and width of the Ha line of hydrogen in dense plasmas*", Physical Review E 47, no.4, 2785 (1993).

[23] Braun, H. H. *et al.*, "*Frequency and Temperature Dependence of Electrical Breakdown at 21, 30, and 39 GHz*", Physical Review Letters 90, no.22, 224801 (2003).

[24] Broks, B. H. P., K. Garloff and J. van der Mullen, "*Nonlocal-thermal-equilibrium model of a pulsed capillary discharge waveguide*", Physical Review E (Statistical, Nonlinear, and Soft Matter Physics) 71, no.1 (2005).

[25] Broks, B. H. P. *et al.*, "*Modeling of a square pulsed capillary discharge waveguide for interferometry measurements*", Physics of Plasmas 14, no.2, 023501 (2007).

[26] Buscher, S. *et al.*, "*The Stark width and shift of the hydrogen Ha line*", Journal of Physics B: Atomic, Molecular and Optical Physics 35, no.13, 2889 (2002).

[27] Campbell, L. P. *et al.*, "*Inverse Cerenkov acceleration and inverse free-electron laser experimental results for staged electron laser acceleration*", IEEE Transactions on Plasma Science 28, no.4, 1143 (2000).

[28] Catravas, P. *et al.*, "*Measurement of Electron-Beam Bunch Length and Emittance Using Shot-Noise-Driven Fluctuations in Incoherent Radiation*", Physical Review Letters 82, no.26, 5261 (1999).

[29] Chen, H. *et al.*, "*High Density Plasma in a High Pressure Hydrogen Capillary Discharge*", in Pulsed Power Plasma Science Conference (IEEE, 2007), pp. 288.

[30] Chen, P., "*A possible final focusing mechanism for linear colliders*", Particle Accelerators 20, 171 (1987).

[31] Chen, P. *et al.*, "*Acceleration of Electrons by the Interaction of a Bunched Electron Beam with a Plasma*", Physical Review Letters 54, no.7, 693 (1985).

[32] Chen, P. *et al.*, "*Energy Transfer in the Plasma Wake-Field Accelerator*", Physical Review Letters 56, no.12, 1252 (1986).

[33] Chen, P. *et al.*, "*Plasma Focusing for High-Energy Beams*", IEEE Transactions on Plasma Science 15, no.2, 218 (1987).

[34] Chiou, T. C. and T. Katsouleas, "*High Beam Quality and Efficiency in Plasma-Based Accelerators*", Physical Review Letters 81, no.16, 3411 (1998).

[35] Clayton, C. E. *et al.*, "*Transverse Envelope Dynamics of a 28.5-GeV Electron Beam in a Long Plasma*", Physical Review Letters 88, no.15, 154801 (2002).

[36] Clayton, C. E. *et al.*, "*Relativistic Plasma-Wave Excitation by Collinear Optical Mixing*", Physical Review Letters 54, no.21, 2343 (1985).

[37] Clayton, C. E. *et al.*, "*Ultrahigh-gradient acceleration of injected electrons by laser-excited relativistic electron plasma waves*", Physical Review Letters 70, no.1, 37 (1993).

[38] Coisson, R., "*Energy-loss calculation of gain in a plane sinusoidal free-electron laser*", IEEE Journal of Quantum Electronics 17, no.8, 1409 (1981).

[39] Collaboration, C. D. F. *et al.*, "*Observation of Top Quark Production in p-p Collisions with the Collider Detector at Fermilab*", Physical Review Letters 74, no.14, 2626 (1995).

[40] Crooks, W., *Radiant Matter* (Twenty First Century Books, 1879).

[41] Dawson, J., "*Nonlinear Electron Oscillations in a Cold Plasma*", Physical Review 113, no.2, 383 (1959).

[42] Dawson, J., "*Personal recollections on the development of Plasma Accelerators and light sources*", in The ninth workshop on advanced accelerator concepts, edited by P. Colestock and S. Kelley (AIP, 2001), pp. 3.

[43] Dawson, J. M., "*Plasma Particle Accelerators*", Scientific American 260, no.3, 54 (1987).

[44] Deng, S. *et al.*, "*Hose Instability and Wake Generation by an Intense Electron Beam in a Self-Ionized Gas*", Physical Review Letters 96, no.4, 045001 (2006).

[45] Deng, S. *et al.*, "*Plasma wakefield acceleration in self-ionized gas or plasmas*", Physical Review E 68, no.4, 047401 (2003).

[46] Eddington, A., "*The Physical Society of London Report on the Relativity Theory of Gravitation*", Nature 103, no.2575, 2 (1919).

[47] Edison, N. *et al.*, "*Characterization of a capillary-discharge plasma*", Physical Review E 47, no.2, 1305 (1993).

[48] Einstein, A., "*Die Feldgleichungen der Gravitation*", Sitzungsberichte der Preussischen Akademie der Wissenschaften zu Berlin, 844 (1915).

[49] England, R. J. *et al.*, "*Sextupole correction of the longitudinal transport of relativistic beams in dispersionless translating sections*", Phys. Rev. ST Accel. Beams 8, no.1 (2005).

[50] Esarey, E., C. B. Schroeder and W. P. Leemans, "*Laser-driven plasma-based accelerators"*,LBNL Technical Report, LBNL-53510 (2006).

[51] Esarey, E. *et al.*, "*Overview of plasma-based accelerator concepts*", IEEE Transactions on Plasma Science 24, no.2, 252 (1996).

[52] Esarey, E. *et al.*, "*Optically guided laser wake-field acceleration*", Physics of Fluids B: Plasma Physics 5, no.7, 2690 (1993).

[53] Escarguel, A. *et al.*, "*A single laser spark in aqueous medium*", Journal of Quantitative Spectroscopy and Radiative Transfer 64, no.4, 353 (2000).

[54] Escarguel, A. *et al.*, "*Highly nonlinear, sign-varying shift of hydrogen spectral lines in dense plasmas*", Physical Review E 62, no.2, 2667 (2000).

[55] Everett, M. *et al.*, "*Trapped electron acceleration by a laser-driven relativistic plasma wave*", Nature 368, no.6471, 527 (1994).

[56] Fainberg, Y., "*The use of plasma waveguides as accelerating structures in linear accelerators*", in CERN Symposium on High Energy Accelerators (CERN, 1956), p. 84.

[57] Fainberg, Y. *et al.*, "*Wakefield excitation in plasma by a train of relativistic electron bunches*", Plasma Physics Reports 20, no.7, 606 (1994).

[58] Faure, J. *et al.*, "*A laser-plasma accelerator producing monoenergetic electron beams*", Nature 431, no.7008, 541 (2004).

[59] Faure, J. *et al.*, "*Controlled injection and acceleration of electrons in plasma wakefields by colliding laser pulses*", Nature 444, no.7120, 737.

[60] Feynman, R., *The character of physical law* (Random House, Inc., 1994).

[61] Flih, S. A., E. Oks and Y. Vitel, "*Comparison of the Stark widths and shifts of the H-alpha line measured in a flash tube plasma with theoretical results*", Journal of Physics B: Atomic, Molecular and Optical Physics 36, no.2, 283 (2003).

[62] Flih, S. A. and Y. Vitel, "*Experimental profiles of hydrogen balmer alpha line emitted in weakly non-ideal plasmas*", in Spectral Line Shapes: Volume 11, 15th ICSLS, edited by J. Seidel (AIP, 2001), pp. 30.

[63] Geddes, C. G. R. *et al.*, "*High-quality electron beams from a laser wakefield accelerator using plasma-channel guiding*", Nature 431, no.7008, 538 (2004).

[64] Gigosos, M., M. Gonzalez and V. Cardenoso, "*Computer simulated Balmer-alpha, -beta and -gamma Stark line profiles for non-equilibrium plasmas diagnostics*", 5th European Furnace Symposium and 10th International Solid Sampling Colloquium with Atomic Spectroscopy 58, no.8, 1489 (2003).

[65] Gonsalves, A. J. *et al.*, "*Transverse Interferometry of a Hydrogen-Filled Capillary Discharge Waveguide*", Physical Review Letters 98, no.2, 025002 (2007).

[66] Griem, H., *Plasma Spectroscopy* (McGraw-Hill, 1964).

[67] Griem, H., *Spectral Line Broadening by Plasmas* (Academic, 1974).

[68] Griem, H., "*Shifts of hydrogen and ionized-helium lines from Delta n=0 interactions with electrons in dense plasmas*", Physical Review A 38, no.6, 2943 (1988).

[69] Griem, H. R., "*Stark Broadening of the Hydrogen Balmer-alpha Line in Low and High Density Plasmas*", Contributions to Plasma Physics 40, no.1-2, 46 (2000).

[70] Griem, R., H. Jacek and O. Wieslaw, "*Comparison of hydrogen Balmer-alpha Stark profiles measured at high electron densities with theoretical results*", Journal of Physics B: Atomic, Molecular and Optical Physics 38, no.7, 975 (2005).

[71] Hemker, R. G. *et al.*, "*Development of a parallel code for modeling plasma based accelerators*", in Proceedings of the Particle Accelerator Conference (IEEE, 1999), pp. 3672.

[72] Hofmann, I. and J. Struckmeier, "*Generalized three-dimensional equations for the emittance and field energy of high-current beams in periodic focusing structures*", Particle Accelerators 21, 69 (1987).

[73] Hogan, M. J. *et al.*, "*E-157: A 1.4-m-long plasma wake field acceleration experiment using a 30 GeV electron beam from the Stanford Linear Accelerator Center Linac*", Physics of Plasmas 7, 2241 (2000).

[74] Hogan, M. J. *et al.*, "*Multi-GeV Energy Gain in a Plasma-Wakefield Accelerator*", Physical Review Letters 95, no.5 (2005).

[75] Hogan, M. J. *et al.*, "*Ultrarelativistic-Positron-Beam Transport through Meter-Scale Plasmas*", Physical Review Letters 90, no.20, 205002 (2003).

[76] Hutchinson, I. H., *Principles of Plasma Diagnostics* (Cambridge University Press, 1987).

[77] Jackson, J., *Classical Electrodynamics* (Wiley, 1998).

[78] Jing, C. *et al.*, "*Observation of Enhanced Transformer Ratio in Collinear Wakefield Acceleration*", in 12th Advanced Accelerator Concepts Workshop, edited by M. Conde and C. Eyberger (AIP, 2006), pp. 511.

[79] Jing, C. *et al.*, "*Observation of Enhanced Transformer Ratio in Collinear Wakefield Acceleration*", Physical Review Letters 98, no.14, 144801 (2007).

[80] Jones, W. M., M. C. Healy and G. L. McCulloch, "*Ratio of Balmer line to spectrally adjacent emission, from the afterglow of a Z-pinch discharge in hydrogen*", Plasma Physics and Controlled Fusion 29, no.8, 1045 (1987).

[81] Joshi, C. *et al.*, "*High energy density plasma science with an ultrarelativistic electron beam*", in Review,Tutorial and Invited Papers from the 43rd Annual Meeting of the APS Division of Plasma Physics (AIP, 2002), pp. 1845.

[82] Joshi, C. *et al.*, "*Ultrahigh gradient particle acceleration by intense laser-driven plasma density waves*", Nature 311, no.5986, 525 (1984).

[83] Kaganovich, D. *et al.*, "*Investigations of double capillary discharge scheme for production of wave guide in plasma*", Applied Physics Letters 71, no.20, 2925 (1997).

[84] Kaganovich, D. *et al.*, "*High efficiency guiding of terawatt subpicosecond laser pulses in a capillary discharge plasma channel*", Physical Review E 59, no.5, R4769 (1999).

[85] Kallos, E. *et al.*, "*High-Gradient Plasma-Wakefield Acceleration with Two Subpicosecond Electron Bunches*", Physical Review Letters 100, no.7, 074802 (2008).

[86] Kallos, E. *et al.*, "*A Multibunch Plasma Wakefield Accelerator*", in Proceedings of the Particle Accelerator Conference (IEEE, 2005), pp. 3384.

[87] Kallos, E. *et al.*, "*Plasma wakefield acceleration utilizing multiple election bunches*", in Proceedings of the Particle Accelerator Conference (IEEE, 2007), pp. 3070.

[88] Kallos, E. *et al.*, "*Resonant Plasma Wakefield Experiment: Plasma Simulations and Multibunched Electron Beam Diagnostics*", in 12th Advanced Accelerator Concepts Workshop, edited by M. Conde and C. Eyberger (AIP, 2006), pp. 520.

[89] Katsouleas, T., "*Physical mechanisms in the plasma wake-field accelerator*", Physical Review A 33, no.3, 2056 (1986).

[90] Katsouleas, T., "*Plasma physics: On the node of a wave*", Nature 444, no.7120, 688 (2006).

[91] Katsouleas, T. and J. M. Dawson, "*Unlimited Electron Acceleration in Laser-Driven Plasma Waves*", Physical Review Letters 51, no.5, 392 (1983).

[92] Katsouleas, T. *et al.*, "*Beam loading in plasma accelerators*", Particle Accelerators 22, 81 (1987).

[93] Keinigs, R. and M. Jones, "*Two-dimensional dynamics of the plasma wakefield accelerator*", Physics of Fluids 30, no.1, 252 (1987).

[94] Kepple, P. and H. Griem, "*Improved Stark Profile Calculations for the Hydrogen Lines H alpha , H beta , H gamma , and H delta*", Physical Review 173, no.1, 317 (1968).

[95] Kim, S.-H. *et al.*, "*Capillary discharge in the open air*", IEEE Transactions on Magnetics 39, no.1, 244 (2003).

[96] Kimura, W. D. *et al.*, "*Detailed experimental results for laser acceleration staging*", Phys. Rev. ST Accel. Beams 4, no.10 (2001).

[97] Kimura, W. D. *et al.*, "*First Staging of Two Laser Accelerators*", Physical Review Letters 86, no.18, 4041 (2001).

[98] Kimura, W. D. *et al.*, "*Subpicosecond Double Electron Bunch Generation*", in 12th Advanced Accelerator Concepts Workshop, edited by M. Conde and C. Eyberger (AIP, 2006), pp. 527.

[99] Kitagawa, Y. *et al.*, "*Beat-wave excitation of plasma wave and observation of accelerated electrons*", Physical Review Letters 68, no.1, 48 (1992).

[100] Kozawa, T. *et al.*, "*Plasma wakefield acceleration experiments in overdense regime driven by narrow bunches*", in Proceedings of the Particle Accelerator Conference (IEEE, 1995), pp. 779.

[101] Kroll, N., P. Morton and M. Rosenbluth, "*Free-electron lasers with variable parameter wigglers*", IEEE Journal of Quantum Electronics 17, no.8, 1436 (1981).

[102] Langmuir, I., "*Oscillations in Ionized Gases*", Proceedings of the National Academy of Science 14, 627 (1928).

[103] Lawrence, E. and S. Livingston, "*The Production of High Speed Light Ions Without the Use of High Voltages*", Physical Review 40, no.1, 19 (1932).

[104] Laziev, E., V. Tsakanov and S. Vahanyan, "*Electromagnetic wave generation with high transformation ratio by intense charged particle bunches*", in EPAC (IEEE, 1988), pp. 523.

[105] Lee, S. *et al.*, "*Energy doubler for a linear collider*", Phys. Rev. ST Accel. Beams 5, no.1 (2002).

[106] Leemans, W. P. *et al.*, "*GeV electron beams from a centimetre-scale accelerator*", Nat Phys 2, no.10, 696 (2006).

[107] Leemans, W. P. *et al.*, "*Plasma guiding and wakefield generation for second-generation experiments*", IEEE Transactions on Plasma Science 24, no.2, 331 (1996).

[108] Levin, M. *et al.*, "*Longitudinal profiles of plasma parameters in a laser-ignited capillary discharge and implications for laser wakefield accelerator applications*", Applied Physics Letters 87, no.26, 261501 (2005).

[109] Li, B. and D. Kwok, "*Multi-dimensional transient process for a pulse ablating capillary discharge: modeling and experiment*", Journal of Plasma Physics 70, no.4, 379 (2004).

[110] Lihn, H.-C., "*Stimulated Coherent Transition Radiation*", Ph.D. Thesis, Stanford University (1996).

[111] Liu, Y. *et al.*, "*Experimental Observation of Femtosecond Electron Beam Microbunching by Inverse Free-Electron-Laser Acceleration*", Physical Review Letters 80, no.20, 4418 (1998).

[112] Lotov, K. V., "*Blowout regimes of plasma wakefield acceleration*", Physical Review E (Statistical, Nonlinear, and Soft Matter Physics) 69, no.4 (2004).

[113] Lu, W., "*Nonlinear Plasma Wakefield Theory and Optimum Scaling for Laser Wakefield Acceleration in the Blowout Regime*", Ph.D. Thesis, (2006).

[114] Lu, W. *et al.*, "*Nonlinear Theory for Relativistic Plasma Wakefields in the Blowout Regime*", Physical Review Letters 96, no.16 (2006).

[115] Lu, W. *et al.*, "*A nonlinear theory for multidimensional relativistic plasma wave wakefields*", Physics of Plasmas 13, no.5 (2006).

[116] Lu, W. *et al.*, "*Limits of linear plasma wakefield theory for electron or positron beams*", Physics of Plasmas 12, no.6, 063101 (2005).

[117] Lu, W. *et al.*, "*Generating multi-GeV electron bunches using single stage laser wakefield acceleration in a 3D nonlinear regime*", Phys. Rev. ST Accel. Beams 10, no.6 (2007).

[118] Maeda, R. *et al.*, "*Possibility of a multibunch plasma afterburner for linear colliders*", Physical Review Special Topics-Accelerators and Beams 7, no.11 (2004).

[119] Malka, V. *et al.*, "*Electron Acceleration by a Wake Field Forced by an Intense Ultrashort Laser Pulse*", Science 298, no.5598, 1596 (2002).

[120] Mangles, S. P. D. *et al.*, "*Monoenergetic beams of relativistic electrons from intense laser-plasma interactions*", Nature 431, no.7008, 535 (2004).

[121] Maxwell, J., "*A Dynamical Theory of the Electromagnetic Field*", Philosophical Transactions of the Royal Society of London 155, 459 (1865).

[122] Modena, A. *et al.*, "*Electron acceleration from the breaking of relativistic plasma waves*", Nature 377, no.6550, 606 (1995).

[123] Muggli, P. *et al.*, "*Meter-Scale Plasma-Wakefield Accelerator Driven by a Matched Electron Beam*", Physical Review Letters 93, no.1 (2004).

[124] Muggli, P. *et al.*, "*Generation and characterization of microbunched beams with a wire mesh mask*", in Proceedings of the Particle Accelerator Conference (IEEE, 2007), pp. 3079.

[125] Murokh, A. *et al.*, "*Bunch length measurement of picosecond electron beams from a photoinjector using coherent transition radiation*", Nuclear Instruments and Methods in Physics Research Section A: Accelerators, Spectrometers, Detectors and Associated Equipment 410, no.3, 452 (1998).

[126] Nakajima, K. *et al.*, "*Plasma wake-field accelerator experiments at KEK*", Nuclear Instruments and Methods in Physics Research Section A: Accelerators, Spectrometers, Detectors and Associated Equipment 292, no.1, 12 (1990).

[127] Nakamura, K. *et al.*, "*GeV electron beams from a centimeter-scale channel guided laser wakefield accelerator*", Physics of Plasmas 14, no.5, 056708 (2007).

[128] Nakanishi, H. *et al.*, "*Wakefield accelerator using twin linacs*", Nuclear Instruments and Methods in Physics Research Section A: Accelerators, Spectrometers, Detectors and Associated Equipment 328, no.3, 596 (1993).

[129] Nakanishi, H. *et al.*, "*Direct observation of plasma-lens effect*", Physical Review Letters 66, no.14, 1870 (1991).

[130] Newton, I., *The Principia: Mathematical Principles of Natural Philosophy* (University of California Press, 1999).

[131] O'Connell, "*Plasma production via field ionization*", Phys. Rev. ST Accel. Beams 9, 101301 (2006).

[132] Ogata, A., "*Plasma Lens and Wake Experiments in Japan*", in 5th Advanced Accelerator Concepts Workshop (AIP, 1993), pp. 420.

[133] Ogata, A. *et al.*, "*Plasma wakefield accelerator experiments in KEK*", in Proceedings of the Particle Accelerator Conference (IEEE, 1989), pp. 618.

[134] Ogata, A. *et al.*, "*Plasma lens and plasma Wakefield acceleration experiments using twin linacs*", in Proceedings of the Particle Accelerator Conference (IEEE, 1993), pp. 3552.

[135] Ogata, A. *et al.*, "*Direct observation of plasma wakefield caused by a train of LINAC bunches*", in Proceedings of the Particle Accelerator Conference (IEEE, 1991), pp. 622.

[136] Oz, E. *et al.*, "*Ionization-Induced Electron Trapping in Ultrarelativistic Plasma Wakes*", Physical Review Letters 98, no.8 (2007).

[137] Palmer, R., "*Interaction of Relativistic Particles and Free Electromagnetic Waves in the Presence of a Static Helical Magnet*", Journal of Applied Physics 43, no.7, 3014 (1972).

[138] Panofsky, W. K. H. and M. Breidenbach, "*Accelerators and detectors*", Reviews of Modern Physics 71, no.2, S121 (1999).

[139] Panofsky, W. K. H. and W. Wenzel, "*Transverse deflection of charged particles in radiofrequency fields*", Review of Scientific Instruments 27, 967 (1956).

[140] Parigger, C., J. W. L. Lewis and D. Plemmons, "*Electron number density and temperature measurement in a laser-induced hydrogen plasma*", Journal of Quantitative Spectroscopy and Radiative Transfer 53, no.3, 249 (1995).

[141] Parigger, C., D. Plemmons and E. Oks, "*Balmer Series Hβ Measurements in a Laser-Induced Hydrogen Plasma*", Appl. Opt. 42, no.30, 5992 (2003).

[142] Planck, M., "*On the Law of Distribution of Energy in the Normal Spectrum*", Annalen der Physik 4, 553 (1901).

[143] Powell, J. D. and A. E. Zielinski, "*Capillary discharge in the electrothermal gun*", IEEE Transactions on Magnetics 29, no.1, 591 (1993).

[144] Power, J. G., W. Gai and A. Kanareykin, "*Transformer ratio enhancement using a ramped bunch train in a collinear wakefield accelerator*", in The ninth workshop on advanced accelerator concepts, edited by P. Colestock and S. Kelley (AIP, 2001), pp. 605.

[145] Pukhov, A. and J. Meyer-Ter-Vehn, "*Laser wake field acceleration: the highly non-linear broken-wave regime*", Applied Physics B: Lasers and Optics 74, no.4, 355 (2002).

[146] Rosenzweig, J. B., "*Nonlinear plasma dynamics in the plasma wake-field accelerator*", Physical Review Letters 58, no.6, 555 (1987).

[147] Rosenzweig, J. B. *et al.*, "*Acceleration and focusing of electrons in two-dimensional nonlinear plasma wake fields*", Physical Review A 44, no.10, R6189 (1991).

[148] Rosenzweig, J. B. *et al.*, "*Experimental Observation of Plasma Wake-Field Acceleration*", Physical Review Letters 61, no.1, 98 (1988).

[149] Rosenzweig, J. B. *et al.*, "*Experimental measurement of nonlinear plasma wake fields*", Physical Review A 39, no.3, 1586 (1989).

[150] Rowlands-Rees, T. P. *et al.*, "*Laser-Driven Acceleration of Electrons in a Partially Ionized Plasma Channel*", Physical Review Letters 100, no.10, 105005 (2008).

[151] Rubens, H. and F. Kurlbaum, "*Untitled*", Proceedings of the Imperial Academy of Science, 929 (1900).

[152] Ruth, R. D. *et al.*, "*A plasma wakefield accelerator*", Particle Accelerators 17, 171 (1985).

[153] Ruth, R. D. and P. Chen, "*Plasma Accelerators"*,SLAC-PUB 3906 (1985).

[154] Schutt, P., T. Weiland and V. M. Tsakanov, "*On the wakefield acceleration using a sequence of driving bunches"*,DESY-M-88-13 (1988).

[155] Serafini, L., "*Micro-bunch production with radio frequency photoinjectors*", IEEE Transactions on Plasma Science 24, no.2, 421 (1996).

[156] Sheffield, J., *Plasma Scattering of Electromagnetic Radiation* (Academic Press, 1975).

[157] Shibata, Y. *et al.*, "*Observation of coherent transition radiation at millimeter and submillimeter wavelengths*", Physical Review A 45, no.12, R8340 (1992).

[158] Spence, D. J., P. Burnett and S. M. Hooker, "*Measurement of the electron-density profile in a discharge-ablated capillary waveguide*", Optics Letters 24, no.14, 993 (1999).

[159] Spence, D. J. and S. M. Hooker, "*Investigation of a hydrogen plasma waveguide*", Physical Review E 63, no.1, 015401 (2000).

[160] Stambulchik, E. *et al.*, "*Stark broadening of high principal quantum number hydrogen Balmer lines in low-density laboratory plasmas*", Physical Review E (Statistical, Nonlinear, and Soft Matter Physics) 75, no.1 (2007).

[161] Steffen, K. G., *High energy beam optics* (John Wiley, 1965).

[162] Steinhauer, L. C. and W. D. Kimura, "*Longitudinal space charge debunching and compensation in high-frequency accelerators*", Phys. Rev. ST Accel. Beams 2, no.8 (1999).

[163] Steinhauer, L. C. *et al.*, "*Analysis of Laser Wakefield Acceleration Using ATF CO2 Laser*", in Advanced Accelerator Concepts: Tenth Workshop (AIP, 2002), pp. 751.

[164] Stolyarov, D. *et al.*, "*Plasma Density Measurements in Hydrogen-Filled and Ablative Discharge Capillaries Based on Stark Broadening of Atomic Hydrogen Spectral Lines*", in 12th Advanced Accelerator Concepts Workshop, edited by M. Conde and C. Eyberger (AIP, 2006), pp. 784.

[165] Stupakov, G. and P. Emma, "*CSR wake for a short magnet in ultrarelativistic limit*", in EPAC (IEEE, 2002), pp. 1479.

[166] Su, J. J. *et al.*, "*Stability of the Driving Bunch in the Plasma Wakefield Accelerator*", IEEE Transactions on Plasma Science 15, no.2, 192 (1987).

[167] Su, J. J. *et al.*, "*Plasma lenses for focusing particle beams*", Physical Review A 41, no.6, 3321 (1990).

[168] Tajima, T. and J. M. Dawson, "*Laser Electron Accelerator*", Physical Review Letters 43, no.4, 267 (1979).

[169] Tonks, L. and I. Langmuir, "*Oscillations in Ionized Gases*", Physical Review 33, no.2, 195 (1929).

[170] Tsung, F. S. *et al.*, "*Near-GeV-Energy Laser-Wakefield Acceleration of Self-Injected Electrons in a Centimeter-Scale Plasma Channel*", Physical Review Letters 93, no.18, 185002 (2004).

[171] Vidal, C. R. and J. Cooper, "*Heat-Pipe Oven: A New, Well-Defined Metal Vapor Device for Spectroscopic Measurements*", Journal of Applied Physics 40, no.8, 3370 (1969).

[172] Vitel, Y. *et al.*, "*Spectra of dense pure hydrogen plasma in Balmer area*", Journal of Quantitative Spectroscopy and Radiative Transfer 83, no.3-4, 387 (2004).

[173] Wiese, W. L., D. E. Kelleher and D. R. Paquette, "*Detailed Study of the Stark Broadening of Balmer Lines in a High-Density Plasma*", Physical Review A 6, no.3, 1132 (1972).

[174] Wilks, S. *et al.*, "*Beam Loading in Plasma Waves*", IEEE Transactions on Plasma Science 15, no.2, 210 (1987).

[175] Wilson, I., "*The compact linear collider CLIC*", Physics Reports 403-404, 365 (2004).

[176] Ya *et al.*, "*Wake field excitation in plasma by a train of relativistic electron bunches*", Plasma Physics Reports 20, no.7, 606 (1994).

[177] Yakimenko, V. *et al.*, "*Generation and Characterization of the Microbunched Beams in the Range from 0.3 to 500 Femtoseconds*", in 28th International Free Electron Laser Conference (BESSY, 2006), pp. 481.

[178] Yakimenko, V. and R. Ischebeck, "*Summary Report of Working Group 4: e-Beam Driven Accelerators*", in 12th Advanced Accelerator Concepts Workshop (AIP, Lake Geneva, Wisconsin (USA), 2006), pp. 158.

[179] Yakimenko, V. *et al.*, "*Cohesive Acceleration and Focusing of Relativistic Electrons in Overdense Plasma*", Physical Review Letters 91, no.1, 014802 (2003).

[180] Zeng, X. *et al.*, "*Laser-induced shockwave propagation from ablation in a cavity*", Applied Physics Letters 88, no.6, 061502 (2006).

[181] Zoler, D. and R. Alimi, "*A proof of the need for consistent treatment in modelling of capillary ablative discharges*", Journal of Physics D: Applied Physics 28, no.6, 1141 (1995).

Appendix A

PWFA Linear Theory

A.1 Impulse Response of a Plasma

In this section the electric field that is excited when a relativistic charged beam enters a plasma is derived. The analysis applies to linear theory, where the beam density n_b is much smaller that the plasma density n_p, $n_b \ll n_p$. Also, we will only deal with two dimensions in a system will cylindrical symmetry, so there is no azimuthal dependence and $\frac{\partial}{\partial \phi} = 0$.

We start by writing Maxwell's equations in a homogeneous linear medium:

$$\begin{aligned} \nabla \times \vec{E} &= -\frac{\partial \vec{B}}{\partial t} \\ \nabla \times \vec{B} &= \mu_0 \vec{J} + \frac{1}{c^2}\frac{\partial \vec{E}}{\partial t} \\ \nabla \cdot \vec{E} &= \frac{\rho}{\varepsilon_0} \\ \nabla \cdot \vec{B} &= 0 \end{aligned} \tag{73}$$

Since in this regime the ion motion is negligible, $\frac{n_b}{n_p} \ll \frac{M_i}{m_e}$, we can assume static ions and only write down Newton's second law of motion for the electrons:

$$\frac{d\vec{p}_e}{dt} = -e\vec{E} - e\vec{v}_e \times \vec{B} \tag{74}$$

Finally the equation of continuity for the electrons is included:

$$\frac{\partial n_e}{\partial t} + \nabla \cdot \left(n_e \vec{v}_e \right) = 0 \tag{75}$$

The electron momentum, the charge density and the current density are defined as follows for an electron beam:

$$\begin{aligned} \vec{p}_e &= \gamma m_e \vec{v}_e = \frac{1}{\sqrt{1 - \frac{v_e^2}{c^2}}} m_e \vec{v}_e \\ \rho &= \rho_{beam} + \rho_{ions} + \rho_{electrons} = -en_b + en_i - en_e \\ \vec{J} &= \vec{J}_{beam} + \vec{J}_{electrons} = -en_b \vec{v}_b - en_e \vec{v}_e \end{aligned} \tag{76}$$

There are 10 unknowns in the above 12 equations: $\vec{E}, \vec{B}, \vec{v}_e, n_e$. There are 2 more equations than unknown variables because Gauss's laws for the electric and magnetic fields can be derived from the other two Maxwell's equations when they are combined with the continuity (or charge conservation) equation.

The next step is to linearize the equations, assuming that the quantities that are examined are just small perturbations over the initial state values (at $t = 0$). The unknowns can be written as follows:

$$\begin{aligned} \vec{E} &\simeq \underbrace{\vec{E}_0}_{0} + \vec{E}_1 \\ \vec{B} &\simeq \underbrace{\vec{B}_0}_{0} + \vec{B}_1 \\ \vec{v}_e &\simeq \underbrace{\vec{v}_0}_{0} + \vec{v}_1 \\ n_e &\simeq n_0 + n_1 \\ n_i &\simeq n_0 \\ \vec{J} &\simeq \vec{J}_b + \underbrace{\vec{J}_0}_{0} + \vec{J}_1 = -en_b \vec{v}_b - en_e \vec{v}_e \simeq -ecn_b \hat{z} - en_0 \vec{v}_1 \end{aligned} \tag{77}$$

There are several items to note here. The plasma starts from a neutral state, so the initial density of electrons is equal to the initial density of ions. Also, since the plasma is assumed homogeneous there is no initial net electric or magnetic field. In addition, the plasma electrons

start out motionless (cold) so there is no initial velocity, and the ions are static so there is no density perturbation assigned to them. Lastly, the beam is assumed to move close to the speed to light in the z-direction, i.e. $\vec{v}_b \simeq c\hat{z}$. The equations now become in the nonrelativistic limit:

$$\begin{aligned}
&\nabla \times \vec{E}_1 = -\frac{\partial \vec{B}_1}{\partial t} \\
&\nabla \times \vec{B}_1 = \mu_0 \vec{J}_1 + \frac{1}{c^2}\frac{\partial \vec{E}_1}{\partial t} \\
&\nabla \cdot \vec{E}_1 = \frac{1}{\varepsilon_0}\left(-en_b + en_0 - en_0 - en_1\right) \\
&\nabla \cdot \vec{B}_1 = 0 \\
&m_e\left(\frac{\partial \vec{v}_1}{\partial t} + \vec{v}_1 \cdot \left(\nabla \cdot \vec{v}_1\right)\right) = -e\vec{E}_1 - e\vec{v}_1 \times \vec{B}_1 \\
&\frac{\partial n_1}{\partial t} + \nabla \cdot \left(\left(n_0 + n_1\right)\vec{v}_1\right) = 0
\end{aligned} \tag{78}$$

By ignoring the second order terms (the products of two first order terms) because these first order perturbations are assumed to be very small compared to the initial values ($n_1 \ll n_0$, etc), the equations become

$$\begin{aligned}
&\nabla \times \vec{E}_1 = -\frac{\partial \vec{B}_1}{\partial t} \\
&\nabla \times \vec{B}_1 = \mu_0 \vec{J}_1 + \mu_0 \vec{J}_b + \frac{1}{c^2}\frac{\partial \vec{E}_1}{\partial t} \\
&\nabla \cdot \vec{E}_1 = -\frac{e}{\varepsilon_0} n_b - \frac{e}{\varepsilon_0} n_1 \\
&\nabla \cdot \vec{B}_1 = 0 \\
&\frac{\partial \vec{v}_1}{\partial t} = -\frac{e}{m_e}\vec{E}_1 \\
&\frac{\partial n_1}{\partial t} + n_0 \nabla \cdot \vec{v}_1 = 0
\end{aligned} \tag{79}$$

The first goal now is just to solve for the density perturbation. Taking the time derivative of the continuity equation and then replacing from the equation of motion:

$$\frac{\partial^2 n_1}{\partial t^2} + n_0 \nabla \cdot \frac{\partial \vec{v}_1}{\partial t} = 0 \qquad \Rightarrow \frac{\partial^2 n_1}{\partial t^2} - \frac{e n_0}{m_e} \nabla \cdot \vec{E}_1 = 0 \tag{80}$$

The electric field can be replaced from Gauss's law to yield:

$$\frac{\partial^2 n_1}{\partial t^2} + \omega_p^2 n_1 = -\omega_p^2 n_b \tag{81}$$

A.2 The Density Perturbation Response

Let's now assume as an input beam a delta function, a single electron at a specific point $\vec{R}$ in time and space moving at a relativistic speed $\vec{v}_b \simeq c\hat{z}$ into the plasma:

$$\begin{aligned} &n_b(r,z,t) = \delta\left(\vec{R} - \vec{v}_b t\right) = \delta(\vec{r})\delta\left(z\hat{z} - ct\hat{z}\right) = \delta(\vec{r})\delta(\xi) \\ &\delta(\vec{r}) = \frac{1}{2\pi r}\delta(r) \end{aligned} \tag{82}$$

since the beam is dependent not simply on the time variable t but on the variable $z - ct$, we expect all the parameters in the system to by finally dependent only on $\xi = z - ct$. This means that the time derivative $\frac{\partial}{\partial t}$ can be replaced with $-c\frac{\partial}{\partial \xi}$.

Equation (81) now becomes

$$\frac{\partial^2 n_1}{\partial \xi^2} + k_p^2 n_1 = -k_p^2 \delta(\vec{r})\delta(\xi) \tag{83}$$

Where $k_p = \frac{\omega_p}{c}$ is the plasma wavenumber. In order to solve this differential equation the Laplace transform is applied (for the ξ variable):

$$\begin{aligned} &s^2 L\{n_1\} - s\underbrace{n_1(0)}_{0} - \underbrace{n_1'(0)}_{0} + k_p^2 L\{n_1\} = -k_p^2 \delta(\vec{r}) \Rightarrow \\ &\Rightarrow L\{n_1\} = -\delta(\vec{r})\frac{k_p^2}{s^2 + k_p^2} \qquad \Leftrightarrow \qquad n_1(r,\xi) = -k_p \delta(\vec{r}) \sin\left(k_p \xi\right) U(\xi) \end{aligned} \tag{84}$$

This is the density perturbation impulse response of the plasma. Here $U(\xi)$ is the Heaviside step function (zero for $\xi<0$, unity for $\xi>0$, and equal to ½ for $\xi=0$). The total density perturbation for a general beam density $n_b(r,\xi)=n_{b\perp}(r)n_{b\|}(\xi)$ is found by integrating the above result (Green's function) over the whole space:

$$n_1(r,\xi)=-k_p\int_{-\infty}^{+\infty}d\xi'\int_0^{+\infty}2\pi r'dr'n_{b\perp}(r')n_{b\|}(\xi')\delta(\vec{r}')\sin\left(k_p(\xi-\xi')\right)U(\xi-\xi')=$$
$$=-k_p\int_{-\infty}^{+\infty}n_{b\|}(\xi')\sin\left(k_p(\xi-\xi')\right)U(\xi-\xi')d\xi'\cdot\underbrace{\int_0^{+\infty}n_{b\perp}(r')\delta(\vec{r}-\vec{r}')2\pi(r-r')dr'}_{n_{b\perp}(r)}\Rightarrow$$

$$\begin{aligned}n_1(r,\xi)&=-k_p n_{b\perp}(r)\int_{-\infty}^{\xi}n_{b\|}(\xi')\sin\left(k_p(\xi-\xi')\right)d\xi'=\\&=-\frac{\varepsilon_0k_p^2}{e}Z(\xi)n_{b\perp}(r)\end{aligned}\qquad(85)$$

Where in the last step we have defined the wakefield function (for reasons that will become apparent later) as

$$Z(\xi)\equiv\frac{e}{\varepsilon_0k_p}\int_{-\infty}^{\xi}n_{b\|}(\xi')\sin\left(k_p(\xi-\xi')\right)d\xi'\qquad(86)$$

A.3 The Electric Field Perturbation Response

Now that the density perturbation is known, the response of the electric can be calculated. First, take the curl of Faraday's law:

$$\nabla\times\left(\nabla\times\vec{E}_1\right)=-\frac{\partial}{\partial t}\left(\nabla\times\vec{B}_1\right)\qquad\Rightarrow\qquad\nabla^2\vec{E}_1-\vec{\nabla}\left(\nabla\cdot\vec{E}_1\right)=\frac{\partial}{\partial t}\left(\nabla\times\vec{B}_1\right)\qquad(87)$$

Now insert the curl of the magnetic field from Faraday's law and the div of the electric field from Gauss's law:

$$\nabla^2\vec{E}_1-\vec{\nabla}\left(-\frac{e}{\varepsilon_0}n_b-\frac{e}{\varepsilon_0}n_1\right)=\frac{\partial}{\partial t}\left(\mu_0\vec{J}_1+\mu_0\vec{J}_b+\frac{1}{c^2}\frac{\partial\vec{E}_1}{\partial t}\right)\Rightarrow$$
$$\Rightarrow\nabla^2\vec{E}_1+\frac{e}{\varepsilon_0}\vec{\nabla}n_b+\frac{e}{\varepsilon_0}\vec{\nabla}n_1=\mu_0\frac{\partial\vec{J}_1}{\partial t}+\mu_0\frac{\partial\vec{J}_b}{\partial t}+\frac{1}{c^2}\frac{\partial^2\vec{E}_1}{\partial t^2}\Rightarrow \quad (88)$$
$$\Rightarrow\nabla^2\vec{E}_1-\frac{1}{c^2}\frac{\partial^2\vec{E}_1}{\partial t^2}=-en_0\mu_0\frac{\partial\vec{v}_1}{\partial t}-ec\mu_0\hat{z}\frac{\partial n_b}{\partial t}-\frac{e}{\varepsilon_0}\vec{\nabla}n_b-\frac{e}{\varepsilon_0}\vec{\nabla}n_1$$

As before, since everything is a function of $\xi=z-ct$, the derivatives with respect to time can be replaced as $\frac{\partial}{\partial t}\to-c\frac{\partial}{\partial\xi}$. Then

$$\nabla^2\vec{E}_1-\frac{\partial^2\vec{E}_1}{\partial\xi^2}=ecn_0\mu_0\frac{\partial\vec{v}_1}{\partial\xi}+ec^2\mu_0\hat{z}\frac{\partial n_b}{\partial\xi}-\frac{e}{\varepsilon_0}\vec{\nabla}n_b-\frac{e}{\varepsilon_0}\vec{\nabla}n_1 \quad (89)$$

The only unknown here (other that the electric field) is the electron velocity perturbation $\vec{v}_1$, which can be simply replaced from Newton's law of motion: $\frac{\partial\vec{v}_1}{\partial t}=-\frac{e}{m_e}\vec{E}_1$ or $\frac{\partial\vec{v}_1}{\partial\xi}=\frac{e}{cm_e}\vec{E}_1$. Then

$$\nabla^2\vec{E}_1-\frac{\partial^2\vec{E}_1}{\partial\xi^2}=ecn_0\mu_0\frac{e}{cm_e}\vec{E}_1+ec^2\mu_0\hat{z}\frac{\partial n_b}{\partial\xi}-\frac{e}{\varepsilon_0}\vec{\nabla}n_b-\frac{e}{\varepsilon_0}\vec{\nabla}n_1\Rightarrow$$
$$\Rightarrow\left(\nabla^2-\frac{\partial^2}{\partial\xi^2}-k_p^2\right)\vec{E}_1=+ec^2\mu_0\hat{z}\frac{\partial n_b}{\partial\xi}-\frac{e}{\varepsilon_0}\vec{\nabla}n_b-\frac{e}{\varepsilon_0}\vec{\nabla}n_1 \quad (90)$$

Now consider that the ∇ operator can be written as

$$\nabla^2=\nabla_r^2+\frac{\partial^2}{\partial^2 z^2}=\frac{1}{r}\frac{\partial}{\partial r}\left(r\frac{\partial}{\partial r}\right)+\frac{\partial^2}{\partial^2 z^2}$$
$$\vec{\nabla}=\hat{r}\frac{\partial}{\partial r}+\hat{z}\frac{\partial}{\partial z} \quad (91)$$

However the variable z is not independent but we have written it as a function of ξ. Therefore since $\xi=z-ct$ we can just replace $\frac{\partial}{\partial z}\to\frac{\partial}{\partial\xi}$. The operators become

$$\nabla^2 = \nabla_r^2 + \frac{\partial^2}{\partial^2 \xi^2} = \frac{1}{r}\frac{\partial}{\partial r}\left(r\frac{\partial}{\partial r}\right) + \frac{\partial^2}{\partial^2 \xi^2}$$
$$\vec{\nabla} = \hat{r}\frac{\partial}{\partial r} + \hat{z}\frac{\partial}{\partial \xi} \tag{92}$$

Now the quantities on the right hand side become

$$\frac{\partial n_b}{\partial \xi} = \frac{\partial}{\partial \xi}\left[\delta(\vec{r})\delta(\xi)\right] = \delta(\vec{r})\delta'(\xi)$$
$$\vec{\nabla} n_b = \hat{r}\frac{\partial n_b}{\partial r} + \hat{z}\frac{\partial n_b}{\partial \xi} = \hat{r}\delta'(\vec{r})\delta(\xi) + \hat{z}\delta(\vec{r})\delta'(\xi)$$
$$\vec{\nabla} n_1 = -\hat{r}k_p\frac{\partial}{\partial r}\left[\delta(\vec{r})\sin(k_p\xi)U(\xi)\right] - \hat{z}k_p\frac{\partial}{\partial \xi}\left[\delta(\vec{r})\sin(k_p\xi)U(\xi)\right] =$$
$$= -\hat{r}k_p\delta'(\vec{r})\sin(k_p\xi)U(\xi) - \hat{z}k_p^2\delta(\vec{r})\cos(k_p\xi)U(\xi) \tag{93}$$

Now substitute back at the electric field wave equation and separate the two vector components, one for the radial direction and one for the longitudinal:

$$\left(\nabla_r^2 - k_p^2\right)E_{1r} = -\frac{e}{\varepsilon_0}\delta'(\vec{r})\left[\delta(\xi) - k_p\sin(k_p\xi)U(\xi)\right]$$
$$\left(\nabla_r^2 - k_p^2\right)E_{1z} = -\frac{e}{\varepsilon_0}k_p^2\delta(\vec{r})\cos(k_p\xi)U(\xi) \tag{94}$$

The last equation for the longitudinal electric field can be easily solved in the ξ dimension but it also requires to be solved in the r dimension, which will yield the field off-axis. The Green's function response $G(\vec{r};\vec{r}')$ to an impulse function $\delta(\vec{r})$ in cylindrical coordinates is the solution to the equation

$$\left(\nabla_r^2 - k_p^2\right)G(\vec{r};\vec{r}') = \delta(\vec{r} - \vec{r}') \tag{95}$$

This solution can written as

$$G(\vec{r};\vec{r}') = -\frac{1}{2\pi}K_0\left(k_p|\vec{r} - \vec{r}'|\right) \tag{96}$$

K_0 is the modified Bessel function of zeroth order. The longitudinal electric field can be written as

$$E_{1z}(r,\xi) = +\frac{e}{2\pi\varepsilon_0} k_p^2 K_0(k_p r)\cos(k_p \xi) U(\xi) \tag{97}$$

This is the longitudinal electric field response of the plasma to an impulse function. It can be divided into two components, a parallel one and a transverse one, namely $E_{\parallel}(\xi)$ and $R(r)$ such that $E_{1z}(r,\xi) = E_{\parallel}(\xi) R(r)$. This yields

$$\begin{aligned} E_{\parallel}(\xi) &= \frac{e}{\varepsilon_0}\cos(k_p \xi) U(\xi) \\ R(r) &= \frac{k_p^2}{2\pi} K_0(k_p r) \end{aligned} \tag{98}$$

It is interesting to observe that while the plasma density perturbation starts from 0 and it is proportional to a sinusoid, the electric field perturbation is actually discontinuous at the starting point as it has a value of ½ of its maximum value and then it evolves as a cosine, being always 90 degrees out of phase compared to the plasma density wave.

Now assume a general beam density distribution of the type

$$n_b(r,\varphi,\xi) = n_{b\parallel}(\xi) n_{b\perp}(r) \tag{99}$$

The perpendicular beam density is assumed unitless with peak amplitude of 1, and therefore the SI units of the longitudinal beam density are m^{-3}. Then the total electric field is found simply by integrating Green's function over the whole beam distribution in space [92, 116]:

$$\begin{aligned} E_{\parallel}(\xi) &= \frac{e}{\varepsilon_0}\int_{-\infty}^{\xi} n_{b\parallel}(\xi')\cos\left(k_p(\xi-\xi')\right) d\xi' \\ R(r,\varphi) &= \frac{k_p^2}{2\pi}\int_{\varphi'=0}^{2\pi} d\varphi' \int_{r'=0}^{+\infty} n_{b\perp}(r') K_0\left(k_p|\vec{r}-\vec{r}'|\right) r' dr' \end{aligned} \tag{100}$$

Here $\left|\vec{r}-\vec{r}'\right|=\sqrt{r^2+r'^2-2rr'\cos\left(\varphi-\varphi'\right)}$. Also notice that $E_{\parallel}\left(\xi\right)=Z'\left(\xi\right)$. For rotationally symmetric bunches where $n_{b\perp}\left(r',\varphi'\right)=n_{b\perp}\left(r'\right)$, by using the property that $\int_{\Delta}^{2\pi+\Delta} f\left(\cos x\right)dx=\int_{0}^{2\pi} f\left(\cos x\right)dx$, one can show that $R\left(r\right)$ reduces to

$$\begin{aligned} R(r) &= \frac{k_p^2}{2\pi}\int_{\varphi'=0}^{2\pi} d\varphi' \int_{r'=0}^{+\infty} n_{b\perp}(r') K_0\left(k_p\sqrt{r^2+r'^2-2rr'\cos\varphi'}\right) r'dr' \\ &= k_p^2 \int_{r'=0}^{r} n_{b\perp}(r') I_0\left(k_p r'\right) K_0\left(k_p r\right) r'dr' + k_p^2 \int_{r'=r}^{+\infty} n_{b\perp}(r') I_0\left(k_p r\right) K_0\left(k_p r'\right) r'dr' \\ &= k_p^2 \int_{r'=0}^{+\infty} n_{b\perp}(r') I_0\left(k_p r_<\right) K_0\left(k_p r_>\right) r'dr' \end{aligned} \quad (101)$$

Here $r_<=\min\left\{r,r'\right\}$ and $r_>=\max\left\{r,r'\right\}$.

A.4 Bi-Gaussian Bunches

Since the Gaussian is the most common type of beam density shape, it shall be analyzed explicitly. For a transversely Gaussian bunch profile $n_{b\perp}\left(r\right)=e^{-\frac{r^2}{2\sigma_r^2}}$, the on-axis perpendicular component of the longitudinal wakefield is

$$R(0)\simeq\begin{cases} k_p^2\sigma_r^2\left[0.05797-\ln\left(k_p\sigma_r\right)\right] & , \quad k_p\sigma_r<0.5 \\ \left(\frac{k_p^2\sigma_r^2}{2}\right)e^{+\frac{k_p^2\sigma_r^2}{2}}\Gamma\left(0,\frac{k_p^2\sigma_r^2}{2}\right) & , \quad \forall\, k_p\sigma_r \\ 1 & , \quad k_p\sigma_r\gg 1 \end{cases} \quad (102)$$

Here $\Gamma\left(0,b\right)=\int_{b}^{+\infty}\frac{e^{-t}}{t}dt=\int_{1}^{+\infty}\frac{e^{-bt}}{t}dt\equiv E_1\left(b\right)$. A longitudinally Gaussian bunch profile is of the form

$$n_{b\parallel}\left(\xi\right)=n_{b0}e^{-\frac{\xi^2}{2\sigma_z^2}}=\underbrace{\frac{N}{\left(2\pi\right)^{3/2}\sigma_r^2\sigma_z}}_{n_{b0}}e^{-\frac{\xi^2}{2\sigma_z^2}} \quad (103)$$

The total number of particles in this bunch is

$$N \equiv \int_V n_b(r,\xi)\,dV = \int_{r=0}^{+\infty} n_{b\perp}(r)\,2\pi r dr \int_{\xi=-\infty}^{+\infty} n_{b\parallel}(\xi)\,d\xi \tag{104}$$

Near the center of the Gaussian bunch the field needs to be evaluated numerically. Near the tail of the bunch though it can be calculated analytically:

$$E_{\parallel}(\xi \gg \sigma_z) = \left(\frac{e}{4\pi\varepsilon_0}\right)\left(\frac{2N}{\sigma_r^2}\right) e^{-\frac{\sigma_z^2 k_p^2}{2}} \cos\left(k_p \xi\right) \tag{105}$$

Or, in normalized units

$$\frac{eE_{\parallel}(\xi \gg \sigma_z)}{mc\omega_p} = \sqrt{2\pi}\left(\frac{n_{b0}}{n_0}\right)\left(k_p \sigma_z e^{-\frac{\sigma_z^2 k_p^2}{2}}\right)\cos\left(k_p \xi\right) \tag{106}$$

Then the total on-axis wakefield left behind a bi-Gaussian electron bunch is

$$E_{1z}(r=0,\xi \gg \sigma_z) = \left(\frac{e}{4\pi\varepsilon_0}\right) N k_p^2 e^{-\frac{\sigma_z^2 k_p^2}{2}} e^{+\frac{k_p^2 \sigma_r^2}{2}} \Gamma\left(0, \frac{k_p^2 \sigma_r^2}{2}\right)\cos\left(k_p \xi\right) \tag{107}$$

Or, in normalized units

$$\begin{aligned} &\frac{eE_{1z}(r=0,\xi \gg \sigma_z)}{mc\omega_p} = \\ &= \sqrt{2\pi}\left(\frac{n_{b0}}{n_0}\right)\cdot\left(k_p \sigma_z e^{-\frac{\sigma_z^2 k_p^2}{2}}\right)\cdot\left(\frac{k_p^2 \sigma_r^2}{2}\right) e^{+\frac{k_p^2 \sigma_r^2}{2}} \Gamma\left(0, \frac{k_p^2 \sigma_r^2}{2}\right)\cos\left(k_p \xi\right) \end{aligned} \tag{108}$$

The absolute wakefield amplitude is increased as $\sigma_z \downarrow$ and $\sigma_r \downarrow$ and $N \uparrow$ (for a constant plasma density). Finally, let's investigate the dependence of the plasma wake amplitude on the plasma density, or equivalently the plasma wavenumber k_p. There are two questions to be answered. First, given all other parameters constant, what is the optimal plasma density? Second, what is the wake that can be obtained for that plasma density?

A.5 Optimal Plasma Density for bi-Gaussian Electron Drivers

In the 1D limit, one can straightforwardly find the plasma density for which (106) is maximized for a *fixed* density perturbation n_{b0}/n_0: it is $k_p\sigma_z=\sqrt{2}$. The maximum normalized wake amplitude then is given by

$$\frac{eE_{||}^{\max}\left(\xi\gg\sigma_z\right)}{mc\omega_p}\simeq 1.3\left(\frac{n_{b0}}{n_0}\right) \tag{109}$$

If the bunch shaped is fixed instead, equation (105) indicates that the absolute wakefield amplitude increases as the plasma density decreases, or $k_p\downarrow$. This will be true as long as the 1D linear regime condition is satisfied, i.e. $n_{b0}\ll n_0$ and $k_p\sigma_r\ll 1$. Therefore, while in that regime, the optimum plasma density is the minimum.

When the 2D effects are included, in order to get the plasma density that optimizes the wake amplitude for a fixed bi-Gaussian bunch, the derivative of the wake amplitude expression (107) with respect to k_p needs to be taken and set to zero:

$$\frac{d}{dk_p}\left\{\left(\frac{e}{4\pi\varepsilon_0}\right)Nk_p^2e^{-\frac{\sigma_z^2k_p^2}{2}}e^{+\frac{k_p^2\sigma_r^2}{2}}E_1\left(\frac{k_p^2\sigma_r^2}{2}\right)\right\}=0\Rightarrow$$

$$\Rightarrow 2E_1\left(\frac{k_p^2\sigma_r^2}{2}\right)-\sigma_z^2k_p^2E_1\left(\frac{k_p^2\sigma_r^2}{2}\right)+\sigma_r^2k_p^2E_1\left(\frac{k_p^2\sigma_r^2}{2}\right)-\sigma_r^2k_p^2E_0\left(\frac{k_p^2\sigma_r^2}{2}\right)=0$$

In this last step we used the expression for the derivative of the exponential integral, $\frac{d}{dx}E_1(x)=-E_0(x)$, where $E_0(x)=\int_1^\infty e^{-xt}dt\overset{t>0}{=}\frac{e^{-x}}{x}$. The result can be written as

$$\frac{k_p^2\sigma_z^2}{2}=1+\left(\frac{k_p^2\sigma_r^2}{2}\right)\left[1-\frac{E_0\left(\frac{k_p^2\sigma_r^2}{2}\right)}{E_1\left(\frac{k_p^2\sigma_r^2}{2}\right)}\right] \tag{110}$$

One would have to solve this nonlinear equation numerically in order to derive the optimum plasma density. However, it is found that in most cases the exact solution can be approximated simply by

$$\frac{k_p^2\sigma_z^2}{2} \simeq 1 \Rightarrow \; k_p\sigma_z \simeq \sqrt{2} \tag{111}$$

This is the 1D result. It is true for example for small aspect ratio bunches where $k_p\sigma_z \gg k_p\sigma_r \; \Rightarrow \frac{\sigma_r}{\sigma_z} \ll 1$ and the second term on the right hand side of (110) can be ignored. When this aspect ratio is larger than about 0.1, the exact optimal k_p differs from the simplified optimal k_p by a large factor; however, the approximate maximum wake amplitude never differs more than 20% from the exact value even if the approximate expression $k_p\sigma_z \simeq \sqrt{2}$ is always used [116]. This is due to the slowly-varying dependence of the wake amplitude on $k_p\sigma_r$.

The wakefield amplitude for the semi-optimal condition $k_p\sigma_z = \sqrt{2}$ (using eq.(108)) is

$$E_{1z}^{\max}\left(r=0,\xi \gg \sigma_z\right) \simeq 0.74\left(\frac{e}{4\pi\varepsilon_0}\right)\left(\frac{N}{\sigma_z^2}\right)\left\{e^{+\frac{\sigma_r^2}{\sigma_z^2}}\Gamma\left(0,\frac{\sigma_r^2}{\sigma_z^2}\right)\right\} \tag{112}$$

In normalized units this reads

$$\frac{eE_{1z}^{\max}\left(r=0,\xi \gg \sigma_z\right)}{mc\omega_p} \simeq 1.3\left(\frac{n_{b0}}{n_0}\right)\cdot\frac{\sigma_r^2}{\sigma_z^2}e^{+\frac{\sigma_r^2}{\sigma_z^2}}\Gamma\left(0,\frac{\sigma_r^2}{\sigma_z^2}\right) \tag{113}$$

This indicates that other than the slowly-varying monotonically decreasing term in the brackets, the optimum absolute wakefield amplitude will scale as $1/\sigma_z^2$ if the plasma density is adjusted accordingly for a given σ_z.

The above results for bi-Gaussian drivers in the linear regime can be summarized as follows:

$$\left.\frac{eE_{1z}^{\max}}{mc\omega_p}\right|_{k_p\sigma_z=\sqrt{2}} \simeq \begin{cases} 1.3\left(\frac{n_{b0}}{n_0}\right)\cdot\frac{\sigma_r^2}{\sigma_z^2}\cdot 2\ln\left(\frac{1}{\sigma_r/\sigma_z}\right) & , \quad k_p\sigma_r \ll 1 \\ 1.3\left(\frac{n_{b0}}{n_0}\right)\cdot\frac{\sigma_r^2}{\sigma_z^2}\cdot e^{+\frac{\sigma_r^2}{\sigma_z^2}}\Gamma\left(0,\frac{\sigma_r^2}{\sigma_z^2}\right) & , \quad \forall\, k_p\sigma_r \\ 1.3\left(\frac{n_{b0}}{n_0}\right) & , \quad k_p\sigma_r \gg 1 \end{cases} \tag{114}$$

And in SI units:

$$E_{1z}^{\max}\Big|_{k_p\sigma_z=\sqrt{2}} \simeq \begin{cases} 0.74\frac{e}{4\pi\varepsilon_0}\frac{N}{\sigma_z^2}\cdot 2\ln\left(\frac{1}{\sigma_r/\sigma_z}\right) & , \quad k_p\sigma_r \ll 1 \\ 0.74\frac{e}{4\pi\varepsilon_0}\frac{N}{\sigma_z^2}\cdot e^{+\frac{\sigma_r^2}{\sigma_z^2}}\Gamma\left(0,\frac{\sigma_r^2}{\sigma_z^2}\right) & , \quad \forall\, k_p\sigma_r \\ 0.74\frac{e}{4\pi\varepsilon_0}\frac{N}{\sigma_r^2} & , \quad k_p\sigma_r \gg 1 \end{cases} \tag{115}$$

The convergence of the above three expressions are compared in the following Figure.

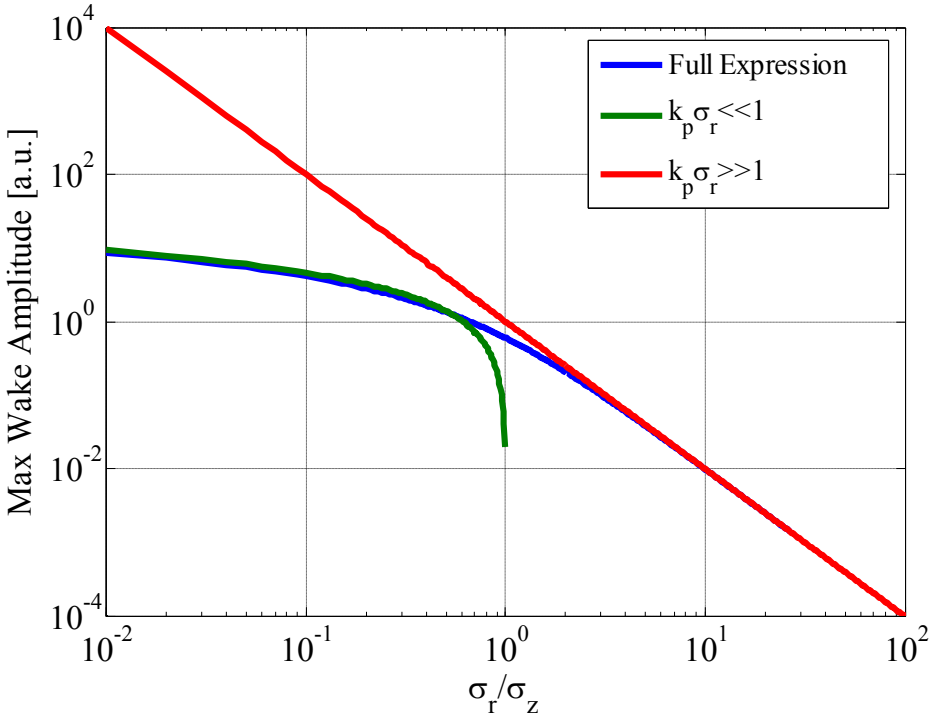

Figure A.1: Comparisons of the maximum wakefield expressions as a function of the beam aspect ratio for bi-Gaussian bunches, when the plasma density is adjusted such that $k_p\sigma_z = \sqrt{2}$.

Appendix B

Upper Limits to the Transformer Ratio

B.1 Symmetric Bunches

It can be proved under very general assumptions that the upper limit to the transformer ratio for a symmetric bunch inside a single mode lossless medium is equal to 2 [10]. Specifically for the plasma wakefield case one can use the results for a linear wakefield excitation. Recollect that the longitudinal wakefield excited from a drive bunch distribution in the 1D linear regime is (from eq.(100))

$$E_z(\xi) = \frac{e}{\varepsilon_0}\int_{-\infty}^{\xi} n_{b\|}(\xi')\cos\left(k_p(\xi-\xi')\right)d\xi'$$

The wakefield at a point ξ inside the bunch with distribution $n_b(\xi)$ is

$$E_z^-(\xi) = \frac{e}{\varepsilon_0}\int_{-\infty}^{\xi} n_{b\|}(\xi')\cos\left(k_p(\xi-\xi')\right)d\xi' =$$
$$= \frac{e}{\varepsilon_0}\cos\left(k_p\xi\right)\int_{-\infty}^{\xi} n_{b\|}(\xi')\cos\left(k_p\xi'\right)d\xi' + \frac{e}{\varepsilon_0}\sin\left(k_p\xi\right)\int_{-\infty}^{\xi} n_{b\|}(\xi')\sin\left(k_p\xi'\right)d\xi'$$

Assuming a symmetric bunch around $\xi = 0$, at the center of the bunch the wakefield is

$$E_z^-(0) = \frac{e}{\varepsilon_0}\int_{-\infty}^{0} n_{b\|}(\xi')\cos k_p\xi' d\xi' \qquad (116)$$

If the wakefield at the center of the bunch is also the peak decelerating wakefield then $E^-_{\max} = E^-_z(0)$. If this is not the case, then it will be larger than this value and $\left|E^-_{\max}\right| > \left|E^-_z(0)\right|$. However in any case $\left|E^-_{\max}\right| \geq \left|E^-_z(0)\right|$. Also, the wakefield at a point ξ after the bunch is (assuming that the bunch distribution is localized around ξ=0 without extending too far):

$$E^+_z(\xi) = \frac{e}{\varepsilon_0}\int_{-\infty}^{+\infty} n_{b\|}(\xi')\cos\left(k_p(\xi-\xi')\right)d\xi' =$$
$$= \frac{e}{\varepsilon_0}\cos k_p\xi \int_{-\infty}^{+\infty} n_{b\|}(\xi')\cos k_p\xi' d\xi' + \frac{e}{\varepsilon_0}\sin k_p\xi \int_{-\infty}^{+\infty} n_{b\|}(\xi')\sin k_p\xi' d\xi'$$

Assuming now that the bunch distribution is symmetric (and the integral is done symmetrically around the bunch), then the second integral in the above expression is 0 because an odd function is integrated symmetrically (the bunch is an even function multiplied by the sinusoidal which is an odd function, resulting in an odd function). Then the maximum value is reached when $\cos k_p\xi = -1$, yielding a result for the maximum accelerating wakefield:

$$E^+_{\max} = -\frac{e}{\varepsilon_0}\int_{-\infty}^{+\infty} n_{b\|}(\xi')\cos k_p\xi' d\xi' =$$
$$= -2\frac{e}{\varepsilon_0}\int_{-\infty}^{0} n_{b\|}(\xi')\cos k_p\xi' d\xi' = 2\left|E^-_z(0)\right| \leq 2\left|E^-_{\max}\right| \Rightarrow$$

$$R \equiv \left|\frac{E^+_{\max}}{E^-_{\max}}\right| \leq 2 \qquad (117)$$

Therefore we conclude that if the peak of the decelerating wakefield happens to be at the center of a symmetric bunch then the transformer ratio peaks at 2; in any other case it will be less than 2.

B.2 Asymmetric Bunches

The transformer ratio can be increased beyond 2 if a proper asymmetric bunch is utilized [9, 104]. The maximum possible transformer ratio (along with the beam to plasma energy transfer efficiency) is achieved when the retarding wakefield inside the bunch is constant. The bunch distribution that satisfies this condition can be calculated analytically as follows.

$$\begin{aligned} &E_{\|}(\xi)=\frac{e}{\varepsilon_0}\int_{-\infty}^{\xi} n_{b\|}(\xi')\cos\left(k_p(\xi-\xi')\right)d\xi' = E_0 U(\xi) \Rightarrow \\ &\Rightarrow \int_{-\infty}^{+\infty} n_{b\|}(\xi')\cos\left(k_p(\xi-\xi')\right)u(\xi-\xi')d\xi' = \frac{\varepsilon_0 E_0}{e}U(\xi) \end{aligned} \tag{118}$$

Here $U(\xi)$ is the Heaviside step function. It is assumed that there is a constant wakefield that starts at $\xi=0$. The longitudinal beam distribution $n_{b\|}(\xi)$ can be solved with the use of the Laplace Transform. By taking the Laplace Transform of both sides and applying the property that the Laplace Transform of a convolution integral is just the product of the Laplace Transforms of the individual functions that are convolved, we get:

$$\begin{aligned} &\wp\left\{\int_{-\infty}^{+\infty} n_{b\|}(\xi')\cos\left(k_p(\xi-\xi')\right)u(\xi-\xi')d\xi'\right\} = \wp\left\{\frac{\varepsilon_0 E_0}{e}U(\xi)\right\} \Rightarrow \\ &\Rightarrow \wp\left\{n_{b\|}(\xi)\right\}\frac{s}{s^2+k_p^2} = \frac{\varepsilon_0 E_0}{e}\frac{1}{s} \Rightarrow \\ &\Rightarrow \wp\left\{n_{b\|}(\xi)\right\} = \frac{\varepsilon_0 E_0}{e}\left(1+k_p^2\frac{1}{s^2}\right) \Rightarrow \\ &\Rightarrow n_{b\|}(\xi) = \frac{\varepsilon_0 E_0}{e}\left(\wp^{-1}\{1\}+k_p^2\wp^{-1}\left\{\frac{1}{s^2}\right\}\right) \Rightarrow \\ &\Rightarrow n_{b\|}(\xi) = \frac{\varepsilon_0 E_0}{e}\left[\delta(\xi)+k_p^2\xi\cdot U(\xi)\right] \end{aligned} \tag{119}$$

So, mathematically the optimal bunch distribution is linear ramp with a delta function at the beginning (required to jump-start the wakefield that remains constant thereafter). The exact bunch distribution and retarding wake can be calculated if we specify a linear ramp with N_1

particles and length $k_p L = M \in \mathbb{Z}$, and a delta function with N_2 particles. This can be written as (for a transversely Gaussian profile):

$$n_b(\xi,r) = \underbrace{\left\{ \underbrace{\frac{\mathrm{N}_2}{2\pi\sigma_r^2}\delta(\xi)}_{n_{b\parallel 2}} + \underbrace{\frac{N_1}{\pi\sigma_r^2 L^2}\cdot\xi\cdot rect\left(\frac{\xi - L/2}{L/2}\right)}_{n_{b\parallel 1}} \right\}}_{n_{b\parallel}} \cdot \underbrace{e^{-\frac{r^2}{2\sigma_r^2}}}_{n_{b\perp}} \tag{120}$$

The wakefield excited inside this bunch is

$$E_{\parallel}(\xi) = \frac{eN_1}{\varepsilon_0 \pi\sigma_r^2 k_p^2 L^2} + \left(\frac{eN_2}{\varepsilon_0 2\pi\sigma_r^2} - \frac{eN_1}{\varepsilon_0 \pi\sigma_r^2 k_p^2 L^2} \right) \cos\left(k_p \xi\right) \tag{121}$$

This wake is constant if

$$\frac{N_1}{N_2} = 2\pi^2 M^2 \tag{122}$$

The wake excited after the bunch is

$$E_{\parallel}(\xi) = -\underbrace{\frac{e\mathrm{N}_1}{2\pi^2\sigma_r^2\varepsilon_0 \mathrm{M}} \frac{\sqrt{1+\left(2\pi M\right)^2}}{2\pi M}}_{E_{\max}^{+}} \cos\left(k_p \xi + \tan^{-1}\left(2\pi M\right)\right) \tag{123}$$

Therefore, the optimum transformer ratio is then

$$R = \frac{E_{\max}^{+}}{E_{\max}^{-}} = \sqrt{1+\left(2\pi M\right)^2} \overset{M \gg 1}{\rightarrow} 2\pi M \tag{124}$$

This is the ultimate limit for the transformer ratio in the linear regime.

Appendix C

Coherent Transition Radiation from an Electron Bunch

In the following pages we will attempt to calculate theoretically the CTR from an electron bunch when going through a metal foil. There are two independent effects that take place in such a phenomenon. First, we will calculate the energy radiated from a single electron when it hits a metal foil (transition radiation). Second, we will calculate how this radiation is altered by the presence of the other electrons nearby (coherent radiation). A more complete description can be found in [110].

C.1 Transition Radiation from a Single Electron

The problem of the radiation emitted from an electron approaching normally a perfectly conducting boundary is handled using the method of images: the perfect conductor is replaced with another electron of equal and opposite charge (i.e., a positron) approaching the first electron from the opposite direction with the same initial speed, such that the two particles are to collide exactly where the boundary was. A significant assumption here is that the two particles decelerate until they meet at the boundary with 0 speed each. Transition radiation will be emitted from both electrons as they decelerate to reach standstill.

The energy radiated from a single charged particle during a collision is given by the following formula [77]:

$$\frac{d^2E}{d\omega d\Omega} = \frac{1}{16\pi^3\varepsilon_0 c}\left|\int \frac{d}{dt}\left[\frac{q\hat{n}\times\left(\hat{n}\times\vec{\beta}\right)}{1-\hat{n}\cdot\vec{\beta}}\right]e^{+i\omega\left(t-\hat{n}\cdot\vec{r}(t)/c\right)}dt\right|^2 \tag{125}$$

The quantity on the left has units of energy per steradian per frequency, in CGS units. $\vec{\beta} = \vec{v}/c$ is the speed of the electron, $\hat{n}$ is the direction of radiation at frequency ω, and $\vec{r}$ is the position of the electron at time t. Since the time τ it takes for en electron to cross the boundary is small, we let $\omega\tau \ll 1$ which will set the exponent inside the integral to go to 0. This is valid if the radiation of interest is at relatively low frequencies. The integral then becomes

$$\frac{d^2E}{d\omega d\Omega} = \frac{1}{16\pi^3\varepsilon_0 c}\left|\left[\frac{-e\hat{n}\times\left(\hat{n}\times\vec{\beta}\right)}{1-\hat{n}\cdot\vec{\beta}}\right]_{\beta_{initial}=\beta}^{\beta_{final}=0} + \left[\frac{+e\hat{n}\times\left(\hat{n}\times\vec{\beta}\right)}{1-\hat{n}\cdot\vec{\beta}}\right]_{\beta_{initial}=-\beta}^{\beta_{final}=0}\right|^2 \tag{126}$$

Here the positron radiation term was also added. Carrying out the calculation

$$\frac{d^2E}{d\omega d\Omega} = \frac{e^2}{16\pi^3\varepsilon_0 c}\left|\frac{2\hat{n}\times\left(\hat{n}\times\vec{\beta}\right)}{1-\left(\hat{n}\cdot\vec{\beta}\right)^2}\right|^2 = \frac{e^2}{4\pi^3\varepsilon_0 c}\frac{\beta^2\sin^2\theta}{\left(1-\beta^2\cos^2\theta\right)^2} \quad , \quad \cos\theta \equiv \hat{n}\cdot\left(-\hat{\beta}\right) \tag{127}$$

So this is the radiation from the transition of the electron approaching perpendicularly a perfect conductor. Note that the exact same expression holds true for the case of an electron emerging from a perfect conductor into the vacuum. Also, observe that due to the low-frequency assumption there is no dependence on frequency in this formula. The peak of the radiation is $\frac{e^2\gamma^2}{16\pi^3\varepsilon_0\beta^2 c}$, located at an angle $\sin\theta = \frac{1}{\beta\gamma}$. More general expressions are available for general cases of oblique incidence [110].

C.2 Coherent Radiation from N electrons

Let us assume N electrons, distributed in space. Each electron is identified by the number j, so $j=1,2,...,N$. Let the center of this electron bunch to be at the origin of the axes, that the observation point is located at $\vec{R}=R\hat{R}$, and that each electron j is located at a distance $\vec{r}_j=r_j\hat{r}_j$ from the center of the bunch. Hence the distance between an electron j and the observation point is $\vec{x}_j=\vec{R}-\vec{r}_j=x_j\hat{n}_j$.

Now, assume that all the electrons are moving at exactly the same speed. This motion can be broken down to a set of frequencies. The field generated by an electron j at the frequency ω is $\vec{E}_j(k)$, where $k=\frac{\omega}{c}$. The field observed at the observation point which is $\vec{x}_j$ away will propagate with a wavevector $\vec{k}_j=k\hat{n}_j$, so its value at that point will be

$$\vec{E}_j(k)e^{+i\vec{k}_j\cdot\vec{x}_j}=\vec{E}_j(k)e^{+ik\hat{n}_j\cdot\left(-\vec{r}_j+\vec{R}\right)}=\vec{E}_j(k)e^{-ik\hat{n}_j\cdot\vec{r}_j}e^{+ikR\hat{n}_j\cdot\hat{R}} \tag{128}$$

Assuming the far-field approximation, i.e. $R\gg r_j$,then $\hat{n}_j\simeq\hat{R}$ and $\vec{E}_j(k)\simeq\vec{E}_e(k)$, which means that the electric field amplitude is same as if the electron is located at the center of the bunch. The field now becomes

$$\vec{E}_e(k)e^{-ik\hat{R}\cdot\vec{r}_j}e^{+ikR\hat{R}\cdot\hat{R}}=\vec{E}_e(k)e^{+ikR}e^{-ik\hat{R}\cdot\vec{r}_j} \tag{129}$$

The *total* field intensity $I_{total}(k)$ in Watts per m^2 generated from *all* the electrons at that observation point for that frequency k is

$$I_{total}(k)=\frac{c\varepsilon_0}{2}\left|E_{total}\right|^2=\frac{c\varepsilon_0}{2}\left|\vec{E}_e(k)e^{+ikR}\right|^2\left|\sum_{j=1}^{N}e^{-ik\hat{R}\cdot\vec{r}_j}\right|^2=I_e(k)\left|\sum_{j=1}^{N}e^{-ik\hat{R}\cdot\vec{r}_j}\right|^2 \tag{130}$$

Here $I_e(k)=\frac{c\varepsilon_0}{2}\left|\vec{E}_e(k)\right|^2$ is the field intensity generated from a single electron. If all the electrons were located in the same point in space, then the phase information would disappear and this would yield a factor N^2 (it's just like having a charge $e\cdot N$ there, which would create an electric field N times stronger and hence intensity N^2 times stronger). However the distribution of the electrons along the bunch will alter this simple dependence.

$$I_{total}(k)=I_e(k)\sum_{j=1}^{N}\sum_{m=1}^{N}e^{-ik\hat{R}\cdot\vec{r}_j}e^{+ik\hat{R}\cdot\vec{r}_m}=I_e(k)\left[N+\sum_{\substack{j=1\\j\neq m}}^{N}\sum_{m=1}^{N}e^{-ik\hat{R}\cdot\left(\vec{r}_j-\vec{r}_m\right)}\right] \tag{131}$$

In order to proceed further, one more assumption needs to be made. Since the number of electrons in each bunch is typically large, we could replace the summations over all the electrons with integrals over a continuous electron distribution. So, let's assume that the number of electrons in a volume element d^3r at a distance $\vec{r}$ from the center of the bunch is $N\cdot S(\vec{r})d^3r$. Then the function $S(\vec{r})$ is just a probability distribution such that $\int S(\vec{r})d^3r=1$. Therefore, the discrete summation can be approximated by the integral (after some short calculations)

$$I_{total}(k)\simeq I_e(k)\left[N+\sum_{\substack{j=1\\j\neq m}}^{N}\int e^{-ik\hat{R}\cdot\left(\vec{r}_j-\vec{r}'\right)}NS(\vec{r}')d^3r'\right]\simeq I_e(k)\left[N+N(N-1)f\left(k;\hat{R}\right)\right] \tag{132}$$

$$f\left(k;\hat{R}\right)\equiv\left|\int e^{+ik\hat{R}\cdot\vec{r}'}S(\vec{r}')d^3r'\right|^2$$

f is traditionally noted as the bunch form factor, a quantity that relates the bunch distribution with the phases of the electrons inside the bunch. For $k\to 0$ (low frequencies, high wavelengths) the factor is close to its maximum value, 1. In this case $I_{total}(k\to 0)\to N^2I_e(k)$. Here the electrons act in harmony, and they produce the same intensity as if they all were

perfectly located at the center of the bunch. Hence in low frequencies the actual distribution of electrons doesn't matter much, because the phase factor is so tiny that it doesn't affect the integral. This is the coherent radiation.

For $k \to \infty$ (high frequencies, low wavelengths) the phase will change with infinitely big steps. Even around a small dr we will ideally have all phases adding up in the integral, and these will eventually cancel out. Hence at this case where the phases are random the bunch form factor will approach 0 and $I_{total}\left(k \to \infty\right) \to N I_e\left(k\right)$. Here the electrons act completely at random, and they produce a total electric field that is only the square root of the electric field they produce when they act in harmony, and hence now the intensity scales linearly with the number of electrons and the charge of the bunch. This is the incoherent radiation.

C.3 The Bunch Form Factor in a more Specific Case

In order to evaluate the bunch form factor for a general frequency, let

$$S\left(\vec{r}'\right) = \frac{1}{2\pi\sigma_{\rho'}^2} e^{-\frac{\rho'^2}{2\sigma_{\rho'}^2}} Z\left(z'\right) \qquad , \qquad \begin{matrix} x' = \rho'\cos\phi' \\ y' = \rho'\sin\phi' \end{matrix} \tag{133}$$

This means that we will have a cylindrical coordinate system to describe the transverse dependence of the bunch which is assumed Gaussian. Since $\hat{R}\cdot\vec{r}' = \rho'\sin\theta\cos\left(\phi-\phi'\right) + z'\cos\theta$, then the BFF reads

$$f\left(k;\phi,\theta\right) = \left| \int_{\rho'=0}^{\rho'=\infty} \int_{\phi'=0}^{\phi'=2\pi} \int_{z'=-\infty}^{z'=+\infty} e^{+ik\left(\rho'\sin\theta\cos\left(\phi-\phi'\right)+z'\cos\theta\right)} \frac{1}{2\pi\sigma_{\rho'}^2} e^{-\frac{\rho'^2}{2\sigma_{\rho'}^2}} Z\left(z'\right)\rho' d\phi' d\rho' dz' \right|^2 = \tag{134}$$

$$= \left| \int_{z'=-\infty}^{z'=+\infty} e^{+ik\cos\theta z'} Z\left(z'\right) dz' \right|^2 \left| \int_{\rho'=0}^{\rho'=\infty} \frac{1}{2\pi\sigma_{\rho'}^2} e^{-\frac{\rho'^2}{2\sigma_{\rho'}^2}} \rho' \left(\int_0^{2\pi} e^{+ik\rho'\sin\theta\cos\left(\phi-\phi'\right)} d\phi' \right) d\rho' \right|^2$$

The inside integral can be calculated as follows:

$$\int_0^{2\pi} e^{+ik\rho'\sin\theta\cos(\phi-\phi')}d\phi' \overset{\phi-\phi'=\psi}{=} + \int_{\phi-2\pi}^{\phi} e^{+ik\rho'\sin\theta\cos\psi}d\psi = 2\pi J_0\left(k\rho'\sin\theta\right) \tag{135}$$

Then using also the identity $\int_0^{\infty} e^{-\alpha^2 t^2} J_\nu\left(bt\right)t^{\nu+1}dt = \frac{b^\nu}{\left(2\alpha^2\right)^{\nu+1}} e^{-\frac{b^2}{4\alpha^2}}$ [4], the bunch form factor can be written as

$$f\left(k;\theta\right) = e^{-\sigma_\rho^2 k^2\sin^2\theta}\left|\int_{-\infty}^{+\infty} Z(z')e^{+ik\cos\theta z'}dz'\right|^2 \tag{136}$$

It is clearly seen that the bunch form factor is directly proportional to the squared amplitude of the Fourier transform of the longitudinal distribution of the bunch. Thus, the geometrical characteristics of the electron distribution are mapped onto the spectrum of the emitted radiation.

C.4 CTR Interferometry

Coherent Transition Radiation is emitted when an electron beam hits a foil, and it is emitted near a wavelength equal to the dimensions of the beam itself. Since the detectors typically are not capable of resolving the picoseconds-long CTR signal in time, interferometry can be used to retrieve time-dependent information of the signal. The electric field is added to a slightly delayed in time version of the same electric field, and the intensity sum is observed, usually time integrated. The output yields information of the shape of the beam, and it is especially useful when more than one bunch of electrons are present.

Let's start with the electric field of the CTR: $E(t)$. This is a spatially integrated time-dependent magnitude of the full field $\vec{E}\left(r,\phi,z,t\right)$. At the exit of the interferometer, this field is

added to a shifted in time version of the field, $E(t-\tau)$. Here τ is the shift in time, which is controlled by adjusting the lengths of the arms of the interferometer. Negative values of τ imply that the second field comes earlier in time than the first, while positive values correspond to an electric field that comes later in time than the original. For a beam that is about 1 mm long, the time shift should be controlled in the 1 mm range, which is about 3 ps. At the exit of the interferometer the total field is $E(t)+E(t-\tau)$.

This field will hit a CTR detector, the same one that was used to measure the plain CTR. The detector will yield a time-integrated value of the intensity of the input fields, which will be proportional to

$$I(\tau)=\int_{-\infty}^{+\infty}\left[E(t)+E(t-\tau)\right]^2 dt = 2I_0 + 2\int_{-\infty}^{+\infty} E(t)\cdot E(t-\tau)dt \tag{137}$$

Where $\int_{-\infty}^{+\infty}\left[E(t)\right]^2 dt = I_0$. Hence the output will be a constant background enhanced by the autocorrelation integral of the beam with itself. For a single Gaussian bunch, i.e.

$$E(t)=E_0 e^{-\frac{(t-t_0)^2}{2\sigma_z^2}} \tag{138}$$

The recorded interferometer CTR signal is

$$I\left(\tau\right)=2I_0\left(1+e^{-\frac{\tau^2}{4\sigma_z^2}}\right) \tag{139}$$

Here $I_0=E_0^2\sqrt{\pi}\sigma_z$. It is therefore another Gaussian, only with a standard deviation that is $\sqrt{2}$ times larger now than the standard deviation of the Gaussian bunch itself. The pattern has a minimum at $2I_0$ and it reaches double this background value at the best case ($\tau=0$) which is when the bunch overlaps with itself. By measuring the width of the CTR Gaussian, one can

therefore measure the width of the initial bunch. An absolute measurement of the intensity will also yield the strength of the bunch.

Let's assume now that there are two distinct electron bunches that comprise the beam, each at different spots along time and with different amplitudes. We have

$$E_1(t) = E_{01} e^{-\frac{(t-t_{01})^2}{2\sigma_{z1}^2}} \qquad E_2(t) = E_{02} e^{-\frac{(t-t_{02})^2}{2\sigma_{z2}^2}}$$
$$E(t) = E_1(t) + E_2(t) \tag{140}$$

The total signal recorder at the detector will be (after some analytical manipulations)

$$I(\tau) = 2I_{01} + 2I_{02} + 4\frac{\sqrt{2I_{01}I_{02}}}{\sqrt{\frac{\sigma_{z2}}{\sigma_{z1}} + \frac{\sigma_{z1}}{\sigma_{z2}}}} e^{-\frac{(t_{01}-t_{02})^2}{2(\sigma_{z1}^2+\sigma_{z2}^2)}} +$$
$$+2I_{01} e^{-\frac{\tau^2}{4\sigma_{z1}^2}} + 2I_{02} e^{-\frac{\tau^2}{4\sigma_{z2}^2}} + \tag{141}$$
$$+2\frac{\sqrt{2I_{01}I_{02}}}{\sqrt{\frac{\sigma_{z2}}{\sigma_{z1}} + \frac{\sigma_{z1}}{\sigma_{z2}}}} e^{-\frac{(t_{01}-t_{02}-\tau)^2}{2(\sigma_{z1}^2+\sigma_{z2}^2)}} + 2\frac{\sqrt{2I_{01}I_{02}}}{\sqrt{\frac{\sigma_{z2}}{\sigma_{z1}} + \frac{\sigma_{z1}}{\sigma_{z2}}}} e^{-\frac{(t_{01}-t_{02}+\tau)^2}{2(\sigma_{z1}^2+\sigma_{z2}^2)}}$$

There are 3 groups of terms in the result. The first group consists of the first 3 terms, and it is just the constant background radiation interference. The second group consists of the next 2 terms, which are the self-correlation terms for each bunch. The third group consists of the last 2 terms, and they are two satellite lobes, each corresponding to a cross term between the first and second bunch and vice versa. It is clear that the location and shape of each satellite lobe can provide information for both bunches.

Appendix D

ThemOsiris Simulation Code

The fully explicit particle-in-cell code OSIRIS [71] is widely used for calculating the beam-plasma and laser-plasma interactions in a plasma accelerator. However, one of the drawbacks of the code is that only a single plasma density can be simulated at any given run. For the multibunch ideas and experiments presented in this dissertation though, it is desirable to get a quick answer regarding the evolution of the wakefield amplitude with respect to the phase of the bunches for different plasma densities. For this reason a simulation code was developed that solves for the wakefield amplitude given an input beam profile. The mathematical analysis behind the code is briefly presented in Section D.1, while Section D.2 offers an example of an implementation of the code in Matlab. This code was used to generate most of the non-OSIRIS simulation figures in the work presented in this dissertation.

D.1 Analytical Formulation

The starting point are Maxwell's equations in a linear medium, explicitly written in equation (73) . Instead of assuming linear approximation, we solve the equations in the fully relativistic nonlinear 1D regime, along with the relativistic Newton's law of motion, equation (74), and the continuity condition for electrons, equation (75). Therefore, assuming $\partial / \partial r = 0$ (and thus no magnetic field) and dependence on the variable $\xi = z - ct$, then $\vec{\nabla} = \hat{z} \cdot d / d\xi$ and we get

$$
\begin{aligned}
0 &= -ecn_b - en_e v_e - \frac{1}{\mu_0 c}\frac{dE}{d\xi} \\
\frac{dE}{d\xi} &= \frac{1}{\varepsilon_0}\left(-en_b + en_0 - en_e\right) \\
\frac{d}{d\xi}\left(\gamma m_e v_e\right) &= \frac{e}{c}E \\
-c\frac{dn_e}{d\xi} + \frac{d}{d\xi}\left(n_e v_e\right) &= 0
\end{aligned}
\tag{142}
$$

The electric field E and the electron velocity v_e can be substituted in the above system of equations. After some analytical manipulation, a differential equation for the total electron density n_e as a function of the length ξ can be written as follows:

$$
\frac{d^2 n_e}{d\xi^2} = \frac{3}{2n_e - n_0}\left(\frac{dn_e}{d\xi}\right)^2 - \left(2n_e - n_0\right)^{3/2} \cdot k_p^2\left(n_e - n_0 + n_b\right) \tag{143}
$$

This equation is equivalent to the one derived by Rosenzweig in [146]. The electric field E is then found from

$$
E = \frac{m_e c^2}{en_0}\frac{1}{\left(2\frac{n_e}{n_0} - 1\right)^{3/2}}\frac{dn_e}{d\xi} \tag{144}
$$

The above equations intrinsically include nonlinear effects, such as the sawtooth-shaped wakefields and the frequency shifts that emerge in the nonlinear regime. However the equations are only valid as long as the plasma can be treated as a fluid, and this does not always hold in the blowout regime due to particle trajectory crossings [116]. Still, these equations can be used to obtain rough wakefield amplitudes and bunch phasing in the mildly nonlinear regime.

Note that in the weakly linear regime we have $n_e / n_0 \ll 1$ and by Taylor-expanding n_e around n_0 the above equations are approximated by

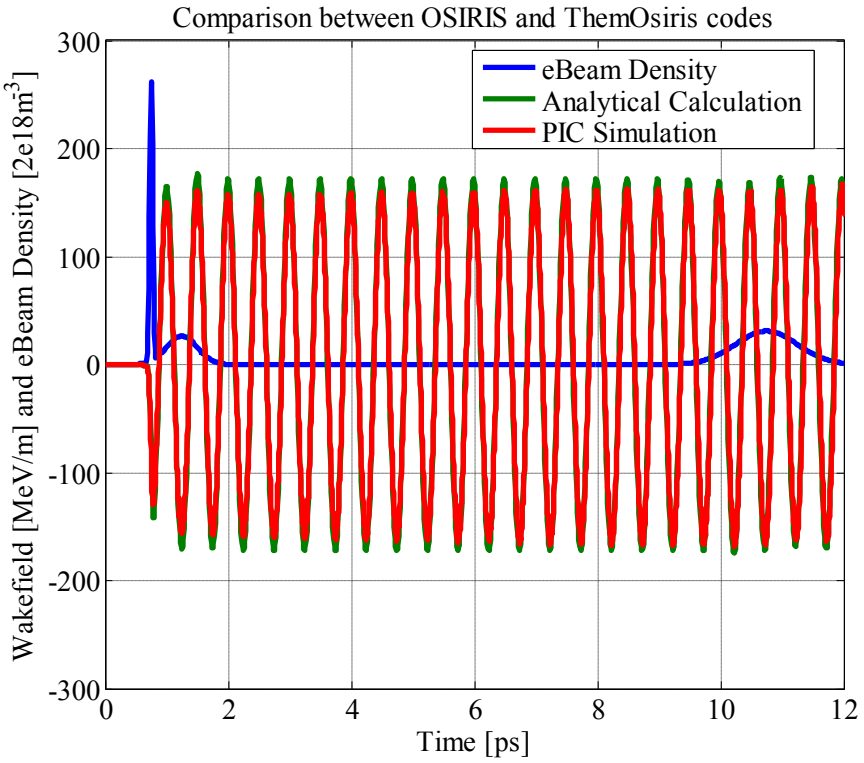

Figure D.1: Comparison between OSIRIS and ThemOsiris codes for the same set of input parameters. Three electron bunches with peak beam density of 2×10^{12} cm^{-3} are fed into a 5×10^{16} cm^{-3} plasma. The deviation between the codes is less than 5% in terms of the wakefield evolution, while ThemOsiris is at least 1,000 times faster.

$$\frac{d^2 n_e}{d\xi^2} \simeq -k_p^2 \left(n_e - n_0 + n_b \right)$$
$$E \simeq \frac{m_e c^2}{e n_0} \frac{d n_e}{d\xi} \tag{145}$$

These are the results of the linear wakefield theory that was presented in Appendix A.1 . In order to obtain a wakefield amplitude that includes 2D transverse effects, the amplitude found through equation (144) can be multiplied (for transversely Gaussian bunches) by $R(0)$ which is defined in equation (9).

A comparison between the outputs of ThemOsiris and OSIRIS is presented in Figure D. An implementation of ThemOsiris in Matlab was written. The input beam electron density

consists of 3 bunches, the last one separated by many plasma wavelengths. We observe that as benchmarked by OSIRIS the code correctly predicts the wakefield amplitude with less than 5% error. Being ≈1000 times faster than OSIRIS, the code can be used to do quick plasma density scans and/or to determine the proper position of the bunches.

In the second revision of this code, the ability to generate the beam energy spectra at the exit of the plasma was added (including intrinsic energy spread). The code is limited to slow variation of the initial neutral plasma density (on a scale longer than the beam length) and assumes that the beam does not evolve with time.

D.2 Sample Code

An example of ThemOsiris code than can run in Matlab is given below. The code outputs the wakefield vs. time as well as the predicted energy spectra of given bunches. The functions that are called are also explicitly written below.

```
% ThemOsiris
% This is a code that will calculate the phase space and energy gain of
% 2D  bunches  into a high density plasma, used for our Brookhaven
% ATF experiment...

clear all;
% Useful physical constants
c = 3e8;
e = 1.6e-19;
m = 9.1e-31;

% Plasma normalization parameters
lamda0 = 250e-6;                % Reference wavelength for normalizations
k0 = 2*pi/lamda0;               % Reference wavevector
n0 = 1e-6*lamdap2n0(lamda0);    % Reference plasma density in cm^-3
wp = 2*pi*c/lamda0;             % Reference plasma frequency in Hz


% INPUT DECK!!!
%--------------------------------------------------------------------------
%--------------------------------------------------------------------------

% Plasma Density
```

```
%---------------
np=1.79e16;                         % in cm^-3

% Input parameters for the 2 bunches
%-----------------------------------

% Energy of the bunches in MeV
Energy0 = [56 57 58 59 60 61];

% Total Charge for drive bunches [pC]
qt=250;

% How many drive bunches?
Nb=4;

% How much of the charge is *not* blocked? [1=none]
b=0.5;

% Charge of each bunch in pC
% (the drive bunch has half the charge)
q = b*[qt/Nb*1 qt/Nb*3 qt/Nb*5 qt/Nb*7 qt/Nb*0.001 qt/4/2];

% Bunch seperation distance in microns
% (relates to plasma density)
sep = n02lamdap(np)*1e6;

% Position of each bunch in sec
 %mean = [250 250+1.5*sep 250+3*sep 250+4.5*sep 1250 1625+125]*1e-6/c;
 mean = [250 250+1.5*sep 250+2*1.5*sep 250+3*1.5*sep 250+6*sep 1562.5]*1e-6/c;

% sigma_z of each bunch in sec
% (such that fraction b goes through)
sigma_z = b/2*[sep sep sep sep sep sep/4/b]*1e-6/c;

% Spot size of each bunch in microns
sigma_r  = 100*[1 1 1 1 1 1];


% Define the spatial grid for the simulation
%-------------------------------------------
zmin = 0.0*k0*1e-3;             % Start of simulation box in mm
zmax = 20.0*k0*1e-3;            % End of simulation box in mm
N = 100;                        % Grid number of points for simulation box
z = linspace(zmin,zmax,N);      % The grid in propagation direction

%-------------------------------------------------------------------------
%-------------------------------------------------------------------------

% Solve for the wakefield generated from the above bunch distribution
% tspan in ps, E in MeV/m, nb in m^-3
[tspan, E, nb] = multi_gaus_wake(np, mean, sigma_z, sigma_r, q);

% INITIALIZE PARTICLE POSITION AND MOMENTUM!!!
```

```
%-------------------------------------------------------------------------
%-------------------------------------------------------------------------

NN=length(tspan);
% Calculate the beam densities seperately


    for i=1:NN
        nb1(i) = square(tspan(i)*1e-12, mean(1), sigma_z(1), 3, q(1),
sigma_r(1));
        nb2(i) = square(tspan(i)*1e-12, mean(2), sigma_z(2), 3, q(2),
sigma_r(2));
        nb3(i) = square(tspan(i)*1e-12, mean(3), sigma_z(3), 3, q(3),
sigma_r(3));
        nb4(i) = square(tspan(i)*1e-12, mean(4), sigma_z(4), 3, q(4),
sigma_r(4));
        nb5(i) = square(tspan(i)*1e-12, mean(5), sigma_z(5), 3, q(5),
sigma_r(5));
        nb6(i) = square(tspan(i)*1e-12, mean(6), sigma_z(6), 3, q(6),
sigma_r(6));
    end

% How many particles do you want in the simulation total???
Np  = 25000*length(q(q>1));

    Np1 = q(1)/sum(q)*Np;    % Number of particles in each bunch
    Np2 = q(2)/sum(q)*Np;    % Number of particles in each bunch
    Np3 = q(3)/sum(q)*Np;    % Number of particles in each bunch
    Np4 = q(4)/sum(q)*Np;    % Number of particles in each bunch
    Np5 = q(5)/sum(q)*Np;    % Number of particles in each bunch
    Np6 = q(6)/sum(q)*Np;    % Number of particles in each bunch

% Renormalize density so that we have this number of particles

    nb1 = nb1.*Np1.*length(nb1)/(tspan(end)-tspan(1))/sum(nb1);
    nb2 = nb2.*Np2.*length(nb2)/(tspan(end)-tspan(1))/sum(nb2);
    nb3 = nb3.*Np3.*length(nb3)/(tspan(end)-tspan(1))/sum(nb3);
    nb4 = nb4.*Np4.*length(nb4)/(tspan(end)-tspan(1))/sum(nb4);
    nb5 = nb5.*Np5.*length(nb5)/(tspan(end)-tspan(1))/sum(nb5);
    nb6 = nb6.*Np6.*length(nb6)/(tspan(end)-tspan(1))/sum(nb6);

% Create the initial particle location matrix
%-----------------------------------------
dz = tspan(2)-tspan(1);                                  % Elementary step
ze1=[]; ze2=[]; ze3=[]; ze4=[]; ze5=[]; ze6=[];
% Initialize the particles location matrix

    for i=2:length(tspan);                                   % for every time
interval dz (dt)

    num_par1 = round(nb1(i)*dz);                         % This is how many
particles are in that interval
    num_par2 = round(nb2(i)*dz);
```

```
    num_par3 = round(nb3(i)*dz);
    num_par4 = round(nb4(i)*dz);
    num_par5 = round(nb5(i)*dz);
    num_par6 = round(nb6(i)*dz);

    tempz1 = linspace(tspan(i-1),tspan(i),num_par1);    % Evenly distribute
the particles over that interval
    tempz2 = linspace(tspan(i-1),tspan(i),num_par2);
    tempz3 = linspace(tspan(i-1),tspan(i),num_par3);
    tempz4 = linspace(tspan(i-1),tspan(i),num_par4);
    tempz5 = linspace(tspan(i-1),tspan(i),num_par5);
    tempz6 = linspace(tspan(i-1),tspan(i),num_par6);

    tempz1 = tempz1(2:end);                             % Ignore the first
overlapping particle
    tempz2 = tempz2(2:end);
    tempz3 = tempz3(2:end);
    tempz4 = tempz4(2:end);
    tempz5 = tempz5(2:end);
    tempz6 = tempz6(2:end);

    ze1 = [ze1 tempz1];                                 % Add those particles
to the location matrix
    ze2 = [ze2 tempz2];
    ze3 = [ze3 tempz3];
    ze4 = [ze4 tempz4];
    ze5 = [ze5 tempz5];
    ze6 = [ze6 tempz6];

    end


Np1=length(ze1);                    % actual number of particles in beam 1
Np2=length(ze2);                    % actual number of particles in beam 2
Np3=length(ze3);
Np4=length(ze4);
Np5=length(ze5);
Np6=length(ze6);

Np = Np1+Np2+Np3+Np4+Np5+Np6;                       % Total actual number of
particles
ze = [ze1 ze2 ze3 ze4 ze5 ze6];                     % Merging the two beams
together!
% Now, the matrix ze contains the positions of the particles with respect
% to the beggining (head) of the beam


% Create the initial particle momentum matrix
%-----------------------------------------
s_th=0.1;                                           % Thermal spread in MeV
Energy1(1:Np1) = Energy0(1) + s_th*randn(1,Np1);     % Energy of the first
beam particles
```

```
Energy2(1:Np2) = Energy0(2) + s_th*randn(1,Np2);     % Energy of the second
beam particles
Energy3(1:Np3) = Energy0(3) + s_th*randn(1,Np3);
Energy4(1:Np4) = Energy0(4) + s_th*randn(1,Np4);
Energy5(1:Np5) = Energy0(5) + s_th*randn(1,Np5);
Energy6(1:Np6) = Energy0(6) + s_th*randn(1,Np6);
Energy = [Energy1 Energy2 Energy3 Energy4 Energy5 Energy6];
% Merge the two energy distributions


% Modify the start and end of simulation box is necessary
loc_z_start = 1;
loc_z_final = length(z);
z_start = z(loc_z_start);
z_final = z(loc_z_final);

%  Create the matrix that holds the momentums of the particles
p = zeros(loc_z_final-loc_z_start+1,Np);
% Initialize the beam electrons at their initial momentum[normalized units]
p(1,:) = sqrt((1+Energy(:)/0.511875).^2-1);
% Now matrix p holds the momentums of all the Np particles of both bunches

% Find each particle location in tspan
par_loc=round(1+((NN-1)/(tspan(end)-tspan(1)))*ze);
par_loc(par_loc>5000)=5000;     % Ignore further away particles
% This can be done because tspan(i)=1000/(NN-1)*(i-1)=linspace(0,1000,N);

%--------------------------------------------------------------------------
%--------------------------------------------------------------------------


% Main loop for pushing particles
%--------------------------------------------------------------------------
for i=loc_z_start:loc_z_final-1       % For each step along z

    % Calculate next step for the beam
    dz = z(i+1)-z(i);

    for j=1:Np      % For each particle along the beam
       % And now the main push!
        p(i+1-loc_z_start+1,j)= p(i-loc_z_start+1,j) +...
            dz/k0*E(par_loc(j))*1e6*e/c^2/m;
    end
end

% Translate momentum to energy in MeV
Energy = 0.511875.*(sqrt(p.^2+1)-1);

% Calculate Transformer Ratio
% -------------------------------------------------------------------------
% Number of driving bunches
Nd = length(q(q>1))-1;
```

```
for i=1:Nd
    % Extend of bunch region in psec
    L_low  = (mean(i)-sigma_z(i))*1e12;
    L_high = (mean(i)+sigma_z(i))*1e12;
    t_low  = length(tspan(tspan<L_low));  % Position in tspan
    t_high = length(tspan(tspan<L_high)); % Position in tspan
    % Maximum decelerating field inside that bunch
    Em(i) = abs(min(E(t_low:t_high)));
end
% Maximum decelerating field inside the drive bunches
Emin = max(Em);

% Up until the beginning of the drive bunch
Lb = (mean(end)-sigma_z(end))*1e12;
tb = length(tspan(tspan<Lb)); % Position in tspan
% Maximum accelerating field after the drive bunches
Emax = max(E(t_high:tb));

% Transformer Ratio
R = Emax/Emin;


% PLOTTING PARAMETERS AND FUNCTIONS
%--------------------------------------------------------------------------
%--------------------------------------------------------------------------

% Define Bin Centers
E_min=53;
E_max=68;
M=linspace(E_min,E_max,200);

figure('Position',[100 100 800 700]);

subplot(2,1,1);
hold on;
area(tspan,(nb1+nb2+nb3+nb4+nb5)/max(nb1+nb2+nb3+nb4+nb5+nb6)*180,'facecolor',
'green');
area(tspan,nb6/max(nb1+nb2+nb3+nb4+nb5+nb6)*180,'Facecolor',[1 0.5 0]);
plot(tspan,E,'linewidth',3);
grid on;
title(['Wakefield and Beam Density,  n_p=',num2str(np,'%2.1e'),'cm^-^3'])
ylabel('Wakefield [MV/m]');
xlabel('Time [ps]');
axis([0 7 -200 200]);
legend('Drive Beam','Witness','Wakefield','location','southwest');
text(5.1,175,['R=',num2str(R,'%1.3g')]);
enhance_plot;

[N0,X0] = hist(Energy(1,:),M);
[N1,X1] = hist(Energy(end,1:Np1),M);
[N2,X2] = hist(Energy(end,Np1+1:Np1+Np2),M);
[N3,X3] = hist(Energy(end,Np1+Np2+1:Np1+Np2+Np3),M);
[N4,X4] = hist(Energy(end,Np1+Np2+Np3+1:Np1+Np2+Np3+Np4),M);
```

```
[N5,X5] = hist(Energy(end,Np1+Np2+Np3+Np4+1:Np1+Np2+Np3+Np4+Np5),M);
[N6,X6] = hist(Energy(end,Np1+Np2+Np3+Np4+Np5+1:Np1+Np2+Np3+Np4+Np5+Np6),M);
%[N7,X7] = hist(Energy(end,Np1+Np2+Np3+Np4+Np5+Np6+1:end),M);
[N ,X ] = hist(Energy(end,:),M);

subplot(2,1,2);
area(X1,N1,'Facecolor',[0 0 1]);

title(['Energy Spectrum after ',num2str(zmax/k0*1000),'mm of plasma']);
ylabel('# of sim particles');
xlabel('eBeam Energy [MeV]');
axis([E_min E_max 0 10000]);

hold on;
area(X2,N2,'Facecolor',[0 0 0.85]);
area(X3,N3,'Facecolor',[0 0 0.60]);
area(X4,N4,'Facecolor',[0 0 0.45]);
area(X5,N5,'Facecolor',[0 0 0.30]);
%area(X6,N6,'Facecolor',[0 0 0.15]);
area(X6,N6,'Facecolor','magenta');
%area(X7,N7,'Facecolor','magenta');
plot(X0,N0,'black:');
plot(X,N,'r','linewidth',3);
%legend('Bunch 1','Bunch 2','Bunch 3','Bunch 4','Bunch 5','Bunch 6','Witness
Bunch','Initial Spectrum','Final Spectrum','location','northwest');
enhance_plot;
```

```
% Solves the 1D nonlinear plasma differential equation
% np in cm^-3
% sigma1, sigma2,in s
% sigma_r in microns, charge in pC


function [t, E, nb] = multi_gaus_wake(np, mean, sigma_z, sigma_r, charge)


c=3e8;
e=1.6e-19;
m=9.1e-31;

wp = 2*pi*c/n02lamdap(np);  % in s^-1

tmin = 0;                                                  % start field time in
ps
tmax = 12;                                                 % End field time in ps
NN=5000;                                                   % Number of points for
field
tspan = linspace(tmin,tmax,NN);                            % in ps
```

```
tspan2 = tspan*1e-12*wp;                                    % Time grid points in
sim units


options=odeset('reltol',1e-3,'abstol',1e-10);               % Solver Options

    [t,v]=ode45(@rhs_multi_gaus,tspan2, [1, 0], options, mean, sigma_z,
sigma_r, charge, np);
    n = v(:,1);                                             % Electron Beam
density
    E = (v(:,2)./(2*n-1).^(1.5))';                          % Electric Field

    sr=sigma_r(1)*1e-6*2*pi/n02lamdap(np);                  % Normalized
transverse radius
    E = E*sr.^2/2*exp(sr.^2/2).*expint(sr.^2/2);            % Account for
transverse effects

t = t/wp*1e12;                                              % time in ps is
returned

for i=1:size(t,1) nb(i)=square(t(i)*1e-12, mean(1), sigma_z(1), 3, charge(1),
sigma_r(1)) +...
      square(t(i)*1e-12, mean(2), sigma_z(2), 3, charge(2), sigma_r(2)); end
% nb is in m^-3
t=t';
Enorm = m*c*wp/e;
E2 = E*Enorm/1e6;    % Return E in MeV/m
E=E2;
```

```
% The function that contains the right hand side of the differential equation
to be solved
% np is plasma density in cm^-3


function out = rhs_multi_gaus(t, y, mean, sigma_z, sigma_r, charge, np)

n = y(1);
u = y(2);

wp = 1/n02lamdap(np)*2*pi*3e8;          % plasma frequency in s^-1
np = np*1e6;                            % in m^-3

% Calculate beam density
for i=1:length(mean)
    temp(i) = square(t/wp, mean(i), sigma_z(i), 3, charge(i), sigma_r(i));
end
beam = sum(temp);

out1 = u;
```

```
out2 = 3/(2*n-1)*u^2 - (2*n-1)^(1.5)*(n - 1 + beam/np);

out = [out1; out2];
```

```
% Returns the value of the gaussian at point x in sec
% mean is the mean value in sec
% sigma is the Half Width of the square in sec
% num is the numbers of sigmas on each side after which the gaussian is 0
% charge is the charge in pC
% sigma_r is the rms spot size in microns
%
% the output is the beam density at the point x in particles per m^3

function out = square(x, mean, sigma_z, num, charge, sigma_r)

charge = charge*1e-12;
sigma_r = sigma_r*1e-6;
e=1.6e-19;
c=3e8;

if abs(x-mean)<=sigma_z
    out = charge/(e*2*pi*sigma_r^2*2*sigma_z*c);
else out=0;
end
```

```
% lamdap in m, n0 in cm^-3

function out = no2lamdap(n0)

c=3e8;
e=1.6e-19;
m=9.1e-31;
e0=8.85e-12;

out = 2*pi*c/e*sqrt(e0*m/n0*1e-6);
```

```
function enhance_plot(fontname,fontsize,linewid,markersiz)

%  enhance_plot([fontname,fontsize]);
%
%  Function to enhance MATLAB's lousy text choices on plots.  Sets the
```

```
%  current figure's Xlabel, Ylabel, Title, and all Text on plots, plus
%  the axes-labels to the "fontname" and "fontsize" input here where
%  the defaults have been set to 'times' and 16.
%  Also sets all plotted lines to "linewid" and all markers to size
%  "markersiz".  The defaults are 2 and 8.
%
%  INPUTS:  fontname:   (Optional,DEF='TIMES') FontName string to use
%                       MATLAB's ugly default is 'Helvetica'
%           fontsize:   (Optional,DEF=16) FontSize integer to use
%                       MATLAB's tiny default is 10
%           linewid:    (Optional,DEF=2) LineWidth integer to use
%                       MATLAB's skinny default is 0.5
%           markersiz:  (Optional,DEF=8) MarkerSize integer to use
%                       MATLAB's squinty default is 6
%  for all inputs, if pass 0, use default
%
% Modifications
%  19-Feb-2002 J. Nelson
%       added linewid and markersiz to help squinting readers
%
%  20-Feb-2002 J. Nelson
%       added check for legend.  If legend exists, increase the
%           line and marker size, also increase the font to
%           fontsize-2 (2 points smaller than title and labels)
%=========================================================================

if (~exist('fontname')|(fontname==0))
  fontname = 'times';
end
if (~exist('fontsize')|(fontsize==0))
  fontsize = 16;
end
if (~exist('linewid')|(linewid==0))
  linewid=3;
end
if (~exist('markersiz')|(markersiz==0))
  markersiz = 8;
end

Hf=gcf;
Ha=gca;
Hx=get(Ha,'XLabel');
Hy=get(Ha,'YLabel');
Ht=get(Ha,'Title');
set(Ha,'LineWidth',.75);
set(Hx,'fontname',fontname);
set(Hx,'fontsize',fontsize);
set(Hy,'fontname',fontname);
set(Hy,'fontsize',fontsize);
set(Ha,'fontname',fontname);
set(Ha,'fontsize',fontsize);
%set(Ha,'YaxisLocation','right')
%set(Ha,'YaxisLocation','left')
```

```
set(Ht,'fontname',fontname);
set(Ht,'fontsize',fontsize);
set(Hy,'VerticalAlignment','bottom');
set(Hx,'VerticalAlignment','cap');
set(Ht,'VerticalAlignment','baseline');
Hn = get(Ha,'Children');
n = length(Hn);
if n > 0
  typ = get(Hn,'Type');
  for j = 1:n
    if strcmp('text',typ(j,:))
      set(Hn(j),'fontname',fontname);
      set(Hn(j),'fontsize',fontsize);
    end
    if strcmp('line',typ(j,:))
      set(Hn(j),'LineWidth',linewid);
      set(Hn(j),'MarkerSize',markersiz);
    end
  end
end
legh=legend;
Hn=get(legh,'Children');
n = length(Hn);
if n > 0
  typ = get(Hn,'Type');
  for j = 1:n
    if strcmp('text',typ(j,:))
      set(Hn(j),'fontname',fontname);
      set(Hn(j),'fontsize',fontsize-2);
    end
    if strcmp('line',typ(j,:))
      set(Hn(j),'LineWidth',linewid);
      set(Hn(j),'MarkerSize',markersiz);
    end
  end
end

figure(Hf);
```

Appendix E

Publication List

"Simulations of a high-transformer-ratio plasma wakefield accelerator using multiple electron bunches", by Efthymios Kallos, Patric Muggli, Tom Katsouleas, Vitaly Yakimenko, Jangho Park and Karl Kusche, in Proceedings of the 2008 Advanced Accelerator Concepts Workshop, Santa Cruz, CA (2008), to appear

"A mask technique for the generation of trains or microbunches with subpicosecond spacing and length", by Patric Muggli, Vitaly Yakimenko, Jangho Park, Efthymios Kallos, Karl Kusche, and Marcus Babzien in Proceedings of the 2008 Advanced Accelerator Concepts Workshop, Santa Cruz, CA (2008), to appear

"Experimental Results of a Plasma Wakefield Accelerator Using Multiple Electron Bunches", by Efthymios Kallos, Tom Katsouleas, Patric Muggli, Jangho Park, Igor Pogorelsky, Daniil Stolyarov, Vitaly Yakimenko and Wayne D. Kimura in Proceedings of the 2008 European Particle Accelerator Conference, Genoa, Italy (2008), to appear

“Generation of Electron Microbunches Trains with Adjustable Sub-picosecond Spacing for PWFA and FEL applications”, by Patric Muggli, Efthymios Kallos, Marcus Babzien, Karl Kusche, Vitaly Yakimenko in Proceedings of the 2008 European Particle Accelerator Conference, Genoa, Italy (2008), to appear

"Generation of Trains of Electron Microbunches with Sub-picosecond Spacing", byPatric Muggli, Vitaly Yakimenko, Wayne D. Kimura, Marcus Babzien, Efthymios Kallos and Karl Kusche in Phys. Rev. Lett. (2008), to appear

"High-gradient Plasma Wakefield Acceleration with two subpicosecond electron bunches", by Efthymios Kallos, Tom Katsouleas, Wayne D. Kimura, Patric Muggli, Igor Pavlishin, Igor Pogorelsky, Daniil Stolyarov, Vitaly Yakimenko in Phys. Rev. Lett. 100, 074802 (2008)

"Plasma Wakefield Acceleration Utilizing Multiple Electron Bunches", by Efthymios Kallos, Tom Katsouleas, Patric Muggli, Igor Pavlishin, Igor Pogorelsky, Daniil Stolyarov, Vitaly Yakimenko, Wayne D. Kimura in Proceedings of the 2007 IEEE Particle Accelerator Conference, Albuquerque, NM, pp.3070-3072 (2007)

"Generation and Characterization of the Microbunched Beams with a Mesh Target", by Patric Muggli, Efthymios Kallos, Vitaly Yakimenko, Marcus Babzien, Karl Kusche, Wayne D. Kimura in Proceedings of the 2007 IEEE Particle Accelerator Conference, Albuquerque, NM, pp.3073-3075 (2007)

"Plasma Wakefield Acceleration Experiments Using Two Subpicosecond Electron Bunches", by Patric Muggli, Wayne D. Kimura, Efthymios Kallos, Tom Katsouleas, Karl Kusche, Igor Pavlishin, Igor Pogorelsky, Vitaly Yakimenko in Proceedings of the 2007 IEEE Particle Accelerator Conference, Albuquerque, NM, pp.3079-3081 (2007)

"Femtosecond Microbunched Electron Beam - A New Tool for Advanced Accelerator Research", by Igor Pogorelsky, Marcus Babzien, Ilan Ben Zvi, Karl Kusche, Igor Pavlishin, Vitaly Yakimenko, C. Dilley, S. Gottschalk, Wayne D. Kimura, S. Steinhauer, Efthymios Kallos, Tom Katsouleas, Patric Muggli, A. Zigler, Sammer Banna, Levi Schächter, David Cline, Feng Zhou, Y. Kamiya, T. Kumita in Proceedings of the Third International Conference on Superstrong Fields in Plasmas, Vol. 827, No. 1., pp. 297-307 (2006)

"Generation and Characterization of the Microbunched Beams in the Range from 0.3 to 500 Femtoseconds", by Vitaly Yakimenko, Marcus Babzien, Karl Kusche, Efthymios Kallos, Patric Muggli, and Wayne D. Kimura in Proceedings of the 28th International Free Electron Laser Conference, Berlin, Germany, pp. 481-484 (2006)

"Plasma Simulations and Multibunched Electron Beam Diagnostics", by Efthymios Kallos, Patric Muggli, Tom Katsouleas, Vitaly Yakimenko, Daniil Stolyarov, Igor Pogorelsky, Igor Pavlishin, Karl Kusche, Marcus Babzien, Ilan Ben-Zvi and Wayne D. Kimura in Proceedings of the 12th Advanced Accelerator Concepts Workshop, Lake Geneva, WI, AIP Conference Proceedings No.877, pp. 520-526 (2006)

"Update on Seeded SM-LWFA and Pseudo-Resonant LWFA Experiments", by W D. Kimura, N. E. Andreev, X. Ding, M.Babzien, I. Ben-Zvi, D. B. Cline, S. M. Hooker, E. Kallos, T. C. Katsouleas, K. P. Kusche, S. V. Kuznetsov, P. Muggli, I. V. Pavlishin, I. V. Pogorelsky, A. A. Pogosova, L. C. Steinhauer, D. Stolyarov, A. Ting, V. Yakimenko, A. Zigler, and F. Zhou in Proceedings of the 12th Advanced Accelerator Concepts Workshop, Lake Geneva, WI, AIP Conference Proceedings No.877, pp. 534-540 (2006)

"Subpicosecond Double Electron Bunch Generation", by Wayne D. Kimura, Vitaly Yakimenko, Marcus Babzien, Xiaoping Ding, Eftymios Kallos, Tom Katsouleas, Karl Kusche, Patric Muggli, Igor Pavlishin, Igor Pogorelsky, Daniil Stolyarov, and Feng Zhou in Proceedings of the 12th Advanced Accelerator Concepts Workshop, Lake Geneva, WI, AIP Conference Proceedings No.877, pp. 527-533 (2006)

"Plasma Density Measurements in Hydrogen-Filled and Plastic Ablation Discharge Capillaries based on Stark Broadening of Atomic Hydrogen Spectral Lines", by Daniil Stolyarov, Igor Pavlishin, Marcus Babzien, Wayne Kimura, Patric Muggli, Efthymios Kallos and Vitaly Yakimenko in Proceedings of the 12th Advanced Accelerator Concepts Workshop, Lake Geneva, WI, AIP Conference Proceedings No.877, pp. 784-791 (2006)

"Plasma-Based Advanced Accelerators at the Brookhaven Accelerator Test Facility", by I. V. Pogorelsky, M. Babzien, K. P. Kusche, I. V. Pavlishin, V. Yakimenko, C. E. Dilley, S. C. Gottschalk, W. D. Kimura, T. Katsouleas, P. Muggli, E. Kallos, L. C. Steinhauer, A. Zigler, N. Andreev, D. B. Cline and F. Zhou in Laser Physics, Vol.16, No.2, pp. 259-266 (2006)

"A Multibunch Plasma Wakefield Accelerator", by Efthymios Kallos, Tom Katsouleas, Patric Muggli, Ilan-Ben Zvi, Igor Pogorelsky, Vitaly Yakimenko, Igor Pavlishin, Karl Kusche, Marcus Babzien, Feng Zhou and Wayne D. Kimura in Proceedings of the 2005 IEEE Particle Accelerator Conference, Knoxville, TN, pp. 3384-3386 (2005)